Bulletin of Romanian Chemical Engineering Society

2 2018

ISSN 2360-4697
Edited by SICR and Matrix Rom

The journal is included in the international database
INDEX COPERNICUS INTERNATIONAL

ISSN 2360-4697

Bulletin of Romanian Chemical Engineering Society

Volume 5 2018 Number 2

Contents

TWO DIMENSION MODEL FOR NICKEL TETRACARBONYL SYNTHESIS

Ștefania Cristina IONESCU, Sorin Ilie DAMIAN*,
Oana Cristina PÂRVULESCU, Tănase DOBRE

University POLITEHNICA of Bucharest, Faculty of Applied Chemistry and Materials Science, Department of Chemical and Biochemical Engineering, 1-7 Gheorghe Polizu, 011061, Bucharest, Romania

Abstract

The first metal carbonyl, $Ni(CO)_4$, was prepared in 1890 by the reaction between CO and metallic Ni. This method is simple and still current. A 2D model has been developed in this paper in order to simulate the synthesis of $Ni(CO)_4$ by the reaction between CO and Ni particles in a fixed bed reactor. The model is based on the diffusion of CO and $Ni(CO)_4$ towards/from the reactive Ni surface. A plug flow of gas phase and a decrease of Ni particle radius over time were assumed. The model consists of partial differential equations expressing the variations of CO molar fraction and total molar flow rate along the bed (z coordinate) and of Ni particle radius over time (τ coordinate). Simulations were performed based on selected values of relevant model parameters, i.e., reactor diameter (D=0.18 m), fixed bed height (H=1 m), initial Ni particle radius (R_0=0.002 m), bed void fraction (ε=0.35 m^3/m^3), CO diffusion coefficient in gas phase ($D_A=3.52\times10^{-5}$ m^2/s), total molar flow rate at reactor input (G_{M0}=0.0089 kmol/s), CO molar fraction in gas phase at reactor input ($y_{A\infty0}$=0.995 kmol/kmol), working temperature (T=390 K), pressure ($p=10^5$ Pa), $y_{As}/y_{A\infty}$ (0.05÷0.55) and $D_A/R_0/k_s$ (0.05 and 0.5), where y_{As} represents CO molar fraction at particle surface and k_s is surface reaction rate constant.

Key words: Nickel tetracarbonyl, modelling, diffusion, nickel particle, fixed bed

1. Introduction

The chemistry of metal carbonyls has been of considerable interest for several decades mainly due to reactivity of these compounds in respect to several classes of organic ligands as well as their applications in catalysis and in production of some electronic devices [1]. The first metal carbonyl, $Ni(CO)_4$, was prepared by Mond et al. (1890) [2] by the reaction between metallic nickel and carbon monoxide. This procedure, consisting in passing, at around 100 °C and

* Corresponding author: Email address: dsorin22@yahoo.com

normal pressure, of carbon oxide over nickel particles, followed by the cooling of resulted gases and $Ni(CO)_4$ condensation, is simple and still current. It has been used for industrial preparation of pure nickel [3]. When a Fe-Ni alloy interacts with carbon monoxide at normal pressure and a temperature between 40 and 140 °C, the nickel attack is preponderant (1), because the formation of iron carbonyl occurs intensely only at higher temperature and pressure (2).

$$Ni + 4CO \xrightarrow{1\,atm,\,40\text{-}140\,^\circ C} Ni(CO)_4 \quad (1)$$

$$Fe + 5CO \xrightarrow{175\,atm,\,150\text{-}200\,^\circ C} Fe(CO)_5 \quad (2)$$

Nickel tetracarbonyl is a colourless liquid having melting point of -25 °C, boiling point of 43 °C and decomposition temperature in the range of 180-200 °C. It is insoluble in water but dissolves in various organic solvents. Concerning the reactivity of $Ni(CO)_4$, the following issues are highlighted [4]: (i) it reacts with concentrated sulphuric acid along with detonation due to simultaneous production of hydrogen and carbon oxide ($Ni(CO)_4 + H_2SO_4 \rightarrow NiSO_4 + H_2 + 4CO$), (ii) with moist nitric oxide it gives a blue coloured compound and a mixture of carbon monoxide and hydrogen ($2Ni(CO)_4 + 2NO + 2H_2O \rightarrow 2Ni(NO)(OH) + 8CO + H_2$), (iii) passing gaseous hydrochloric acid through a heterogeneous medium where the discrete phase is nickel tetracarbonyl, results in the decomposition with a pale green water phase ($Ni(CO)_4 + 2\,HCl \rightarrow NiCl_2 + H_2 + 4CO$). Moreover, the vapour of $Ni(CO)_4$ can self-ignite and decompose quickly in air, with a half-life between 30 and 70 s, depending on the air temperature (10 and 50 °C) [5]. The thermal decomposition of $Ni(CO)_4$ as gas in a mixture with an inert (N_2) and CO can be used for synthesis of Ni nanoparticles [5-7]. Nickel nanoparticle diameter (d_p) mainly depends on process temperature (t), nickel tetracarbonyl concentration in gas (c_{NiTC}), carbon oxide concentration in gas (c_{CO}) and residence time (τ) inside a tubular reactor [7]. TEM images of nickel nanoparticles are shown in Fig. 1 [7]. Nickel tetracarbonyl decomposition is also successfully used for the deposition of nickel on ceramics, plastics, and others [6, 8].

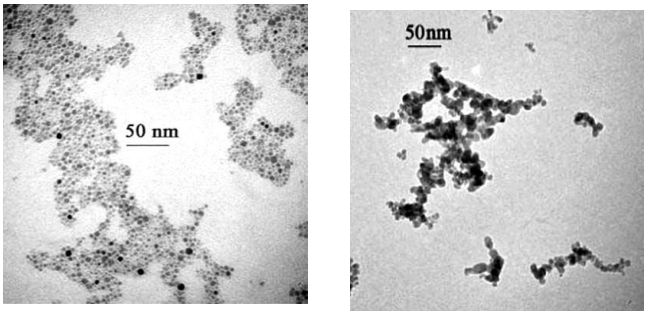

Fig. 1. Nickel nanoparticles obtained by nickel tetracarbonyl decomposition [7]
(left: c_{NiTC}=25 ppm, c_{CO}=1.13%, t=260 °C, τ=0.05 s, d_p=4 nm;
right: c_{NiTC}=9 ppm, c_{CO}=1.13%, t=400 °C, τ=0.05 s, d_p=12 nm).

The synthesis of $Ni(CO)_4$ as well as its uses in different applications are strongly marked by the high toxicity of this compound, which may be fatal if it is inhaled or absorbed through the skin. The process design and control based on modelling could offer relevant information that may be applied to protect the human health and diminish the expenses related to the process [9].

This paper has aimed at developing a mathematical model for $Ni(CO)_4$ synthesis in a fixed bed reactor with countercurrent feeding of CO and Ni particles and further using the model to simulate the synthesis process. Simulation could be very helpful to control and optimize the process, because it involves a decrease in the number of experimental runs, which can heavily affect the health of operators and process costs.

2. Modelling

Molar balance for a Ni particle

It was assumed that the synthesis process at Ni particle level occurred by countercurrent diffusion of CO and $Ni(CO)_4$ towards/from Ni particle coupled with the reaction (1) taking place at its surface. This process is schematically presented in Fig. 2, where N_{Ar} and N_{Br} represent the fluxes of CO and $Ni(CO)_4$, whereas $y_{A\infty}$ and y_{As} are CO molar fraction in gas phase (at a distance $r \to \infty$ of Ni particle centre) and at its surface ($r=R$), respectively. Due to the surface reaction, Ni particle radius (R) decreases over time.

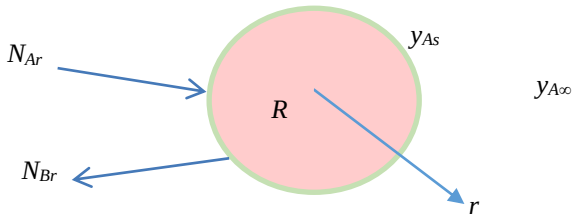

Fig. 2. Scheme for $Ni(CO)_4$ synthesis by surface reaction between Ni and CO.

Molar fluxes N_{Ar} and N_{Br} were correlated by Eqs. (3) and (4), which were obtained according to the countercurrent diffusion of CO (A) and $Ni(CO)_4$ (B) and stoichiometry of reaction (1), respectively. Substituting Eq. (4) in Eq. (3), Eq. (5) was obtained, where D_A is the diffusion coefficient of CO in gas phase and C the total molar concentration. CO flow rate towards Ni particle (n_{Ar}) was expressed depending on N_{Ar} and r radius by Eq. (6), which was further integrated based on boundary conditions given by Eqs. (7) and (8) resulting in Eq. (9), which links n_A to R, C, D_A, y_{As} and $y_{A\infty}$.

$$N_{Ar} = CD_A \frac{dy_A}{dr} + y_A(N_{Ar} - N_{Br}) \quad (3)$$

$$N_{Br} = N_{Ar}/4 \quad (4)$$

$$N_{Ar} = \frac{CD_A}{1-\frac{3}{4}y_A}\frac{dy_A}{dr} \quad (5)$$

$$n_{Ar} = 4\pi r^2 \frac{CD_A}{1-\frac{3}{4}y_A}\frac{dy_A}{dr} \quad (6)$$

$$r = R \qquad y_A = y_{As} \quad (7)$$

$$r \to \infty \qquad y_A = y_{A\infty} \quad (8)$$

$$n_A = \frac{16}{3}\pi RCD_A \ln\left(\frac{1-\frac{3}{4}y_{As}}{1-\frac{3}{4}y_{A\infty}}\right) \quad (9)$$

If the ratio $y_{As}/y_{A\infty}$ tends to zero, the process is controlled by external diffusion, whereas if it goes to unity, the process is kinetically controlled. A first order reaction rate given by Eq. (10), where k_s is the reaction rate constant, was assumed at Ni particle surface. This assumption is widely considered for surface reaction coupled with species diffusion [10]. Substituting Eq. (10) into Eq. (9), Eq. (11) was obtained. A Taylor series development for $\ln\left(1-\frac{3}{4}\frac{n_A}{4\pi R^2 k_s C}\right)$ in Eq. (11) led to Eq. (12), expressing n_A depending on R, C, D_A, $y_{A\infty}$ and k_s. Very high values of k_s lead to a ratio $y_{As}/y_{A\infty}$ tending to zero, accordingly the process is controlled by CO diffusion towards the Ni particle.

$$N_{Ar} = k_s c_{As} = k_s C y_{As} \tag{10}$$

$$n_A = \frac{16}{3}\pi R C D_A \ln\left(\frac{1-\frac{3}{4}\frac{n_A}{4\pi R^2 k_s C}}{1-\frac{3}{4}y_{A\infty}}\right) \tag{11}$$

$$n_A = \frac{\frac{16}{3}\pi R C D_A}{1+\frac{D_A}{R k_s}} \ln\left(\frac{1}{1-\frac{3}{4}y_{A\infty}}\right) \tag{12}$$

Molar balance for fixed bed Ni particles

A scheme of molar balance for a control volume in the fixed bed (dV defined by Eq. (13)) is presented in Fig. 3, where n_{bA} and n_{bB} represent the molar flow rates of CO and Ni(CO)$_4$ in the bed, G_M the total molar flow rate of gases, D the tubular reactor diameter, z the distance in the bed and $y_{A\infty}$ the CO molar fraction in the gas phase flowing through the bed. A plug flow of gas phase was assumed. Moreover, taking into account the stoichiometry of reaction (1), the total molar flow rate and CO molar fraction decrease along the bed, *i.e.*, dG_M/dz<0 and d$y_{A\infty}$/dz<0.

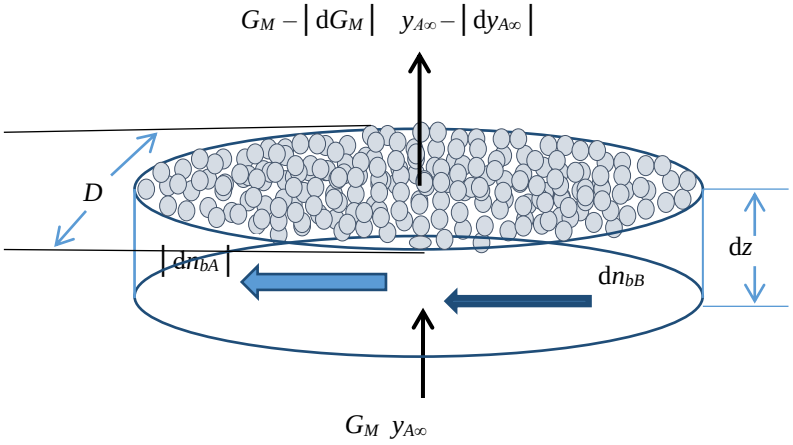

Fig. 3. Scheme of species balance for Ni(CO)$_4$ synthesis by surface reaction between Ni and CO.

Based on Eqs. (13) and (14), expressing the volumes of a Ni particle (V_p), the number of Ni particles within the control volume (n_p) was estimated using Eq. (15), where ε is the bed void fraction. Further, taking into account Eqs. (9) and (15), the molar flow rate of CO within the control volume (dn_{bA}) was determined by Eq. (16). The correlation between the molar flow rates of CO (dn_{bA}) and $Ni(CO)_4$ (dn_{bB}) within the control volume given by Eq. (17), Eq. (18) expressing the total molar flow rate (dG_M) depending on dn_{bA} and dn_{bB} along with Eq. (16) led to Eq. (19) showing the evolution of total molar flow rate along the bed (dG_M/dz).

$$\mathrm{d}V = \frac{\pi D^2}{4}\mathrm{d}z \tag{13}$$

$$V_p = 4\pi R^3/3 \tag{14}$$

$$n_p = \frac{\mathrm{d}V(1-\varepsilon)}{V_p} = \frac{3D^2(1-\varepsilon)}{16R^3}\mathrm{d}z \tag{15}$$

$$\left|\mathrm{d}n_{bA}\right| = n_p n_A = \frac{\pi D^2(1-\varepsilon)CD_A}{R^2}\ln\left(\frac{1-\frac{3}{4}y_{As}}{1-\frac{3}{4}y_{A\infty}}\right)\mathrm{d}z \tag{16}$$

$$\mathrm{d}n_{bB} = \frac{1}{4}\left|\mathrm{d}n_{bA}\right| \tag{17}$$

$$\left|\mathrm{d}G_M\right| = \left|\mathrm{d}n_{bA}\right| - \mathrm{d}n_{bB} = \frac{3}{4}\left|\mathrm{d}n_{bA}\right| \tag{18}$$

$$\frac{\mathrm{d}G_M}{\mathrm{d}z} = -\frac{3\pi D^2(1-\varepsilon)CD_A}{4R^2}\ln\left(\frac{1-\frac{3}{4}y_{As}}{1-\frac{3}{4}y_{A\infty}}\right) \tag{19}$$

The molar balance of A species within the control volume led to Eq. (20) and further, taking into account Eqs. (16) and (18), Eq. (21), expressing the variation of molar fraction of carbon monoxide along the bed, was obtained.

$$\left|\mathrm{d}y_{A\infty}\right| = -\frac{\left|\mathrm{d}n_{bA}\right| - y_{A\infty}\left|\mathrm{d}G_M\right|}{G_M} \tag{20}$$

$$\frac{dy_{A\infty}}{dz} = -\frac{\left(1-\frac{3}{4}y_{A\infty}\right)}{G_M}\frac{\pi D^2(1-\varepsilon)CD_A}{R^2}\ln\left(\frac{1-\frac{3}{4}y_{As}}{1-\frac{3}{4}y_{A\infty}}\right) \tag{21}$$

Nickel particle radius (R) is variable over time due to the nickel consumption. A molar balance of Ni consumption is given by Eq. (22), where ρ_{Ni} is the nickel density and M_{Ni} the nickel molar mass. Based on Eq. (22), Eq. (23), expressing the time evolution of Ni particle radius, was derived.

$$-\frac{d}{d\tau}\left(\frac{4\pi R^3\rho_{Ni}}{3M_{Ni}}\right) = \frac{n_A}{4} = \frac{4}{3}\pi RCD_A\ln\left(\frac{1-\frac{3}{4}y_{As}}{1-\frac{3}{4}y_{A\infty}}\right) \tag{22}$$

$$\frac{dR}{d\tau} = -\frac{M_{Ni}CD_A}{2\rho_{Ni}R}\ln\left(\frac{1-\frac{3}{4}y_{As}}{1-\frac{3}{4}y_{A\infty}}\right) \tag{23}$$

Consequently, a two dimension model was developed to describe the process of $Ni(CO)_4$ synthesis in a fixed bed reactor. It can be used to design or simulate the process [11]. Characteristic equations, initial and boundary conditions of the model are given by Eqs. (24)-(32). In order to keep a constant bed height ($z=H$), Ni particles were continuously fed to the top of the reactor. Dynamics of Ni particle flow rate can be predicted using the model.

$$\frac{\partial y_{A\infty}}{\partial z} = -\frac{\left(1-\frac{3}{4}y_{A\infty}\right)}{G_M}\frac{\pi D^2(1-\varepsilon)CD_A}{R^2}\ln\left(\frac{1-\frac{3}{4}y_{As}}{1-\frac{3}{4}y_{A\infty}}\right) \tag{24}$$

$$\tau = 0 \qquad 0 \le z \le H \qquad y_{A\infty} = 0 \tag{25}$$

$$\tau > 0 \qquad z = 0 \qquad y_{A\infty} = y_{A\infty 0} \tag{26}$$

$$\frac{\partial G_M}{\partial z} = -\frac{3}{4}.\frac{\pi D^2(1-\varepsilon)CD_A}{R^2}\ln\left(\frac{1-\frac{3}{4}y_{As}}{1-\frac{3}{4}y_{A\infty}}\right) \tag{27}$$

$$\tau = 0 \qquad 0 \le z \le H \qquad G_M = 0 \tag{28}$$

$$\tau > 0 \qquad z = 0 \qquad G_M = G_{M0} \tag{29}$$

$$\frac{\partial R}{\partial \tau} = -\frac{M_{Ni} C D_A}{2\rho_{Ni} R} \ln\left(\frac{1-\frac{3}{4}y_{As}}{1-\frac{3}{4}y_{A\infty}}\right) \tag{30}$$

$$\tau = 0 \qquad 0 \le z \le H \qquad R = R_0 \tag{31}$$

$$\tau > 0 \qquad z = H \qquad R = R_0 \tag{32}$$

3. Results and discussions

The model was used to simulate the synthesis of nickel tetracarbonyl in a fixed bed reactor, assuming a plug flow of mobile phase. Simulations were performed based on the values of characteristic factors of the model which are summarized in Table 1. Tabulated values were selected according to the data reported in the related literature. The curves simulated based on the values of process factors specified in Table 1 are presented in Figs. 4-10.

Table 1

Values of model factors used to simulate $Ni(CO)_4$ synthesis in a fixed bed reactor

No.	Factor	Symbol	Selected value	Reference
1	Reactor diameter	D	0.18 m	[2, 7]
2	Ni particle fixed bed height	H	1 m	[2, 7]
3	Initial Ni particle radius	R_0	2×10^{-3} m	[12]
4	Bed void fraction	ε	0.35 m^3/m^3	[11]
5	CO diffusion coefficient in gas phase	D_A	3.52×10^{-5} m^2/s	[13]
6	Total mass flow rate at reactor input	G_{m0}	0.25 kg/s	[12]
7	CO molar fraction in gas phase at reactor input	$y_{A\infty 0}$	0.98 kmol/kmol	[2]
8	Working temperature	T	390 K	[2]
9	Working pressure	p	10^5 Pa	[2]

Carbon monoxide molar fraction ($y_{A\infty}$), total molar flow rate (G_M) and nickel particle radius (R) depending on the distance in the fixed bed (z) for different values of $y_{As}/y_{A\infty}$ (0.05÷0.55) and time (τ=120÷600 s) are given in Figs. 4-6, whereas time variations of mass flow rate of nickel particles (G_{mp}) at the gas exit from the bed for $y_{As}/y_{A\infty}$=0.05÷0.55 are shown in Fig. 7.

Curve 3 in Fig. 4 shows that, as the process is controlled by external diffusion ($y_{As}/y_{A\infty}$=0.05), a stationary state is attained at τ=600 s and CO is almost completely consumed ($y_{A\infty}\approx0$) at a distance in the fixed bed (z) larger than 0.4 m. Curves 3 in Figs. 5 and 6 ($y_{As}/y_{A\infty}$=0.05, τ=600 s) highlight values almost constant for total molar flow rate (G_M) and nickel particle radius (R) at z>0.4 m, suggesting a complete consumption of CO. Moreover, curve 1 in Fig. 7 ($y_{As}/y_{A\infty}$=0.05)

indicates a stationary state at τ=600 s characterized by a constant value of mass flow rate of nickel particles (G_{mp}=0.269 kg/s).

Curve 6 in Fig. 4 indicates that, for an increase in the contribution of surface reaction ($y_{As}/y_{A\infty}$=0.25), the stationary state is attained at τ=600 s and $y_{A\infty}\approx$0 at $z=H$=1 m, whereas curve 2 in Fig. 7 ($y_{As}/y_{A\infty}$=0.25) shows a stationary state at τ=600 s characterized by G_{mp}=0.267 kg/s.

Curves 7, 8 and 9 in Fig. 4, curves 4, 5 and 6 in Figs. 5 and 6 reveal that for $y_{As}/y_{A\infty}$=0.55, the stationary state can not be attained at $\tau\leq$600 s and $z\leq$1 m. Moreover, curve 3 in Fig. 7 ($y_{As}/y_{A\infty}$=0.55) shows that the stationary state can not be attained at $\tau\leq$900 s.

The effect of surface reaction rate constant (k_s) on the space and time variations of CO molar fraction ($y_{A\infty}$) and nickel particle radius (R) is indicated by the curves presented in Figs. 8 and 9, whereas the influence of k_s on the dynamics of mass flow rate of nickel particles (G_{mp}) is revealed by the curves in Fig. 10.

Two values of k_s were used for simulations, *i.e.*: (i) $k_s=3.5\times10^{-1}$ m/s ($D_A/R_0/k_s$=0.05) corresponding to a process controlled by external diffusion; (ii) $k_s=3.5\times10^{-2}$ m/s ($D_A/R_0/k_s$=0.5) highlighting an important role of surface reaction. Curves 1-3 in Figs. 8 and 9 and curve 1 in Fig. 10 ($k_s=3.5\times10^{-1}$ m/s) are similar with curves 1-3 in Figs. 4 and 6 and curve 1 in Fig. 7 ($y_{As}/y_{A\infty}$=0.05) and correspond to external diffusion as rate determining step. On the other hand, curves 4-6 in Fig. 8 and curve 2 in Fig. 10 ($k_s=3.5\times10^{-2}$ m/s) correspond to $y_{As}/y_{A\infty}$=0.35. Curve 2 in Fig. 10 shows that for H=1 m the stationary state can not be attained at $\tau\leq$900 s.

The time required for complete consumption of a Ni particle (τ_c) can de estimated based on Eq. (33), which was obtained by separating the variables in Eq. (23). Effects of $y_{A\infty}$ and y_{As} on τ_c are highlighted by Fig. 11. Depicted data justify the selection of time range in Figs. 4-10.

$$\tau_c = \frac{2\rho_{Ni}R_0^2}{M_{Ni}CD_A \ln\left(\frac{1-\frac{3}{4}y_{As}}{1-\frac{3}{4}y_{A\infty}}\right)} \tag{33}$$

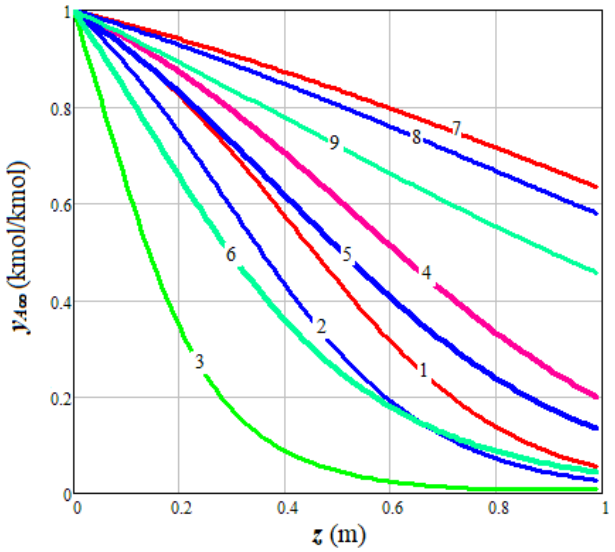

Fig. 4. Space and time variations of carbon monoxide molar fraction:
(1) $y_{As}/y_{A\infty}$=0.05, τ=120 s; (2) $y_{As}/y_{A\infty}$=0.05, τ=300 s; (3) $y_{As}/y_{A\infty}$=0.05, τ=600 s;
(4) $y_{As}/y_{A\infty}$=0.25, τ=120 s; (5) $y_{As}/y_{A\infty}$=0.25, τ=300 s; (6) $y_{As}/y_{A\infty}$=0.25, τ=600 s;
(7) $y_{As}/y_{A\infty}$=0.55, τ=120 s; (8) $y_{As}/y_{A\infty}$=0.55, τ=300 s; (9) $y_{As}/y_{A\infty}$=0.55, τ=600 s.

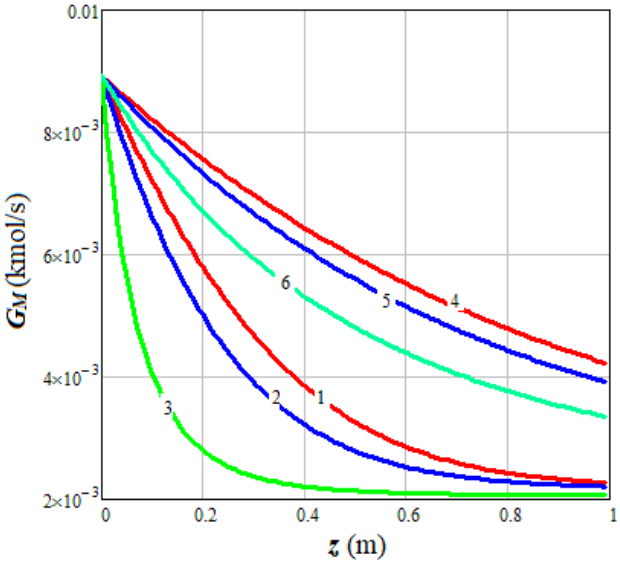

Fig. 5. Space and time variations of total molar flow rate:
(1) $y_{As}/y_{A\infty}$=0.05, τ=120 s; (2) $y_{As}/y_{A\infty}$=0.05, τ=300 s; (3) $y_{As}/y_{A\infty}$=0.05, τ=600 s;
(4) $y_{As}/y_{A\infty}$=0.55, τ=120 s; (5) $y_{As}/y_{A\infty}$=0.55, τ=300 s; (6) $y_{As}/y_{A\infty}$=0.55, τ=600 s.

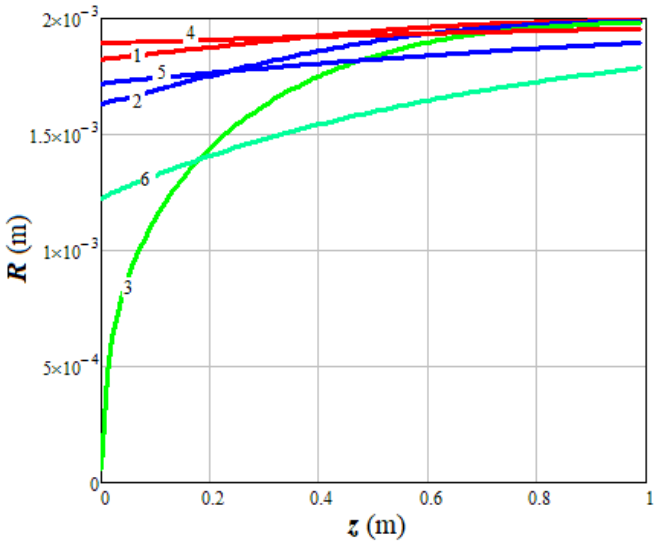

Fig. 6. Space and time variations of nickel particle radius:
(1) $y_{As}/y_{A\infty}$=0.05, τ=120 s; (2) $y_{As}/y_{A\infty}$=0.05, τ=300 s; (3) $y_{As}/y_{A\infty}$=0.05, τ=600 s;
(4) $y_{As}/y_{A\infty}$=0.55, τ=120 s; (5) $y_{As}/y_{A\infty}$=0.55, τ=300 s; (6) $y_{As}/y_{A\infty}$=0.55, τ=600 s.

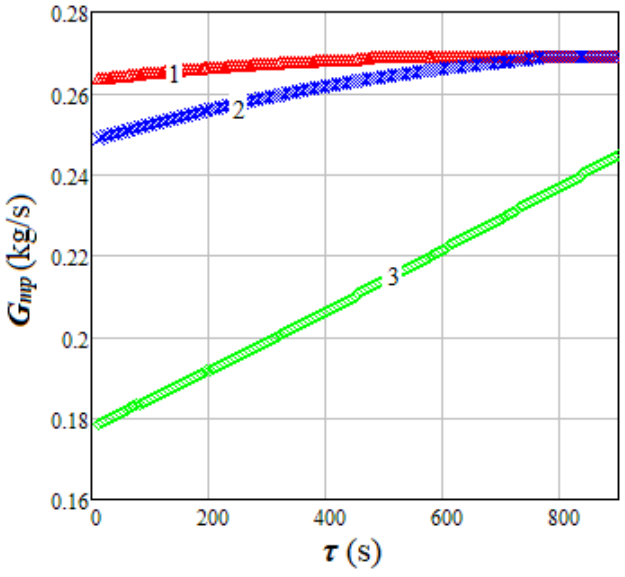

Fig. 7. Time variations of mass flow rate of nickel particles:
(1) $y_{As}/y_{A\infty}$=0.05; (2) $y_{As}/y_{A\infty}$=0.25; (3) $y_{As}/y_{A\infty}$=0.55.

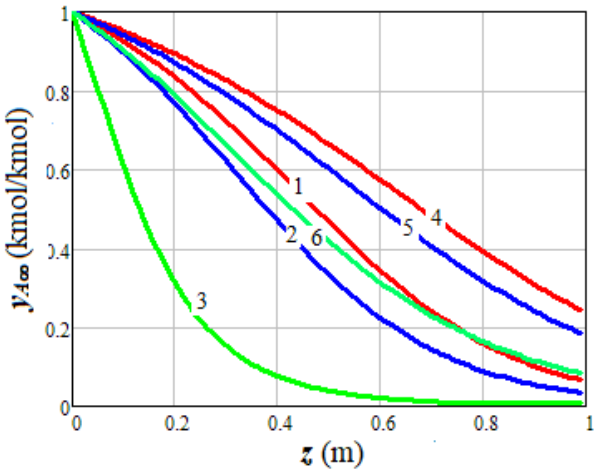

Fig. 8. Effect of surface reaction rate constant on space and time variations of carbon monoxide molar fraction:
(1) k_s=3.5×10^{-1} m/s, τ=120 s; (2) k_s=3.5×10^{-1} m/s, τ=300 s; (3) k_s=3.5×10^{-1} m/s, τ=600 s;
(4) k_s=3.5×10^{-2} m/s, τ=120 s; (5) k_s=3.5×10^{-2} m/s, τ=300 s; (6) k_s=3.5×10^{-2} m/s, τ=600 s.

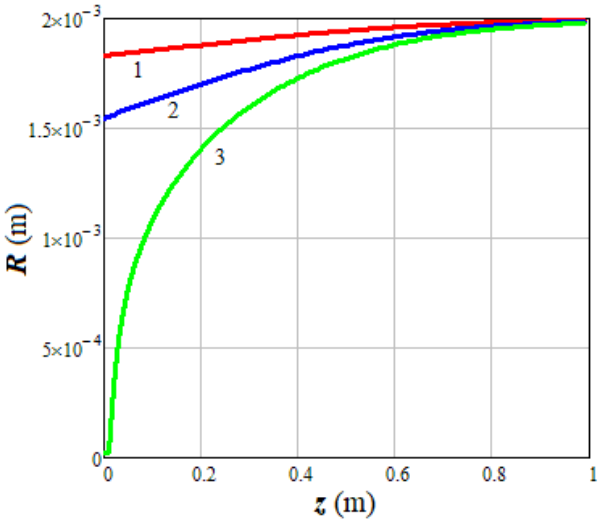

Fig. 9. Effect of surface reaction rate constant on space and time variations of nickel particle radius: (1) k_s=3.5×10^{-1} m/s, τ=120 s; (2) k_s=3.5×10^{-1} m/s, τ=300 s; (3) k_s=3.5×10^{-1} m/s, τ=600 s.

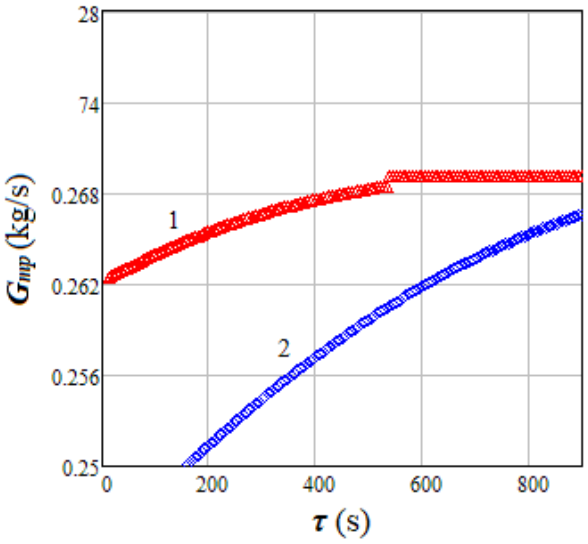

Fig. 10. Effect of surface reaction rate constant on time variations of mass flow rate of nickel particles: (1) k_s=3.5×10^{-1} m/s; (2) k_s=3.5×10^{-2} m/s.

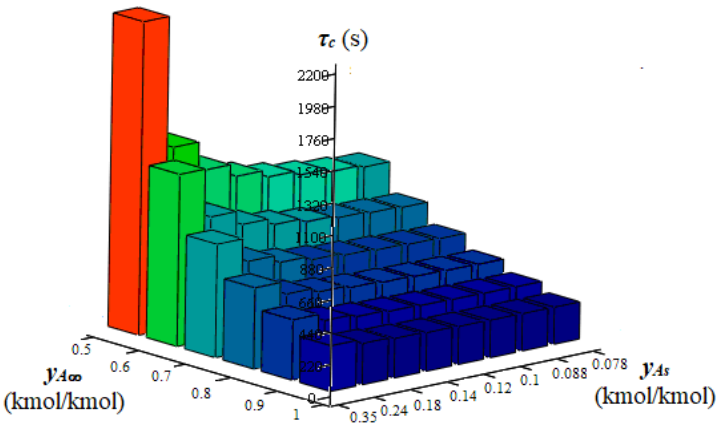

Fig. 11. Effects of $y_{A\infty}$ and y_{As} on the time of complete consumption of a Ni particle (R_0=2×10^{-3} m).

4. Conclusions

A two dimension model has been developed in order to simulate the synthesis of nickel tetracarbonyl ($Ni(CO)_4$) by the reaction between Ni particles and CO in a fixed bed reactor. The model was relied on diffusion with the mobile boundary of CO (A) and $Ni(CO)_4$ (B) coupled with surface reaction. It consisted of partial differential equations expressing the variation over time and along the

fixed bed of process responses in terms of CO molar fraction ($y_{A\infty}$), total molar flow rate (G_M) and Ni particle radius (R). Simulations were conducted based on selected values of relevant parameters of the model, *i.e.*, reactor diameter (D=0.18 m), fixed bed height (H=1 m), initial Ni particle radius (R_0=0.002 m), bed void fraction (ε=0.35 m^3/m^3), CO diffusion coefficient in gas phase ($D_A=3.52\times10^{-5}$ m^2/s), total molar flow rate at reactor input (G_{M0}=0.0089 kmol/s), CO molar fraction in gas phase at reactor input ($y_{A\infty0}$=0.995 kmol/kmol), working temperature (T=390 K) and pressure ($p=10^5$ Pa). Different values for $y_{As}/y_{A\infty}$ (0.05÷0.55) and $D_A/R_0/k_s$ (0.05 and 0.5), where y_{As} is CO molar fraction at particle surface and k_s represents surface reaction rate constant, were used in order to assess the contribution of external diffusion and surface reaction. Aspects related to the time and space variations of process responses were discussed and interpreted.

REFERENCES

[1] Casagrande Jr. O. L., Tomita K., Vollet D. R., On metal carbonyl synthesis and applications, *Polyhedron*, 15, (1996), 4179-4187.

[2] Mond L., Langer C., Quincke F., On nickel tetracarbonyl synthesis, *Journal of the Chemical Society*, 57, (1890), 749-753.

[3] Wender I., Pino P., *Organic Synthesis via Metal Carbonyls*, Vol.1, Interscience Books, New York, 1968.

[4] Bath D.V., *Essential of Coordination Chemistry* (*Selected topics in coordination chemistry-Module 1, Metal Carbonyls*, https://nptel.ac.in/courses/104106064/lectures.pdf), Academic Press, 2015.

[5] Stedman D. H., Hikade D. A., Pearson R. Jr., Yalvac E. D., Nickel carbonyl: Decomposition in air and related kinetic studies, *Science*, 208, no. 4447, (1980), 1029-1031.

[6] Bjorklund B. R., Burwell L. R. Jr., The reaction of nickel tetracarbonyl with γ alumina, *Journal of Colloid and Interface Science*, 70, (1979), 383-391.

[7] Kauffeldt E., Kauffeldt T., Thermodyamic – controlled gas phase for the synthesis of nickel nanoparticles of adjustable size and morphology, *Journal of Nanoparticle Research*, 8, (2006), 477-488.

[8] Hoover B.T., *Process of coating with nickel by the decomposition of nickel carbonyl*, Patent US2881994A, 1959.

[9] Dobre T., Zicman L.R., Pârvulescu O.C., Neacșu E., Ciobanu C., Drăgolici F.N., Species removal from aqueous radioactive waste by deep-bed filtration, Environmental Pollution, 241, (2018), 303-310.

[10] Levenspiel O., *Chemical Reaction Engineering*, Chapter 25, Third Edition, John Wiley, 1999.

[11] Dobre T., Sanchez Marcano J., *Chemical Engineering – Modelling, Simulation and Similitude*, Wiley VCH, 2007.

[12] Ziolkowska I., Ziolkowski D., Modelling of gas interstitial velocity radial distribution over cross-section of a tube packed with granular catalyst bed; Effects of granule shape and of lateral gas mixing, *Chemical Engineering Science*, 62, (2007), 2491-2502.

[13] Chen H. N., Othmer F. D., New generalized equation for gas diffusion coefficient, *Journal of Chemical & Engineering Data*, 7, no. 1, (1962), 37-41.

SELECTIVE TRANSPORT AND REMOVAL OF Cd (II) FROM THE Ni-Cd BATTERIES LEACHING WITH POLYMER INCLUSION MEMBRANES (PIMs)

Larisa MELIȚĂ*

Chemistry and Materials Science Group, Technical University of Civil Engineering Bucharest, 122-124 Lacul Tei Blv, district 2, Bucharest

Abstract

Cadmium is known as an extremely toxic industrial and environmental pollutant and however it is used in different industries and in the fabrication of Ni-Cd batteries. PIMs have been involved as affinity membranes for recovery of cadmium by facilitating transport from the aqueous solutions using selective carriers. In this paper a couple of carrier and plasticizer as tricaprylmethylammonium chloride (Aliquat 336) and 2-nitrophenyl octylether (NPOE) respectively were tested in PIMs with cellulose triacetate (CTA) as base polymer support for selective removal of Cd(II) from the Ni-Cd batteries leaching. In this separation system the effect of carrier and plasticizer content and the transported metal flux (J_i) through membranes were studied. The influence of chloride concentration, in feed and stripping phases, on metal transport and the influence of Cd(II) concentration on the membrane flux has been also investigated. The Cd(II) recovery efficiency obtained in 7 h were 90,6 % and the transport metal flux were about 1.7 $\mu mol \cdot m^{-2} \cdot s^{-1}$. In presence of Ni(II) from the acid leaching Ni-Cd battery the Alliquat 336-based PIMs showed greater selectivity towards Cd(II). After repeated experiments the PIMs have shown a very good stability and a constancy of the transmembrane transport flux. The goal of this study was to propose an alternative solution to remove and recovery of Cd(II) with PIMs from the waste Ni-Cd batteries, which is important not only for the environmental reasons but also for the economic ones.

Key words: Cadmium, Polymer Inclusion Membranes, Aliquat 336, NPOE, Ni-Cd batteries

1. Introduction

Cadmium is known to be an environmental pollutant with toxic effects for humans and living organisms in aquatic ecosystems, causing various diseases. In water systems it enters through the industrial discharges from different industries such as metallurgy, electroplating, pigmenting and from the fabrication of Ni-Cd

* Email address: larisamelita@gmail.com

batteries [1, 2]. Modern risk assessment procedures compare directly the concentrations of harmful substances in water and in the tissues of concern. It is already widely accepted nowadays that sub-lethal concentration pose more serious threats for humans and species, individuals and ecosystems and not necessarily the lethal dosage [3]. In the European Union, any chemical with a wet mass bioconcentration factor $BCF_w > 100$ is considered to be potentially accumulation in consumers and is therefore considered as being deleterious for aquatic biota and food webs [4]. Because of the toxic effects of cadmium, the identification of this heavy metal and then determination of their concentration in different environmental samples is of major importance.

Nickel-cadmium batteries are virtually 100% recyclable once they have been collected. Today, there are 9 major Ni-Cd battery recycling plants located in the United States, Europe and Japan capable of recycling approximately 20,000 mt of industrial and consumer Ni-Cd batteries and their manufacturing scraps. There is more than adequate capacity to recycle all Ni-Cd batteries presently being collected [5].

Through the several technologies that can be used to remove toxic metals from liquid effluents, polymer inclusion membranes (PIMs) have been demonstrated to be useful for the selective extraction and recovery of numerous cations and anions with the advantage that the extraction and back-extraction can be accomplished in a single step. Usually, the PIMs are composed of a base polymer such as poly(vinyl chloride) (PVC) or cellulose triacetate (CTA), a plasticizer or a modifier and an extractant (carrier). The last one is responsible for the binding with the species of interest and transporting it across the PIM, the base polymer supplies the membrane with mechanical strength and the plasticizer supplies elasticity and flexibility. A modifier is occasionally added to the membrane composition to improve the solubility of the extracted species in the membrane liquid phase.

In this paper, a separation system based on PIMs made of CTA as a base polymer and Aliquat 336 (liquid quaternary ammonium salt) as a carrier is proposed for the transport of cadmium, contained in the aqueous samples collected from the acid leaching of the waste Ni-Cd batteries. The transported metal flux through the membranes, the influence of the chloride concentration in feed and striping phases and the Cd(II) concentration in the analyzed samples were investigated, as well as membranes selectivity between Ni and Cd cations. Finally, the proposed separation system has been evaluated by Cd(II) recovery efficiency of aqueous samples derived from a waste Ni-Cd battery.

2. Experimental

Reagents

In all experiments the standard samples of Cd(II) and Ni(II) were prepared by dilution of the stock solutions (1000 $mg \cdot L^{-1}$) of $CdCl_2$, $Cd(NO_3)_2 \cdot 4H_2O$ and $NiCl_2 \cdot 6H_2O$ (Merck and Fluka, Germany) respectively with concentrated HCl (32%) or NaCl (99.5%) (Chimopar, Romania) and deionized water. All used reagents were analytical chemicals grade. The tricaprylmethylamonium chloride (Aliquat 336) carrier, the CTA polymer, the 2-nitrophenyl octyl ether (NPOE) (99%) plasticizer were purchased from Fluka Chemie (Germany) and the chloroform from Chemical Company S.A. (Romania).

The real samples containing Cd and Ni respectively were obtained from the waste Ni-Cd batteries leaching. The powder inside of battery (the inner) was treated with 2M HCl, heated up to complete dissolution and then was filled, until the volume of 200 cm^3, with the same acid. The obtained solution was used as feed phase in the membrane separation cell.

Polymer inclusion membranes (PIMs) preparation

The PIMs preparation were made using a chloroform solution of CTA (250 mg in 25 mL), a NPOE plasticizer (0.3 mL) and different quantities of Aliquat 336 carrier using a technique presented elsewhere [6-8]. The obtained solution was stirred for 30 minutes to homogenize and then was cast into a flat bottom glass Petri dish; this was loosely covered and kept over 24 hours, at room temperature, to allow the evaporation of solvent. The resulted thin film was peeled off the bottom of the Petri dish and placed in the membrane permeation.

Transport experiments through membranes

The transport experiments through PIMs were carried out at 20±0.1 ^0C using a two compartments membrane cell of 200 cm^3 each (V_{cell}) and presented elsewhere [9]. The membrane working area (S_m) was 11.33 cm^2 and placed on the circular window separating the two compartments. The feed and stripping solutions were placed in each compartment of the cell and vigorously agitated by a mechanical stirrer with 800 rpm velocity. The feed phase consisted of a solution with ppm amounts of Cd(II) and Ni(II) respectively in HCl media or NaCl media. The stripping phase consisted of deionized water in all experiments [10]. The concentrations of metal ions in both, feed and stripping, solutions were determined periodically in respective withdrawn samples by atomic absorption spectrometry (ANALYTIK JENA - VARIO AA6 type). An average uncertainty of metal ions determination was in all cases < 1%.

The transported metal flux through the membrane (J, mole/cm^2·sec) was evaluated from the initial slope of the concentration versus time plot. The rate can be calculated by using a linear regression technique:

$$J = (V_{cell} / S_m) \times (dC / dt) \quad (1)$$

where V_{cell} is the volume of the aqueous stripping solution, S_m is the membrane working area, C is the concentration of ion under interest in the stripping solution and t is time.

The *removal efficiency* of the metal was calculated according with relation:

$$E_{Cdtransported}(\%) = \frac{C_{Cd_{stripp_t}}}{C_{Cd\,feed_0}} \times 100 \quad (2)$$

where $C_{Cd\ feed\ o}$ is the initial metal concentration in feed solution and $C_{Cd\ stripp\ t}$ is the metal concentration in stripping solution at time t_i.

3. Results and discussions

Mechanism of Cd transport

The overall transport process is quite similar for all types of carriers. The carrier, Aliquat 336 as quaternary ammonium chloride compound, extract the anionic metal species based on an ion-exchange mechanism. It works on the presence of the extractable anionic chlorocomplexex of cadmium, which are ion paired by the cation of the reagent, dissolved in a suitable solvent [11, 12]. For low concentrations of cadmium the predominant anionic species $CdCl_3^-$ and $CdCl_4^{2-}$ respectively, in chloride solutions, are presented. The reactions between the metal and the carrier ($R_4N^+Cl^-$) suggest the following mechanism of transport:

$$R_4N^+Cl^-_{(m)} + CdCl_3^-{}_{(aq)} \longrightarrow (NR_4)CdCl_{3\,(m)} + Cl^-_{(aq)} \quad (3)$$

$$2R_4N^+Cl^-_{(m)} + CdCl_4^{2-}{}_{(aq)} \longrightarrow (NR_4)_2CdCl_{4\,(m)} + 2Cl^-_{(aq)} \quad (4)$$

where the subscripts *"m"* and *"aq"* indicate the membrane and aqueous phases, respectively.

For obtained PIMs because of their viscosity, higher than that of an organic solvent (chloroform), it is suggested that the $CdCl_3^-$ species are preferentially extracted into the membranes and the diffusion of metallic ions in complex forming ion exchange is known to proceed by the "*relay*" mechanism [13]. Also, because the stripping phase contain water, after the metal transport through membrane, the predominant form of the metal, in that media, is Cd^{2+} and don't allow the reaction with Alliquat 336 carrier.

Carrier and plasticizer composition

The influence of the Aliquat 336 carrier content in the synthetized PIMs on the metal transport was studied. At the beginning, the transfer of 10 mg·L^{-1} of Cd(II) in 2M NaCl through a PIM with CTA and 0.3 mL NPOE in chloroform (without carrier) was tested and no metal was found in the stripping solution. That indicates that the metal transport from feed to stripping solutions by metal diffusion through the membrane does not occur. Subsequent, the transfer of 10 mg·L^{-1} of Cd(II) through the same PIM but with different amounts of Aliquat 336 carrier has been made. Figure 1 shows the variation of Cd transport flux versus Aliquat 336 content in the membranes as a result of the reaction between the metal and carrier. Thus to establish the optimum amount of carrier in membrane, 6 membranes with different contents of carrier: from 0.3 to 4 mg·cm^{-2} approximatively was prepared and the metal flux, *J*, through membranes was calculated with eq. 1.

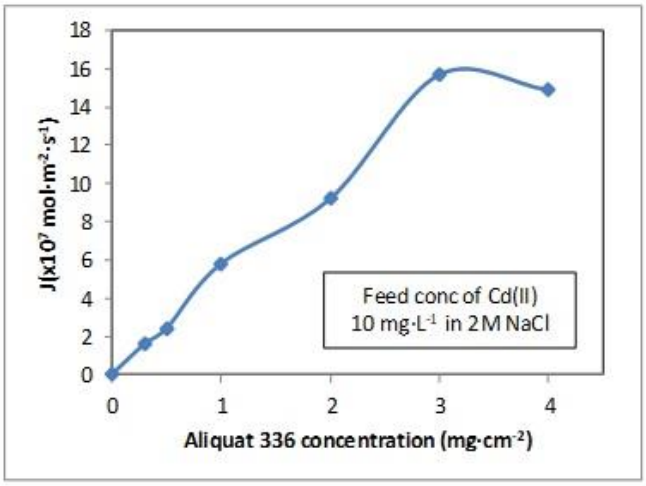

Fig. 1. Variation of Cd transport flux vs. Aliquat 336 carrier content in PIMs

A good separation of Cd(II) at 3.108 mg·cm^{-2} Aliquat 336 in membrane and highest metal flux of 15.8·10^{-7} mol·m^{-2}·s^{-1} were observed. It is interesting to mention that at a low concentration of Aliquat 336 in membrane, such as 0.3 mg·cm^{-2}, a Cd(II) transport flux was observed and could be explained that a small quantity of carrier is enough to create the pathways filled by the organic phase (which contain carrier and plasticizer) that facilitated the interfacial transport of Cd(II) through the ion-exchange mechanism.

The effect of NPOE plasticizer in PIMs is well-known in polymer processing to ensure flexibility and to avoid brittleness and cracking of the membranes. Also, the plasticizer serves as a solvent and constitutes a medium for

the extractant-mobility within the CTA polymer. To verify the effect of plasticizer content from the PIMs to Cd(II) transport through membranes, Figure 2 shows the concentrations profile of cadmium in feed and stripping solutions after 4 hours of separation, determined with FAAS. The initial concentration of Cd(II) in feed solution is 10 mg·L^{-1}. The plasticizer quantity in the membrane composition is 0.3 mL [14] and the quantity of Aliquat 336 is 3.108 mg·cm^{-2}.

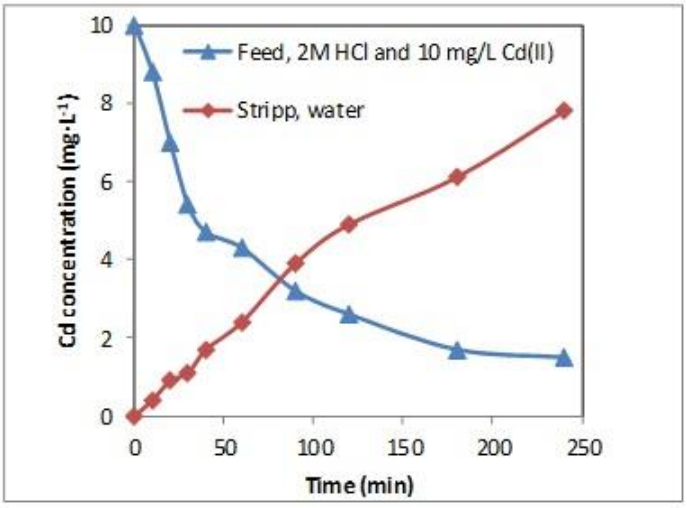

Fig. 2 Effect of NPOE plasticizer content to Cd transport through PIMs

It can be observed that after 10 minutes, the Cd transport through the PIMs was started if NPOE is present in the membrane composition and the value of metal in the stripping solution is 0.389 mg·L^{-1}. In this section the obtained results suggest that the couple of carrier and plasticizer, used in the PIMs synthesis, works well in case of Cd(II) removal from the aqueous solution.

Initial concentration of Cd(II)

The effect of initial Cd(II) concentration from analyzed samples versus separation process was presented, accordingly with the results obtained at FAAS from feed and stripping solutions. At the initial time the Cd(II) concentrations in feed solutions were between 0.02 and 0.5 mM respectively in 2M HCl. It was chosen HCl towards NaCl, even the last one is more used by researchers as chlorine source because of better metal flux through the membranes, but the goal of this paper is to removal/recovery of cadmium from waste Ni-Cd batteries and the leaching contain HCl. Also, from literature the extractant role of carrier Aliqaut 336 is not affected by the concentrated solutions of HCl [15]. In table 1

the influence of feed Cd concentration on the metal flux through membrane, which contains 3.108 mg·cm^{-2} Aliquat 336, is presented.

Table 1

Variation of transported metal flux through a PIM that contain 3.108 mg·cm^{-2} Aliquat 336 carrier with Cd(II) concentration from 2M HCl feed solution

Cd concentration (mM)	J (x10^{-7} mol·m^{-2}·s^{-1})
0.02	4.6
0.05	13.4
0.1	19.9
0.2	49.3
0.3	21.9
0.5	24.1

As it can be seen from the data presented in table 1 the metal flux through the PIM increase if the concentrations of Cd(II) from feed solution are between 0.02 and 0.2 mM respectively. If the concentration of Cd(II) in feed solution increase over 0.2 mM the metal flux decrease. Also, another experiment with a higher concentration of Cd(II) in the feed solution, about 5 mM, during 7 hours, was performed. In all cases, the obtained results by measuring the Cd(II) concentrations in water stripping solutions with FAAS where in the range of 0.0145 and 0.018 mM respectively. These low values could be explained by an interfacial saturation of the metal-carrier complex, thus limiting the metal flux through the membrane. The decrease of Cd transport flux through the PIM can be given by changes to the speciation in the aqueous feed solution and/or to some crystallization process at the interface or inside of membrane, in the pores that are formed at the PIMs synthetization by the CTA polymer chains and where the carrier and plasticizer are found. Not be excluded, at high Cd(II) concentrations, the possibility of microcrystalline species appearance at the membrane-feed solution interface, which can block the free metal-carrier diffusion through the membrane as well as increasing the viscosity of organic liquid phase which is found in the PIMs pores [16]. The obtained results suggest that these PIMs can be used for cadmium recovery from the waste Cd-Ni batteries since the leaching contains small amounts of this metal.

Application of the PIMs to Cd removal from a leaching Ni-Cd battery

After establishing the optimum work conditions for the synthetized PIMs, three experiments were accomplish in order to observe the membranes separation efficiency in case of the Cd and Ni matrices in feed solutions, especially from a waste Ni-Cd battery. The used PIMs contain CTA as base polymer support, Alliquat 336 as carrier 3.108 mg·cm^{-2} and NPOE as plasticizer 0.3 mL. The feed solutions are made up of different ppm quantities of Ni(II) and Cd(II) dissolved in

2M HCl or 2M NaCl and of an acid Ni-Cd lixiviate which is obtained from a Ni-Cd battery. Table 2 shows the obtained results.

Table 2

Cd separation from synthetic and real matrices using PIMs

Feed metal	Feed metal concentration ($mg \cdot L^{-1}$)	Feed solution	Metal flux, J ($x10^{-7}$ $mol \cdot m^{-2} \cdot s^{-1}$)
Cd Ni	1.005 20.07	2M NaCl	2.12 0
Cd Ni	0.978 20.79	2M HCl	1.93 0
Cd Ni	15.87 19.21	Ni-Cd battery lixiviate	17.7 0

It can be observed that in all experiments cadmium was preferentially transported against the Ni(II) even, last one, has a large concentration in both NaCl and HCl media feed solution. After 420 minutes of experimentation a quantitative transport of cadmium to the stripping solution was reached. It is important to mention that in case of a real acidic sample, obtained from a lixiviate of a Ni-Cd battery leaching, where the Cd concentration was 16 times higher, approximatively than of the Cd concentration from the synthetic samples and where the separation conditions were the same, only Cd was transported through the PIMs also. The results could be explained by the competition between extractable anionic chlorocomplexes of Ni(II) and Cd(II) formed with Aliquat 336 carrier and where a weak diffusion of Ni(II) in stripping water phase was observed. So, in the presence of other metal ions the Aliquat 336-based PIM showed greater selectivity towards Cd(II) compared to NI(II) [17].

To evaluate the Cd removal efficiency in a separation process with synthetized PIMs used in a chlorine media, the same with a lixiviate media from a Ni-Cd battery leaching, another experiment with a matrix that contain 10 $mg \cdot L^{-1}$ of Cd(II) in 2M HCl as feed solution was performed. After measuring the Cd quantities from the feed solution and from the stripping phase that contain water, the Cd removal efficiency was calculated (eq. 2) and analyzed. The results are presented in Figure 3. After 240 minutes of experimentation the Cd removal efficiency was 86.5% and after 420 minutes of experimentation the Cd removal efficiency was 90.6%.

Requirements for fast and selective transport as well as good membrane stability a careful choice of carrier/plasticizer combination were necessary. Studies from this paper have revealed that the transport of Cd(II) through PIMs is still often carrier-metal complex diffusion-controlled and the proposed membrane system is a promising separation technique to consider when dealing with different Cd-polluted environmental samples and with aqueous Cd samples originating from the waste Ni-Cd batteries.

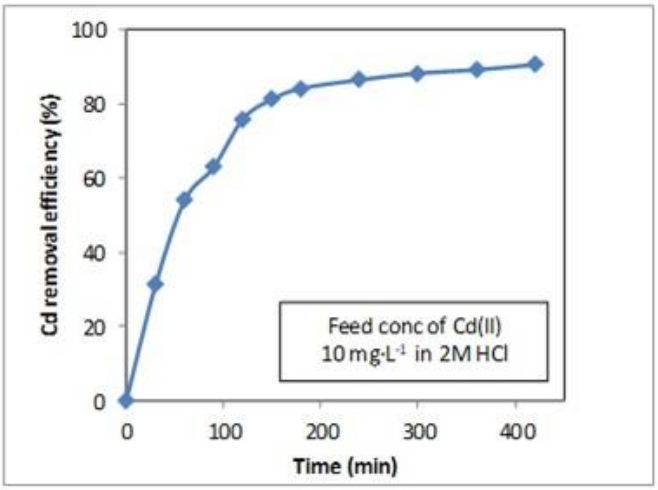

Fig. 3 Variation on time of Cd removal efficiency with PIMs

4. Conclusions

This study demonstrated that:

- The polymeric inclusion membranes (PIMs) obtained with CTA as base polymer support, with Aliquat 336 as carrier and with NPOE as plasticizer can be used for Cd(II) removal from the chloride aqueous solutions to a water-stripping phase. The analyzed samples are made from synthetic matrices, with different concentrations of Cd(II) (0.02 - 0.5 mM) and from a real sample obtained from a Ni-Cd battery leaching which contain 15.87 $mg \cdot L^{-1}$ Cd(II) and 19.21 $mg \cdot L^{-1}$ Ni(II) respectively.
- The optimum concentration of Aliquat 336 carrier in the synthetized membranes was 3.108 $mg \cdot cm^{-2}$. The quantity of plasticizer NPOE was 0.3 mL in 5 mL of $CHCl_3$, to ensure better results in terms of metal transport through the membranes. Cd(II) was carried by PIMs, from feed solution containing 2M HCl or 2M NaCl respectively to stripping solution which contain water.
- The metal quantities from feed and stripping solutions were determined by flame atomic absorption spectrometry (FAAS). It was observed that good results at low concentration of Cd(II) 0.2 mM in feed solution were obtained, where the highest metal flux, *J*, was of 4.93·μmol·m^{-2}·s^{-1} and where the complex $(NR_4)CdCl_{3\ (m)}$ or $(NR_4)CdCl_{4\ (m)}$ between cadmium and Aliquat 336 allowed Cd(II) carrying in good conditions from the feed to stripping solutions.
- The membrane system selectivity towards Cd has been demonstrated in case of the real sample, obtained from a lixiviate of a Ni-Cd battery leaching

which contain a matrix of Ni(II) and Cd(II) in 2M HCl and where the cadmium flux, *J*, through membrane was $1.7 \cdot \mu mol \cdot m^{-2} \cdot s^{-1}$.

- For a matrix which contains 10 $mg \cdot L^{-1}$ of Cd in 2M HCl feed solution, after 7 hours of treatment with PIMs, the Cd(II) recovery efficiency was 90.6%.
- Thus, in this paper the proposed PIMs system with Aliquat 336 as carrier and NPOE as plasticizer offers a simple and efficient procedure for removal/recovery of Cd(II) from samples of contaminant effluents and from the Ni-Cd batteries leaching, which represent a significant wastes for environment.

REFERENCES

[1] Vernet J.P., *Heavy Metalsin the Environment,* Elsevier, Amsterdam, 1991.
[2] Bertin G., Averbeck D., Cadmium: cellular effects, modification of biomolecules, modulation of DNA repar and genotoxic consequences (a review), *Biochemie*, 88, (2006), 1549-1559.
[3] Geyer H.J., Rimkus G.G., Scheunert I., Kaune A., et al. *Bioaccumulation and Occurrence of Endocrine-Disrupting Chemicals (EDCs), Persistent Organic Pollutants (POPs) and Other Organisms Including Humans, The Handbook of Environmental Chemistry*, Springer-Verlag, Berlin/Heildelberg, 2000.
[4] Jitar O., Teodosiu C., Oros A., Plavan G., Nicoara M., Bioaccumulation of heavy metals in marine organisms from the Romanian sector of the Black Sea, *New Biotechnology*, 32(3), (2015), 369-378.
[5] www.cadmium.org/collection-and-recycling-of-nickelcadmium-nicd-batteries
[6] Sugiura M., Coupled-ion transport through a solvent polymeric membrane, *Journal of Colloid Interface Science*, 81, (1980), 385-389.
[7] Sugiura M., Transport of lanthanide ions through cellulose triacetate membranes containing hinokitol and flavonol as carriers, *Separation Science Technology,* 25, 1189-1199, 1990.
[8] Sugiura M., Kikkawa S., Urita S., Carrier mediated transport of rare earth ions through cellulose triacetate membranes, *Journal of Membrane Science,* 42(1-2), (1989), 47-55.
[9] Melita L., Popescu M., Removal of Cr (VI) from industrial water effluents and surface waters using activated composite membranes, *Journal of Membrane Science,* 312, (2008), 157-162.
[10] Fontas C., Pont N., Hidalgo M., Salvado V., Separation and preconcentration of Cd (II) from chloride solutions using supported liquid membranes systems, *Desalination*, 200, (2006), 114-116.
[11] He D., Liu X., Ma M., Transfer of Cd (II) chlorine species by tri-n-octylamine-secondary octyl alcohol-kerosene multimembrane hybrid system, *Sovent Extraction and Ion Exchange*, 22(3), (2004), 491-510.
[12] Fu F., Wang Q., Removal of heavy metal ions from wastewaters: A review, *Journal of Environmental Management,* 92, (2011), 407-4018.
[13] Wang L., Paimin R., Cattrall R.W., Shen W., Kolev S.D., The extraction of cadmium (II) and cooper (II) from hydrochloric acid solutions using an Aliquat 336/PCV membrane, *Journal of Membrane Science*, 176(1), (2000), 105-111.
[14] Kebiche-Senhadji O., Mansouri L., Tingry S., Seta P., Benamor M., Facilitated Cd (II) transport across CTA polymer inclusion membrane using anion (Aliquat 336) and cation (D2EHPA) metal carriers, *Journal of Membrane Science,* 310, (2008), 438-445.

[15] He D., Ma M., Zhao Z., Transport of cadmium ions through a liquid membrane containing amine extractants as carriers, *Journal of Membrane Science,* 169(1), (2000), 53-59.
[16] Nghiem L.D., Mornane P. et al, Extraction and transport of metal ions and ionic organic compounds using polymer inclusion membrane (PIMs), *Journal of Membrane Science*, 281(1-2), (2008),7-41.
[17] Ines M., Almeida G.S., Cattrall R.W, Kolev S.D., Recent trends in extraction and transport of metal ions using polymer inclusion membranes (PIMs), *Journal of Membrane Science*, 415-416, (2012), 9-23.

THE INFLUENCE OF HYDROCARBON CHAIN LENGTH ON THE SURFACE PROPERTIES OF GLUCONOLACTONE-BASED SURFACTANTS

Irina Elena CHICAN, Dana VĂRĂȘTEANU[1], Sanda Maria DONCEA, Raluca SOMOGHI, Ana-Maria GĂLAN

National Institute for Research and Development in Chemistry and Petrochemistry- ICECHIM Bucharest, 202 Splaiul Independentei, 060021, Bucharest, Romania

Abstract

In this paper we present the synthesis of bolaform gluconolactone-based surfactants with C_8 and C_{12} hydrocarbon chains, in mild reaction conditions and the influence of hydrocarbon chain length on the surface properties of synthesized surfactants. The structural characterization of 1,12-digluconamidododecane and 1,8-digluconamidooctane was made by Fourier transform infrared spectroscopy. The visualization of aggregates was performed by optic microscopy in the case of 1,12-digluconamidododecane and transmission electron microscopy for 1,8-digluconamidooctane. It was found that 1,12-digluconamidododecane undergoes a crystallization process, hexagonal crystals being visualized by optic microscopy. We note the vesicular aggregates formed in the 1,8 - digluconamidooctane solution with dimensions between 200-300 nm, visualized by transmission electron microscopy. The surface activity of surfactants was evaluated with a KSV Sigma 700 automated tensiometer, using DuNouy Ring technique. 1,12-digluconamidododecane solutions present a moderate efficiency in reducing the surface tension of water, while 1,8-digluconamidooctane is more efficient in reducing the surface tension of water at low concentrations.

Key words: Surfactants, carbohydrates, surface properties, self-assembly

1. Introduction

The class of carbohydrate-based surfactants had been developed by major manufacturers of active substances and detergents after the increase of legislative restrictions on environmental protection. Carbohydrates, as natural raw materials, derived from renewable vegetal resources are used in fabrication of alkyl polyglycosides, sorbitan fatty acid esters, sucrose fatty acid esters, ethoxylated

[1] Corresponding author; Email address: dvarasteanu @icechim-rezultate.ro

sorbitane fatty acid esters and sucrose fatty acid esters. [1, 2, 3]. Carbohydrates are nontoxic substances to human health and benign to the environment, and as a consequence so are carbohydrate-based surfactants. Moreover, carbohydrates allow numerous structural variations because of their molecular diversity, which allow designing surfactants with desired performance properties. The most representative products in the class of carbohydrate-based surfactants are alkyl polyglycosides. The increasing market demand for alkyl polyglycosides is driven by their excellent cleaning properties, high biodegradability, high tolerance to salts and other such electrolytes. Major applications for alkyl polyglycosides include household detergents, industrial cleaners, personal care and agricultural chemicals. Household detergents dominate the global demand for alkyl polyglycosides. Carbohydrate-based surfactants containing the amide group, such as N-alkanoyl-N-methylglucamine are used in detergent industry in combination with alkyl sulphates or alkyl ether sulphates [4]. In addition to carbohydrate-based surfactants with one hydrophilic group, studies have been made on bolaform surfactants, bearing two hydrophilic groups attached to a hydrocarbon chain. In many cases the second polar group induces higher solubility compared with that of surfactants containing only one polar group. In this paper we present the synthesis of bolaform gluconolactone-based surfactants with C_8 and C_{12} hydrocarbon chains, in mild reaction conditions and the influence of hydrocarbon chain length on the surface properties of synthesized surfactants.

2. Experimental

Materials and methods

The carbohydrate-based surfactants used in this study were synthesized from 1,12-diaminododecane or 1,8 diaminooctane (Sigma-Aldrich) and D-(+)-glucono-δ-lactone (Sigma-Aldrich). In a reaction vessel of 250 mL capacity, equipped with thermometer and electric stirrer 0.01 mole D-(+)-glucono δ-lactone was introduced in 100 mL methanol and allowed to dissolve. Diaminoalkane is gradually added at a molar ratio diaminoalkane : gluconolactone of 1:2. After the diaminoalkane addition the reaction mass is kept under stirring for 24 hours. The resulting precipitate is filtered off and washed with methanol and then dried.
In Figure 1 the structures of synthesized surfactants are presented.

The structure of the synthesized surfactants was analysed by Fourier transform infrared spectroscopy (FTIR), KBr pellet procedure. FTIR spectra of 1, 12-digluconamidododecane and 1,8-diglucoamidooctane were recorded on a Perkin Elmer GX spectrophotometer, with a resolution of 4 cm^{-1}, from 4000 cm^{-1} to 400 cm^{-1}. Pellets were prepared by pressing a mixture of about 1 mg, from each type of sample, and of about 200 mg of KBr (spectroscopy grade, Sigma-Aldrich).

The surface tension was measured with a KSV Sigma 700 automated tensiometer, using the DuNouy Ring technique.

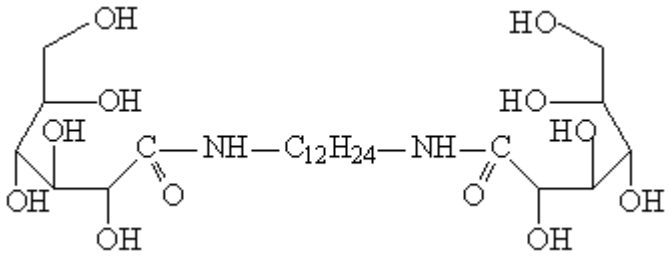

(I)

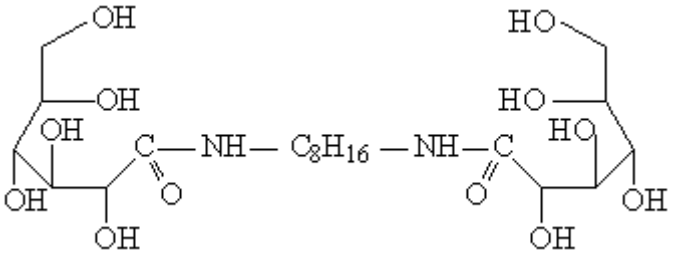

(II)

Fig. 1. Structures of carbohydrate-based surfactants
(I) 1,12-digluconamidododecane; (II) 1,12-digluconamidooctane

The crystalline phase of 1,12-digluconamidododecane was examined on the Carl Zeiss Axiovert 40 CFL Inverted Microscope. Aqueous solution of 1,8-digluconamidooctane were examined using a Tecnai ™ G2 F20 TWIN Cryo-TEM 2015 - FEI Company ™ electronic microscope at cryogenic temperature (<-190 ° C) after immersing the Quantifoil grids with liquid ethane samples for better structural observation; this method minimizes or avoids totally degradation of aggregates at room temperature. Apart from this, vitreous ice is transparent to the electron beam. For improving the cryogenic performances, the microscope is equipped with a copper cryo-shield cooled down by liquid nitrogen.

3. Results and discussions

The bolaform carbohydrate-based surfactants (I) and (II) were synthesized directly by condensation between gluconolactone, the cyclic ester of D-gluconic acid, produced on the industrial scale by enzymatic oxidation of glucose, and fatty diamines with eight or twelve carbon atoms. Besides the advantage to obtain the surfactants in one step synthesis, temperatures above room temperature are not necessary for the reaction to take place. In these conditions yields of 95% were obtained for both products.

The structures of 1,12-digluconamidododecane and 1,8-digluconamidooctane were characterized by FTIR spectroscopy, as presented in Figure 2.

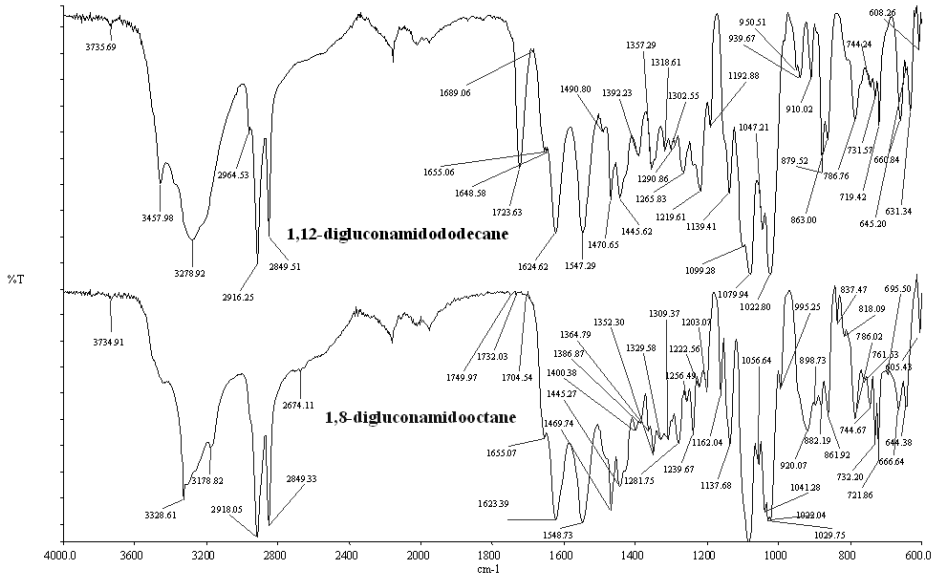

Fig. 2. FTIR spectra of 1,12-digluconamidododecane and 1,8-digluconamidooctane

Specific absorption bands for amide group, -CONR, from 1,12-digluconamidododecane are found at 1658 cm^{-1} and 1625 cm^{-1} (Amide I), 1547 cm^{-1} (Amide II) and 1266 cm^{-1} (Amide III). This fact confirms that amidation has occurred.

FTIR spectra of 1,12-digluconamidooctane confirmed that amidation took place by the appearance of specific absorption bands for amide group –CONR: Amide I bands at 1655 cm^{-1} and at 1623 cm^{-1} characteristic for C = O bond, Amide II band at 1549 cm^{-1} characteristic for NH bond and Amide III band at 1240 cm^{-1} characteristic also for NH bond.

Upon solubilisation, the synthesized surfactants behave differently. 1,12-digluconamidododecane is slightly soluble in water. By heating a 0.2% suspension in water: ethanol 1: 1 to 70 ° C, followed by cooling, it was found that 1,12-digluconamidododecane undergoes a crystallization process, hexagonal crystals with dimensions between 50-200 μm being visualized by optic microscopy (Fig. 3a). In order to establish the type of aggregates formed by 1,8 - digluconamidooctane in 0.5% aqueous solution cryo-TEM technique was applied. We note the vesicular aggregates of 1,8 - digluconamidooctane with dimensions between 200-300 nm (Fig. 3b).

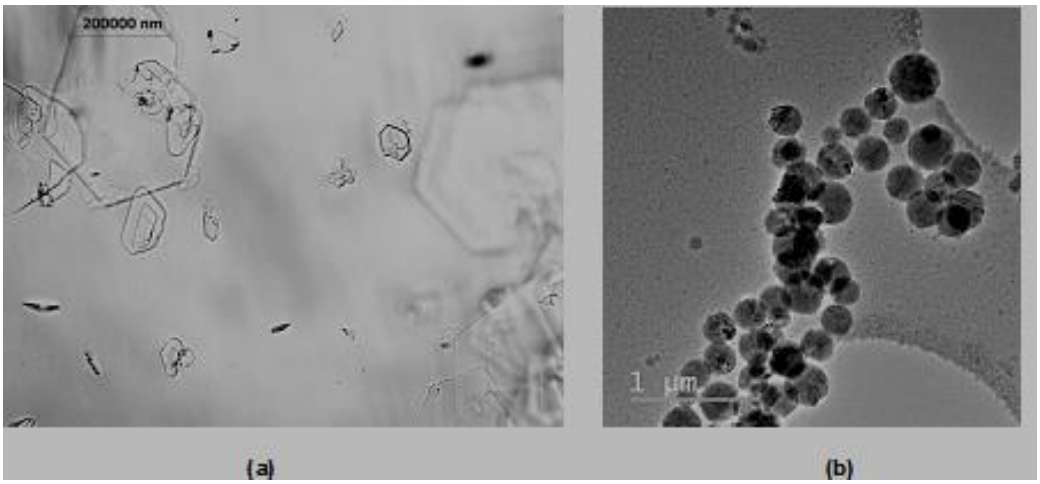

Fig. 3. Microscopy images of 1,12-digluconamidododecane crystals (a) and 1,8-digluconamidooctane vesicles (b)

Surfactants have assembling capacity at the water / air or water / solvent interface, reducing surface or interfacial tension of the medium in which it dissolve. These molecules are able to organize in micelles or can form more or less complex supramolecular aggregates. The amphiphilic substances having a hydrophobic and hydrophilic chain (classical surfactants), but also amphiphilic substances consisting of a hydrophobic chain in the central part of the molecule and two hydrophilic groups at the two ends are assembled into a variety of structures depending on the temperature, nature and composition of the solvent, the critical packing parameter, i.e. the relative size of the hydrophilic portions relative to the hydrophobic portions, thereby obtaining aggregates with specific properties and structures.

Surfactants with one carbohydrate head group were obtained through the aminolysis of D-(+)-glucono δ-lactone with n-octylamine ($CH_3(CH_2)_7$-NH-CO-Gal). Compared to the product synthesized in the present study, 1,8-digluconamidooctane, which contains two carbohydrate head groups and aggregates into vesicles, spontaneous aggregation of octyl- D- and L-gluconamide in water resulted in the formation of double-helical fibres with several micrometers in length. The width of the crossing points was equivalent to the lengths of four molecules of amphiphiles, arranged tail-to-tail. The octyl-D-gluconamide forms right-handed double helices while the L-enantiomer forms left handed double helices [5, 6].

Crystal structures were observed in unsymmetrical bolaform amphiphiles (Gal-NH-CO-$(CH_2)_{12}$-COOH) with 1-galactosamide group as large head group and smaller carboxyl group at the other end. They self-assembled in water to form nanotubes and microtubes simultaneously, depending on the polymorphism of the monolayer lipid membranes. The nanotubes transformed into single crystals by

acidification. The carboxyl groups bind to the primary OH group of galactose, which is fixated by bifurcated hydrogen bonds, as well as to the oxygen in the pyranose ring, thus producing a hydrogen-bond chain. The galactose and carboxyl planes are almost parallel when viewed along the *a*-axis. The structure is stabilized without the need of water molecules [7].

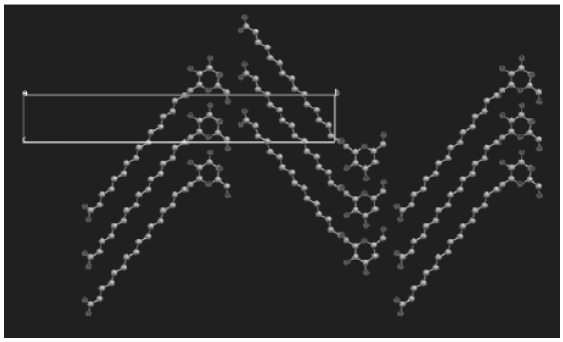

Fig. 4. α,*ω*-Crystal packing of an α -carboxy-*ω* -glucosamide bola [7]

A different situation is observed in symmetrical α, *ω* -bis-galactosamides, where a water molecule binds to the axial hydroxyl group and connects it to neighbors. The number of methylene groups in the connecting chains influences the crystal packing drastically. Even-numbered 1-glucosamide bolas could not be crystallized. Only the axial OH group of the C-12 galactonamide bola (Gal-NH-CO-$(CH_2)_{12}$CO-NH-Gal) allowed a close contact of the CH_2OH-6 groups in hydrogen bonds, allowing for construction of a macrocycle made of two pyranose units, and it produced crystals. Short alkyl chains (≤ (CH_2)10) have the tendency to coil up at room temperature [8].

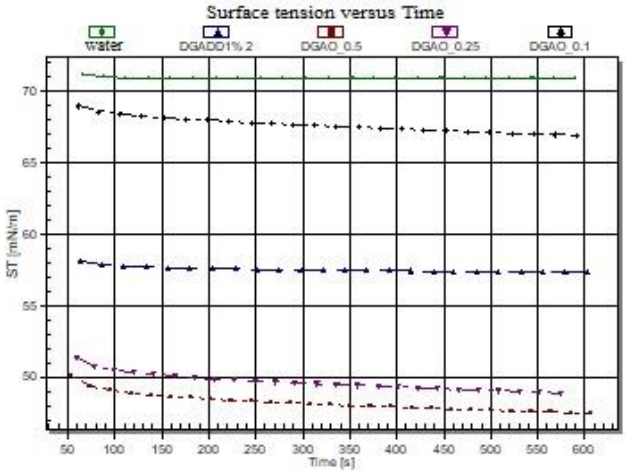

Fig. 5. Surface tension of 1,8-digluconamidooctane (DGAO) and 1,12-digluconamidododecane (DGAD) solutions, compared to surface tension of distilled water

Surface tensions at different concentrations for synthesized surfactants were done, the results being shown in Fig. 5.

1,12-digluconamidododecane (1% solution in distilled water) has an efficiency to reduce the surface tension of distilled water from 71 mN /m to 57 mN/m. The reduction of alkyl chain to eight carbon atoms as in 1,8-digluconamidooctane leads to higher superficial activity for 0.5% and 0.25% solutions in distilled water.

6. Conclusions

Bolaform surfactants are versatile substances with a major contribution to supramolecular chemistry. The chain length influences the rigidity of the molecular assemblies. An appropriate length of the hydrocarbon chain is necessary for bolaform surfactants to self-organize into supramolecular structures. The headgroups affects interactions with solvents. The hydrocarbon chain length of the synthesized bolaform surfactants with sugar head groups affects the behaviour of surfactants in terms of solubility, surface properties and the self-assembling properties. The chain with eight carbon atoms is optimum to form vesicles in water. The introduction of a C12 chain confers to the bolaform surfactant a lipophilic character, with the formation of hexagonal crystals. The efficiency of reducing surface tension of distilled water was in direct relationship with alkyl chain length. The ability of 1,12-digluconamidooctane to self-assemble into the vesicles makes it possible to use it as encapsulating agent.

Acknowledgements

This work was financially supported by the Romanian National Authority for Scientific Research and Innovation –*UEFISCDI*, Contract No. 70PCCDI/2018.

REFERENCES

[1] von Rybinski W., Hill K., Alkyl polyglycosides. In *Novel surfactants: preparation, Applications and Biodegradability: Second Edition, Revised and Expanded,* CRC Press 2003.

[2] Hill K., Rhode O., Sugar-based surfactants for consumer products and technical applications, *Lipid/Fett*, 101(1), (1999), 25-33.

[3] Plat T., & Linhardt R. J., Syntheses and applications of sucrose-based esters, *Journal of Surfactants and Detergents*, 4(4), (2001), 415-421.

[4] Burczyk B., Novel saccharide-based surfactants. In *Novel surfactants: preparation, Applications and Biodegradability: Second Edition, Revised and Expanded*, CRC Press, 2003.

[5] Fuhrhop J. H., Schnieder P., Rosenberg J., Boekema E., The chiral bilayer effect stabilizes micellar fibers, *Journal of the American Chemical Society*, 109(11), (1987), 3387-3390.
[6] Amabilino D. B., Stoddart J. F., Interlocked and intertwined structures and superstructures, *Chemical reviews*, 95(8), (1995), 2725-2828.
[7] Masuda M., Yoza K., Shimizu T., Polymorphism of monolayer lipid membrane structures made from unsymmetrical bolaamphiphiles, *Carbohydrate research*, 340(16), (2005), 2502-2509.
[8] Fuhrhop J. H., Wang T., Bolaamphiphiles, *Chemical Reviews*, 104(6), (2004), 2901-2938.

THE EFFECT OF OXIDATIVE PROCESSES ON THE MIGRATION OF ELEMENTS IN HISTORICAL TAILINGS

Marius ZLAGNEAN, Antoneta FILCENCO-OLTEANU•, Eugenia PANTURU, Aura Daniela RADU, Nicolae TOMUS

Research and Development National Institute for Metals and Radioactive Resource, 70, Carol I, Bvd, Bucharest, Romania,

Abstract

The problem of sulphide oxidation and the associated generation of acid rock drainage (ARD), as well as the dissolution and precipitation processes of metals and minerals, are the most important environmental concern in mining today. The objective of the present study was to characterize and evaluate the Romanian historical tailing of Sasar-Red Valley, near Baia Mare. Tailings samples collected from different depths were characterized in term of mineralogical and chemical composition of the materials, weathering profile characteristics, its acid generating potential (ARD) and elements distribution in depth. Acid base accounting (ABA) tests in conjunction with net acid generation (NAG) tests classified the samples into the category of 'potentially acid generating'. The chemical and mineralogical analyses reveal the presence of a strong oxidation process at the tailings pond surface due to the weathering of sulphide minerals, in particular pyrite which is responsible for production of acidic water. Three zones were identified on the tailing surface: an upper oxidation zone (reddish-brown-yellow coloured, acid generation and metal release), a hardpan layer (acid neutralization and metal accumulation) and a reduction zone (grey coloured, limited water movement, low oxygen diffusivity). As a result of acid generation process the pH of the water decreases once sulphide oxidation starts. Under low pH conditions, ferric sulphate may be oxidized to ferric iron, which is capable of oxidizing other minerals such as copper, zinc or cadmium sulphides. With gradual increasing of the pH level, the dissolved metal load generally decreasing. This paper presents a synthesis of works performed in the Improve Resource Efficiency and Minimize Environmental Footprint (REMinE) project.

Key words: tailing, acid rock drainage, oxidative process

• Corresponding author: Email address antonetafilcenco@yahoo.ro

1. Introduction

The modern mining industry is of considerable importance to the world economy and the consequence of the large size of mining and mineral processing industry is not only the large volume of materials processed but also the large volume of wastes produced.

High content of metals and minerals in historical tailings and waste rock dumps, due to the earlier lack of efficient methods for extraction or low economical profitable at that time, could in many cases be a potential risk for environmental impact. Major and minor environmental concerns with tailings dam are: a) the visual impact; b) the structural stability of the dam and the potential release of tailings into the environment [1]; c) closure and associated capping and vegetation of the tailings dam [2, 3]; d) air and soil pollution through dust generation [4-6]; e) seepage from tailings through the embarkment and base into ground and surface waters. [7,8]

In terms of water contamination, acid rock drainage (ARD) represents the key impact in areas exhibiting sulphide-bearing tailings in the form of rejected pyrite and other sulphide minerals. If sulfidic tailings are exposed to atmospheric oxygen or to dissolved oxygen in the vadose zone of tailings, the oxygen infiltrating in the waste may cause sulphide oxidation and trigger ARD. Acid producing, acid buffering reactions and secondary mineral formation will occur, and low pH pore water with high concentration of dissolved constituents will be generated. [9-11] Indicator for sulphide oxidation – such as abundant oxyhydroxide and hydroxide precipitates or acid, sulphate and metal-rich tailing liquids – are generally observed in the upper part and vadose zone of tailing impoundments. [12,13] As a consequence, ARD is associated with the release of sulphate, heavy metals (Fe, Cu, Pb, Zn, Cd, Co, Cr, Ni, Hg), metalloids (As, Sb) and other elements (Al, Mn, Si, Ca, Na, Mg, Ba, F). [14]

The activities of extraction, processing and preparation of complex ore from the mining basin Baia Mare left behind tens of dumps and mine tailings ponds, located mainly in the river valleys from this area. According to the standard international practice, waste waters and materials resulted from the extraction and processing of ore are stored in different types of tailings management facilities (TMFs). There are also approximately seventeen TMFs (tailing ponds) and eight gold concentrate and pyrite gold deposits, identified by the local Environmental Protection Agency (EPA) in Maramures Country. [15]

The present study will mainly focus on Sasar TMF. Tailings samples collected from different depths were characterized in term of mineralogical and chemical composition of the materials, weathering profile characteristics, elements distribution in depth and its acid generating potential (ARD).

2 Experimental

2.1 Study area

The Maramures Country, situated at northern border of Romania with Ukraine, encloses the old "lands" of Maramures-Chioarul, Lapus and Baia Mare Basin.

Baia Mare Basin is a contact basin that interposes between the Somesana Plain and the Carpathian Mountains as a lower morphological unit, from the surrounding areas, presenting a waved surface, characterized by a convergent system of valleys and interfluves. It was formed due to the tertiary tectonic movement that took to the fragmentation and sinking of the crystalline in the North-Western part of Transylvania, as well as due to the volcanic chain of the Gutin-Oaş Mountains [16].

The area belongs to the undifferentiated Quaternary characterized by deluvial deposits, andesitic blocks and alluvial deposits. Under the action of the external agents the andesites were altered and eroded and formed alluvial and deluvial deposits that make the transition from the deposits of Sasar River upper terrace. The sedimentary in Baia-Mare Basin is represented by grey-purple marls, clays marls and sands with sandstone horizons. [17]

The Sasar (Red Valley) tailing pond (presented in Fig. 1), located in the west part of Baia Mare, secured the storage of flotation tailings from the Processing Plant which was closed in 1982. It contains around 8.5 million m^3 of fine grained waste ores embodying the acidic water producing mineral pyrite.

.

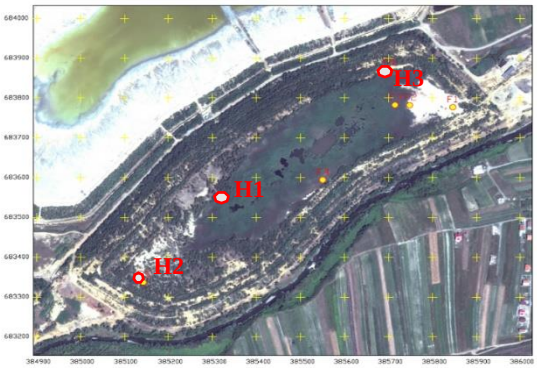

Fig. 1. The Sasar tailing impoundment and sampling points

From mineralogical point of view, the tailings disposed in the Sasar tailing pond contain silicates (from the amphiboles and pyroxenes), sulphide minerals (pyrite, FeS_2, chalcopyrite, $CuFeS_2$, arsenopyrite, FeAsS, pyrrhotite, $Fe_{(1-x)}S$, marcasite, FeS_2, jamesonite, $Pb_4FeSb_6S_{14}$, galena, PbS, sphalerite, ZnS) etc., other metallic minerals like oxides, hydroxides, as hematite, Fe_2O_3, specularite, rarely ilvaite, $CaFe_{22}+Fe_3+[OOH\ Si_2O_7]$, oxi-hydroxi - iron sulphides (HOF), mineral

associations (muscovite), clay minerals, carbonates and some secondary minerals (goethite, α-FeO(OH), hematite Fe_2O_3). [18]

2.2 Sampling

Tailings samples were collected from six depth intervals: 0-1m, 1-2 m, 2-3m, 3-4m, 4-5m and 5-6m, using a soil auger. Drill samples were preserved in polyethylene bags, transported and processed separately. Prior to analysis, the samples collected were split with a riffle splitter, and half of each sample was kept for potential future analysis.

2.3 Experimental methodology

The determination of total element contents was performed using digestion followed by ICP AES (inductively coupled plasma atomic emission spectroscopy) analysis using a Perkin Elmer Optima 3100 RL spectrometer. Additionally, a routine mineral characterization was carried out by optical microscopy using a Carl Zeiss Axio Imager A1m.

The soil moisture content was determined by drying 10g soil sub-samples at 105ºC for 24h.

Static geochemical tests provide the basis for understanding potential reactivity and therefore ARD potential of a sample. The static geochemical tests were performed on pulverized samples (<75μm) collected in drill 2 from 1 m, 3 m and 6 m depth. The purpose of acid-base account (ABA) test is to increase the dissolution of samples which contain not only carbonated compounds but also mineral groups as silicates, and feldspars with concentrated acid solutions. The ABA involves static laboratory procedures that evaluate the balance between acid producing components (oxidation of sulphide minerals such as pyrite) and the acid consuming components (dissolution of alkaline carbonates, displacement of exchangeable bases, and weathering of silicates) of the tailing sample. The acid consuming capacity of the sample, usually termed the neutralization potential (NP) and the acid producing potential, (AP) are expressed in kg $CaCO_3$/ tonne of tailing, and the difference between the two values is termed the net neutralization potential (NetNP) (Equation 1). [19]

$$\boldsymbol{NetNP}\left(\frac{\boldsymbol{kgCaCO_3}}{\boldsymbol{t}}\right) = \boldsymbol{NP} - \boldsymbol{AP} \quad (1)$$

For the purpose of calculating the acid potential (AP), it is generally assumed that 4 moles of H^+ are formed per mole of pyrite oxidized. This in common usage of the factor 31.25 to convert percent contained sulphur to kg $CaCO_3$ equivalent per tonne material (Equation 2). [20,21]

$$\boldsymbol{AP}\left(\frac{\boldsymbol{kgCaCO_3}}{\boldsymbol{t}}\right) = (\boldsymbol{Total}\%\boldsymbol{S}) * \mathbf{31.25} \quad (2)$$

The acid neutralization potential (NP) of the studied samples was determined using the Sobek static test [22]. With this method, approximately 0.5 g

of the sample is tested for its fizz rating by the addition of a few drops of 25% HCl (hydrochloric acid). The resulting fizz (denoted by none, slight, moderate, or strong) determines the volume and the normality of HCl to be added to a 2g sample for NP determination. The samples were subsequently almost boiled at 90ºC for 3 h. The volume of the solution was fixed at the initial value for all the experiments. Then excess acid was determined by titrating with 0.1 mol/L of NaOH to pH=7.0 at room temperature. The NP was obtained in terms of kg $CaCO_3$ equivalent per tonne material using the following formula (3) [22]:

$$NP\ (\frac{\boldsymbol{kgCaCO_3}}{\boldsymbol{t}}) = \frac{50 \cdot a[x-(\frac{b}{a})] \cdot y}{c} \quad (3)$$

Where: *a* – normality of HCl, *b* – normality of NaOH, *c* – sample weight in grams, *x* – volume of HCl added in mL, and *y* – volume of NaOH added to pH7 in mL.

The samples previously prepared for the ANC procedure were used in the net acid production (NetAP) test. This method uses hydrogen peroxide (250 ml of 30% H_2O_2 solution) to react with sulphides contained in a finely ground sample (5 g) of the waste material. The samples were placed on magnetic stirrer for 1 hour. The acid remained after reaction was titrated with standard NaOH 0.1M solution to pH 7 using a Consort C832 conductivity and pH meter. The Net acid production (NetAP) of the samples is given by (equation 4).[22,23]

$$\mathbf{NetAP}\ (\frac{\mathbf{kgCaCO_3}}{\mathbf{t}}) = \frac{\mathbf{50 \cdot a \cdot b}}{\boldsymbol{c}} \quad (4)$$

where *a* represents normality of NaOH, *b* – volume of NaOH added to pH 7 (mL) and *c* represents weight of sample (g).

The paste pH/EC was determined by equilibrating the sample in deionised water for approximately 12 hours at a solid to water ratio of 1:2 (w/w) and then measuring the pH and EC using a Consort C832 conductivity and pH meter. This gives an indication of the inherent acidity and salinity of the waste material when initially exposed in a waste emplacement area. [22]

3. Results and discussions

3.1. Mineralogical and chemical analysis of the tailings

The mineralogical results derived from the optical microscopy analysis showed that the sample consisted of quartz, SiO_2 (high refractive index; no twinning or cleavage); calcite, $CaCO_3$ (very high birefringence); microcrystalline aggregates of plagioclase and pyroxene, feldspar $NaAlSi_3O_8$-$CaAlSiO_2O_6$, (parallel cleavage, multiple twinning and first order birefringence) and microcrystalline goethite FeOOH, and iron hydroxide $Fe(OH)_2$ (opaque to sub-translucid, strong cleavage). The reflective property of pyrite FeS_2, galena's

cleavage structure, the brown and fragile nature of sphalerite (blenda) ZnS, the typical yellowish green colour of chalcopyrite $CuFeS_2$ and the glassy appearance of quartz is clear in the microscope at high magnification as shown in the photomicrograph (Figure 2).

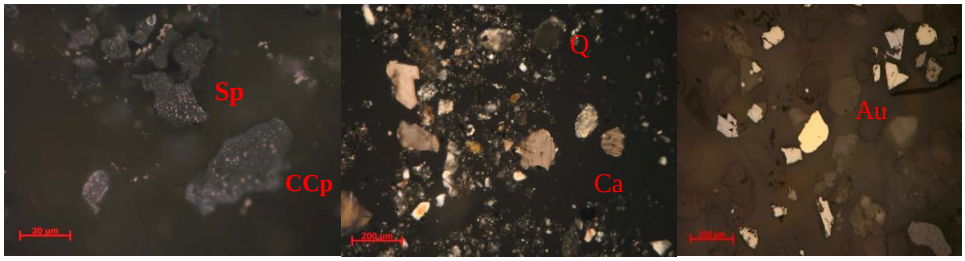

Fig.2. Optical microscopy of a tailing sample showing Sphalerite (Sp), Chalcopyrite (Ccp), Quartz (Q) , Calcite (Ca) and gold (Au)

Table 1 summarizes the chemical compositions of the tailings samples collected form drill 2 (H2). As shown in Table 1, major elements in the tailings were Mn, Zn, Pb, P, Cu, Ba, and As, whereas the minor elements were identified as Ca, Na, Mg, and Hg. The gold and silver content of the tailing samples were 0.43 g/t and 3.70 g/t, respectively.

Table 1.

The chemical compositions of elements content in tailing profile

Element	Content	Element	Content	Element	Content
Au g/t	0.43	Co ppm	9.17	Mo ppm	2.00
Ag g/t	3.70	Cr ppm	16.83	Na %	0.02
Al %	1.01	Cu ppm	199.17	Ni ppm	9.00
As ppm	175.00	Fe %	3.57	P ppm	365.00
B ppm	10.00	Hg ppm	1.33	Pb ppm	490.17
Ba ppm	165.00	K %	0.29	B ppm	14.50
Ca %	1.02	Mg %	0.39	Sr ppm	18.00
Cd ppm	8.95	Mn ppm	2940	Zn ppm	1451.33

3.2. Weathering profile characteristics and elements distribution in depth

In Sasar impoundment three zones were identified (Figure 3): an upper oxidation zone (reddish-brown-yellow coloured, acid generation and metal release), a hardpan layer (acid neutralization and metal accumulation) and a reduction zone (grey coloured, limited water movement, low oxygen diffusivity). If the precipitation (of secondary materials) layer dries out and cement, it forms a so-called hardpan, which act as horizontal barrier to the vertical flow of pore waters.

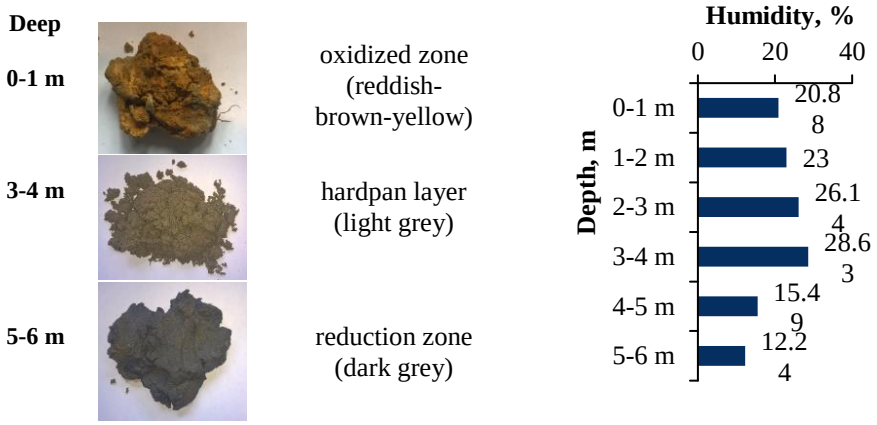

Fig.3. The colours for oxidation zone, hardpan layer and reduction zone and weathering profile for studied drill.

This distinct vertical colour change in tailing, generally indicates the transition from an oxidized layer to reduced material.

It was noted that moisture was increasing from 20.88% (a dry state) on surface to 28.63% at 3-4 m depth on studied drill core. At 5-6 m depth the moisture decreases to 12%.

The changes in pH will also affect the solubility and bio-availability of elements originally present in the soil.

The pH of the pore water rapidly rises due to carbonate dissolution and iron precipitates as iron hydroxides which cement the waste. The oxidation of sulfuric minerals and dissolution of calcium minerals in the upper zone are presented in Figure 4.

In oxidation zone (pH=1.5) the lowest contents of Ca and S and the highest content of Fe can be noted. In this zone, the carbonate minerals are dissolved and the sulphides are oxidised.

The obtained data showed that the Ca content increases from 0.88% in oxidation zone (pH=1.5) to 1.17% in the reduction zone (pH=7.5) and the S content increases with depth from 1.58% in oxidation zone (pH=1.5) to 1.99% in the reduction zone (pH=7.5). The Fe content decreases with depth from 4.18% in oxidation zone to 3.09% in reduction zone, due to oxidative processes that occur on sulfide minerals (pyrite, blenda, etc.).

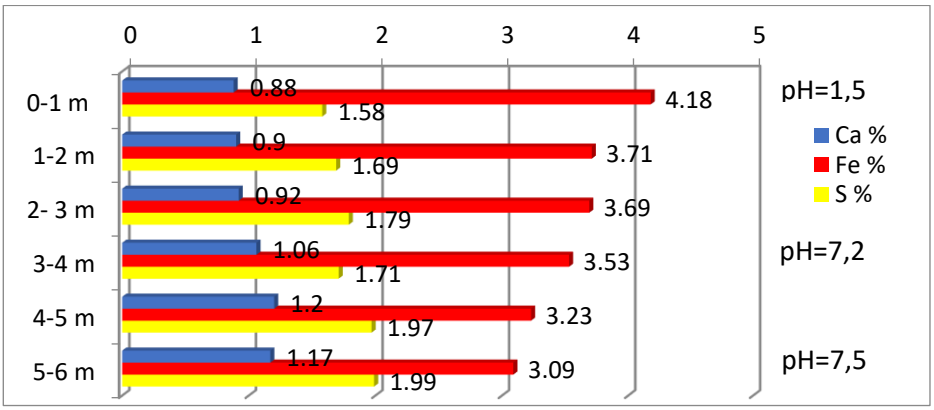

Fig.4. Calcium, iron and sulphur content distributions in depth for H2 drill core

3.3 Static tests results

The implemented static test procedures consisted of neutralisation potential (NP) and Net Acid Production (NetAP) tests.

3.3.1 Paste pH

Table 2 provides data related to paste pH and electric conductivity of samples collected from 1m, 3m and 6 m respectively.

Table 2.

Paste pH and electric conductivity

Sample	Time, h	$pH_{1:2}$	$EC_{1:2}$(µS/cm)
D1	1	1.57	351
	12	2.93	638
D3	1	7.02	1080
	12	7.06	1466
D6	1	7.11	654
	12	7.18	1710

D1 sample showed a paste pH below 4 and an electrical conductivity > 20 µS/cm, meaning that it contains a high amount of dissolved salts. As a consequence, the D1 sample could be included in the category of samples with acid production potential. The values of pH over 7 obtained in the case of D3 and D6 samples indicate that those can either be potentially-acid-forming or non-acid forming, depending on their acid-base balance.

3.3.2 Acid -Base Accounting test

Net neutralization potential (NetNP) data, including neutralization potential (NP) acid potential (AP), NP to AP ratio and net acid production (NetAP), are provided in Table 3.

Table 3

The static test results of the tailing samples

Sample	ABA pH	Fizz rate	S, (%)	NP (kg $CaCO_3$/t)	AP (kg $CaCO_3$/t)	NetNP(kg $CaCO_3$/t)	NP:AP ratio	NetAP pH	NetAP(kg $CaCO_3$/t)	Class
D1	1,45	0	1,58	-0,75	49.37	-14,75	-0,015:1	2,77	6,6	PAF
D3	1,16	1	1,79	32,5	55.94	-20,5	0,58:1	3,22	9,7	PAF
D6	1,32	2	1,99	50	62.19	-14	0,80:1	3,15	7,15	PAF

According to the standard method, sample having a net neutralizing potential (Net NP) less than - 5 kg$CaCO_3$/ tone is classified as *a potential source of acidic drainage (PAF).* In our case study, the obtained net neutralizing potential (NetNP) values were negative, which indicated that the samples were potentially acid forming materials. Results obtained by static tests (Table 3) are graphically plotted in Figure 5.

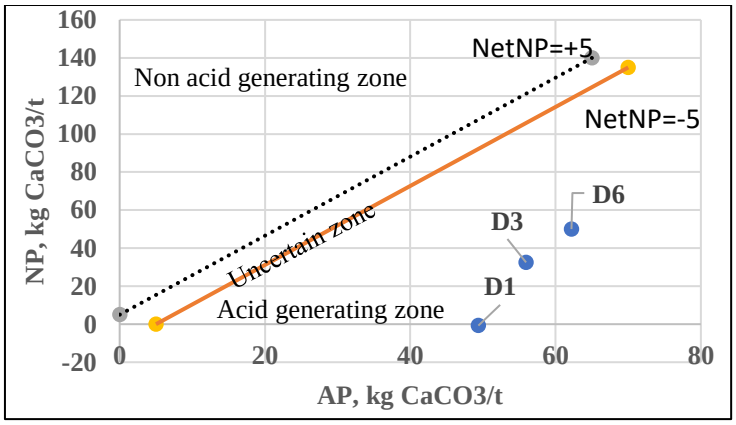

Fig.5. Classification of the samples in terms of AP and NP according to Ferguson and Morin [24]

It has been suggested that the ratio between NP and AP values might provide a more reliable guideline for classification of samples, with suggestions that NP:AP ratios below 1 indicate *potential source of acidic drainage*. [19]

The NetAP positive values obtained show that the samples are potential sources of acid waters, a fact that results from the Figure 6 as well.

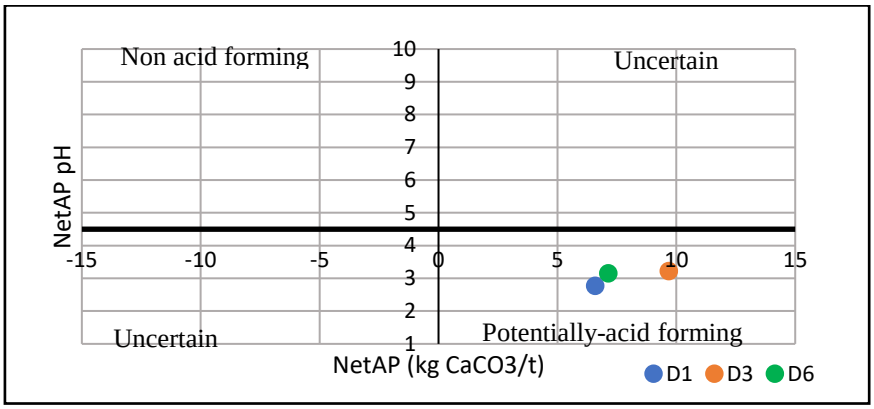

Fig. 6. Distribution of the tailing samples in the NetAP pH/ NetAP diagrams

The NetNP results obtained compared with NetAP results confirmed that samples would produce acidity upon exposure to oxygen and water.

4. Conclusions

Tailings from mineral processing of polymetallic ore stored in Sasar (Red Valley) impoundments, located in the western part of Baia Mare (Romania), were characterized in term of mineralogical and chemical composition of the materials, weathering profile characteristics, elements distribution in depth and its acid generating potential (ARD). The main conclusions related to this study can be summarized as follows:

- The mineralogical results showed that the sample consisted of quartz, SiO_2; calcite, $CaCO_3$; pyrite FeS_2, galena ZnS, and chalcopyrite $CuFeS_2$
- Results have indicated that tailings exhibit very high contamination degree for soil, especially with Mn, Zn, Pb, Cu, thus, gold mine tailings can be considered as a primary source of soil and groundwater contamination in mining areas.
- The gold and silver content of the tailing samples were 0.45 g/t and 4.59 g/t, respectively, reprocessing of tailing could be considered as an economically feasible possibility;
- In Sasar impoundment three zones were identified: an upper oxidation zone (reddish-brown-yellow coloured, acid generation and metal release), a hardpan layer (acid neutralization and metal accumulation) and a reduction zone (grey coloured, limited water movement, low oxygen diffusivity).

- It was noted that moisture was increasing from 20.88% on surface to 28.63% at 3-4 m depth on studied drill core. At 5-6 m depth the moisture decreases to 12%.
- Both the ABA and the NetAP test classified the samples into the category of 'potentially acid generating'.
- Comparison of Net Acid Production (NetAP) and Net Neutralization Potential (NetNP) results confirmed that samples would produce acidity upon exposure to oxygen and water.
-

Acknowledgment: This work was funded under the scope of the "3rd ERA-MIN Joint Call (2015) on Sustainable Supply of Raw Materials in Europe" by a grant of the Romanian National Authority for Scientific Research and Innovation, CCCDI – UEFISCDI, project: Improve Resources Efficiency and Minimize Environmental Footprint - REMinE, Contract no.13/2016. Coordinator: Luleå University of Technology (LTU), Sweden; Partners: Research and Development National Institute for Metals and Radioactive Resource, Romania, University of Porto, Portugal.

REFERENCES

[1] Davies M.P, Martin T.E, Upstream constructed tailings dams – a review of the basics. In: Tailings and mine waste'00. *Balkema, Rotterdam*, 3-15, 2000
[2] Hutchison I., Ellison R., *Mine waste management*, Lewis Publisher, Boca Raton, 1992.
[3] Patterson B.M, Robertson B.S, Woodbury R.J., Talbot B., Davis G.B, Long-term evaluation of a composite cover overlaying a sulfidic tailings facility, *Mine Water Environ*., 25, (2006), 137-145.
[4] Djebbi C, Chaabani F., Font O., Queralt I., Querol X. Atmospheric dust deposition on soils around an abandoned fluorite mine (Hammam Zriba, NE Tunisia*), Environ Res*., 158, (2017), 153-166.
[5] Anawar H.M. Sustainable rehabilitation of mining waste and acid mine drainage using geochemistry, mine type, mineralogy, texture, ore extraction and climate knowledge. *J Environ Manage.* 1; 158, (2015), 111-21.
[6] Huang L., Baumgartl T, Mulligan D. Is rhizosphere remediation sufficient for sustainable revegetation of mine tailings? , *Ann Bot.*, 110(2), (2012), 223-38.
[7] Mittal H.K., Morgenstern N. R, Seepage control in tailings dams, C*anadian Geotechnical Journal*, 13(3), (2011), 277-293.
[8] Chabukdhara M. Gupta K.S., Kotecha Y., Nema A.K., Groundwater quality in Ghaziabad district, India: multivariate and health risk assessment, *Chemosphere*, 179, (2017), 167-178.
[9] Edwards K.J., Bond P.J., Druschel G.K., McGuire M.M., Hamers R.J., Banfield J.F., Geochemical and biological aspects of silfide mieneral dissolution: lessons learned from IRON Mountain, California. *Chem Geol*, 169, (2000), 383-397.
[10] Dold B, Spangenberg J.E., Sulfur speciation and stable isotope trends of water-soluble sulfates in mine tailings profiles. *Environ Sci Technol.*, 39, (2005), 5650-5656.

[11] Romero N.F., Armienta M.A, Gonzales-Hernandez G., Solide phase control on the mobility of potentially toxic elements in an abandoned lead/zinc mine tailings impoundment, Taxco, Mexico, *Appl.Geochem.*, 22, (2007), 109-127.

[12] Schippers A., Kock D, Schwartz M., Bottcher M.E., Vogel H., Hagger M., Geomicrobiological and geochemical investigation of a pyrothite-containing mine waste tailings dam near Selebi-Phikwe in Botswana, *J. Geochem Explor.*, 92, (2007), 151-158.

[13] Heikkinen P.M, Raisanen M.L., Mineralogical and geochemical alteration of Hitura sulphide mine tailings – indicators of spatial distribution of sulphide oxidation in active tailings imjpoundments, *Appl. Geochem.*, 24, (2008), 1224-1237.

[14] Geldenius S., Bell F.G, Acid mine drainage at a coal mine in the eastern Tranvaal, South Africa, *Environ. Geol.*, 34, (1998), 234-242.

[15] Gurzau E.S., Baciu C., Gurzau A.E., Surdu S., Damian Ghe., Impact of the tailings impoundments on groundwater quality in Bozânta area (Baia Mare – NW Romania) and human exposure, *Carpathian Journal of Earth and Environmental Sciences*, 7(4), (2012), 231-240.

[16] Modoi, O.C., Vlad, S.N., Stezar I.C., Manciula,D., Gagiu. A.C. Marginean S., Integrated tailing dams management in Baia Mare area, Romania, *Environ Engineering and Management Journal*, 10, (2011), 43-51.

[17] Mutihac V., *The Geological Structure of the Romanian Territory*, (in Romanian), Technical Press, Bucharest, Romania. 1990

[18] Benciu F., *Heavy Metal Pollution*,(in Romanian), Didactic and Pedagogic Publishing House, Bucharest, Romania, 2007,

[19] MEND Project 1.16.1b, *Acid rock drainage prediction manual, A manual of chemical evaluation procedures for the prediction of acid generation from mine wastes*, Coastech Tesearch Inc. 2008

[20] Schumann R., Stewart W., Miller S., Kawashima N., Li. J., Smart R Acid–base accounting assessment of mine wastes using the chromium reducible sulfur method, *Science of the Total Environment*, 424, (2012)289-296.

[21] Weber P.A, et al. Methodology to determine the acid-neutralization capacity of rock samples, *The Canadian Mineralogist*, 43(4), (2005), 183.

[22] Sobek, A.A, Schuller W.A, Freeman J.R, Smith R.M., *Field and laboratory methods applicable to overburdens and minesoils*, EPA 600/2-78-054, 203, 1978

[23] Finkelman, R.B., Giffin, D.E., Hydrogen-peroxide oxidation - an improved method for rapidly assessing acid-generating potential of sediments and sedimentary-rocks. *Reclam. Reveg. Res.*, 5, (1986), 521-534.

[24] Ferguson KD, Morin KA. The prediction of acid rock drainage—lessons from the data base. In: *Proceedings of the 2nd ICARD*, vol 3. Montreal, QC, Canada, (1991), 83–106.

APPLICATION OF CORRELATION ALGORITHMS ON MONITORING DATA FOR QUALITY ASSESSMENT OF THE AQUATIC ECOSYSTEMS

Petra IONESCU[1*], Alexandru A. IVANOV[1], Elena DIACU[2], György DEÁK[1], Monica -V. RADU[1], Carmen TOCIU[1]

[1]National Institute for Research & Development in Environmental Protection, 294 Spl. Independentei, 6-th District, Code 060031, Bucharest, Romania
[2]University "Politehnica" of Bucharest, 1-7 Gh. Polizu street, 1-st District, Code 011061, Bucharest, Romania

Abstract

Water pollution is a critical issue worldwide, the need for an integrated management of water resources leading to a continuous monitoring of its quality. The multitudes of data from monitoring programs require the use of indices and algorithms for evaluating water quality as suggestive as possible. Development of sets of indices and ecological indicators is a priority at European level.

This paper aims to assess the surface water quality in relation to the heavy metals content according to national and European regulations by a modern approach of data processing from monitoring programs. To achieve the propose, a data set obtained from a monitoring program conducted during January - April 2015 under the contract 53/2015 entitled "Monitoring of environmental impact of the works for improvement of navigation conditions on the Danube between Călăraşi and Brăila, km 375 and km 175" has been used, and the following data correlation algorithm have been developed and applied: Heavy Metal Pollution Index (HPI), Metal Index (MI) and Multi-Parametric Quality Index (ICPM) applied to metal concentrations.

Key words: Heavy Metal Pollution Index, Metal Index, Multi-Parametric Quality Index, aquatic ecosystem

1. Introduction

At a global level, the quality of surface waters is a very sensitive issue. The assessment of health of aquatic ecosystems represents one of the worldwide research priorities. Through the Water Framework Directive/2000/60/EC [1] a number of priority monitoring programs were launched followed by centralization

*Corresponding author; E-mail: petraionescu2012@yahoo.ro

of a large amount of data regarding the contamination and ecological status of surface waters in Europe [2].

The multitude of data obtained from monitoring programs requires the use of indices and algorithms for evaluating surface water quality as suggestive as possible in accordance to Water Framework Directive/2000/60/EC [3].

The environmental indices represent an aggregation of several mathematical indicators (named *variables*) used to present a spatial or temporal change in the environmental state [3]. Among the main pollutants to be monitored in order to obtain an overall picture of the aquatic ecosystem health are the heavy metals, due to the high toxicity, non-biodegradability and high tendency to bio-accumulate in the food chain [7-10].

For the heavy metals, pollution indices can be grouped into three types: (i) contamination indices; (ii) background enrichment indices and (iii) ecological risk indices [5]. And of these, the most commonly used indicators are: (i) individual indices calculated to evaluate the degree of contamination with a single metal and including: the contamination factor, the environmental risk factor, the enrichment factor and the index of geo-accumulation and (ii) integrated indices which are based on individual indices for a larger number of metals [6].

In the present study, in order to assess the surface water quality in relation to the heavy metal content according to national legislation, the following indices were implemented: Heavy Metal Pollution Index (HPI), Metal index (MI) and Multi-Parametric Quality Index (ICPM) applied to metal concentrations.

2. Experimental

For the development and application of mathematical models mentioned, a data set has been used, obtained from the monitoring program conducted during January - April 2015 under the contract entitled *"Monitoring of Environmental Impact of the Works for Improvement of the Navigation Conditions on the Danube Between Calarasi and Braila, km 375 - km 175"* [11]. To develop mathematical models, the following heavy metals were considered: chromium (Cr), copper (Cu), zinc (Zn), arsenic (As), barium (Ba), selenium (Se), cobalt (Co), lead (Pb), cadmium (Cd), iron (Fe), mercury (Hg), manganese (Mn) and nickel (Ni).

Heavy Metal Pollution Index

The calculation of Heavy Metal Pollution Index (HPI) involves three steps: first, to each metal (Mi) a weight (Wi) is assigned, calculated as the value inversely proportional to the standard recommended for each metal; the second stage consists in calculation of the parameter (Qi) for each metal; in the final stage sub-indexes computed in a global index are summed (Eq. (1), Eq. (2) and Eq. (3)) [12, 13]. Generally, the critical value of metal pollution index is 100 [14].

To develop this index, limit values specified by M.O. 161/2006 for quality class I (Ii = ideal value) and class III quality have been counted (Si = maximum permissible value) [15].

Table 1

Standard used for HPI computation based on M.O. 161/2006

Mi (µg/L)	I_i (µg/L)	S_i (µg/L)	W_i
Cr	25	100	0,01
Cu	20	50	0,02
Cd	0,50	2	0,50
Zn	100	500	0,002
Ni	10	50	0,02
Pb	5	25	0,04
As	10	50	0,02
Ba	0,05	0,50	2
Se	1	5	0,20
Co	10	50	0,02
Hg	0,10	0,50	2
Ni	10	50	0,02
Fe	300	500	0,002
Mn	50	300	0,0033

$$W_i = \frac{k}{S_i} \quad (1)$$

$$Q_i = \sum_{i=1}^{n} \frac{\{M_i(-)I_i\}}{(S_i - I_i)} \; x\; 100 \quad (2)$$

$$HPI = \frac{\sum_{i=1}^{n} W_i Q_i}{\sum_{i=1}^{n} W_i} \quad (3)$$

Metal Index

Metal index (MI) is the sum of reports monitored and maximum permissible concentration values for each metal, representing a quality indicator for both surface water and drinking water [16]. According to Water Quality Classification Using MI there are six classes of quality, starting from very pure as Class I to Class VI, as the most affected [12].

Multi-Parametric Quality Index

Starting from the premise that to each indicator a different weight might be assigned in order to highlight the significance of those having a greater impact on water quality, on the environment and hence on human health, a multiparametric quality index (ICPM) for the evaluation of water quality has been developed, using a total of 41 physical-chemical indicators [11, 18].

3. Results and discussions

For the development and application of the three mathematical models, the average values obtained from the monitoring program for the following heavy metals: Cr, Cu, Zn, As, Ba, Se, Co, Pb, Cd, Fe, Hg, Mn and Ni have been considered.

Heavy Metal Pollution Index

Figure 1 shows the temporal variation of Heavy Metal Pollution Index for the average values of each month for monitoring. Following the analysis it has been observed that the HPI shows the following variation for the 4 months of monitoring: January < April < March < February. The values for Heavy Metal Pollution Index do not exceed the limit of 100.

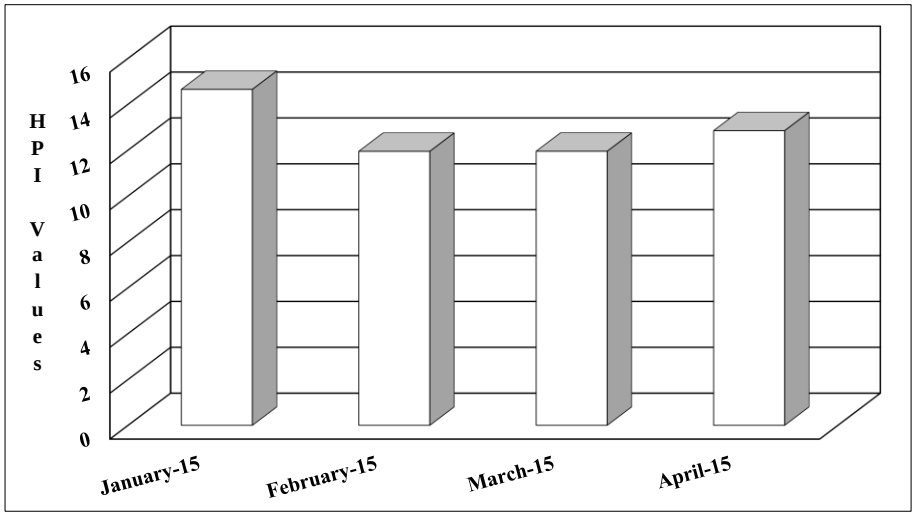

Fig. 1. Temporal variation of HPI

Metal Index

Similar to the first index, for the development of Metal Index the average values recorded during the 4 months of monitoring have been considered, been reported to the limit values according to MO 161/2006 (Class III of quality). In Figure 2 the temporal variation of Metal Index for the four months of monitoring is being represented.

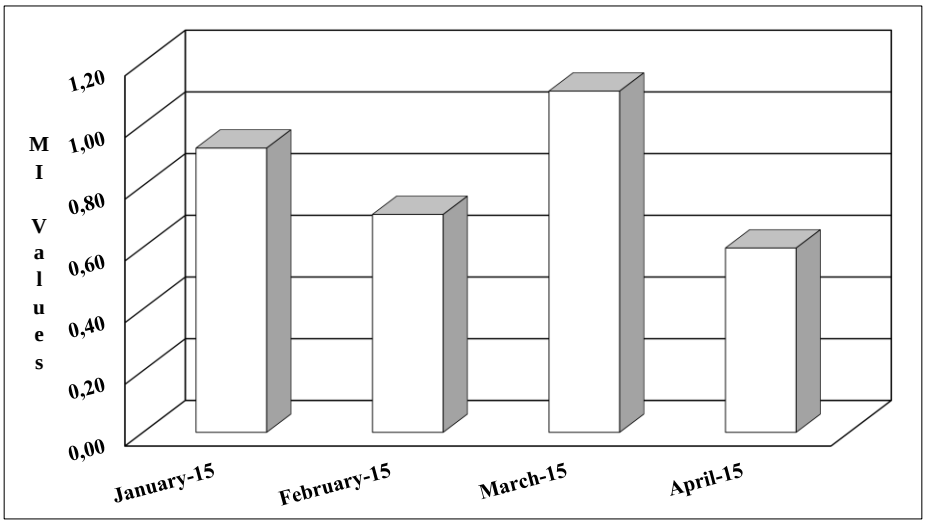

Fig. 2. Temporal variation of MI

Multi-Parametric Quality Index

With the purpose of comparison to other indices of ecosystem quality focused on indicators from heavy metals class, the ICPM algorithm (developed originally for 41 quality indicators) was applied only to the heavy metals class comprised of 13 quality indicators. Figure 3 presents the results of ICPM applied to the metals group.

No.	Quality Indicator (QI)	Intermediary ICPM Value /QI				Contributions to ICPM /QI			
		Luna 41	Luna 42	Luna 43	Luna 44	Luna 41	Luna 42	Luna 43	Luna 44
20	Cr total, µg/L	69,6%	80,6%	94,9%	66,7%	4,1E-02	4,8E-02	5,6E-02	4,0E-02
21	Cu, µg/L	59,4%	71,2%	94,8%	35,8%	4,4E-02	5,3E-02	7,1E-02	2,7E-02
22	Zn, µg/L	60,1%	69,7%	90,4%	61,5%	3,7E-02	4,3E-02	5,5E-02	3,8E-02
23	As, µg/L	-0,6%	2,1%	71,3%	10,9%	-6,4E-04	2,1E-03	7,3E-02	1,1E-02
24	Ba, mg/L	18,9%	15,4%	40,4%	19,9%	1,7E-02	1,4E-02	3,7E-02	1,8E-02
25	Se, µg/L	22,1%	35,5%	76,9%	29,5%	2,0E-02	3,2E-02	6,8E-02	2,6E-02
26	Co, µg/L	31,7%	40,3%	70,8%	36,2%	1,7E-02	2,2E-02	3,8E-02	1,9E-02
27	Pb, µg/L	49,9%	65,8%	77,6%	45,1%	3,8E-02	5,0E-02	5,9E-02	3,5E-02
28	Cd, µg/L	0,0%	0,0%	28,7%	11,2%	0,0E+00	0,0E+00	2,7E-02	1,0E-02
29	Fe total, mg/L	79,1%	53,2%	83,4%	39,8%	7,9E-02	5,3E-02	8,3E-02	4,0E-02
30	Hg, µg/L	0,0%	0,0%	0,0%	0,0%	0,0E+00	0,0E+00	0,0E+00	0,0E+00
31	Mn total, mg/L	56,0%	43,6%	87,4%	42,0%	3,6E-02	2,8E-02	5,5E-02	2,7E-02
32	Ni, µg/L	56,9%	60,1%	91,4%	64,7%	3,7E-02	3,9E-02	6,0E-02	4,2E-02
		Type A summed value ICPM(A)				37%	38%	68%	33%
					ICPM	**37%**	**38%**	**68%**	**33%**

Fig. 3. Intermediary values and individual quality indicator contributions in the final ICPM value

Following the analysis of data, Figure 3 revealed that ICPM (heavy metals) shows the following variation for the four months of monitoring (January - April 2015): April < January < February < March.

6. Conclusions

The Heavy Metal Pollution Index (HPI) has been an effective tool for assessing the level of pollution of surface waters in terms of heavy metal content, providing information on the influence of each metal in particular to the overall water pollution. The application of Metal Index (MI) on monthly average values has led to the classification of the Lower Danube as water quality Class II (good) according to regulations.

With the purpose of comparison to other indices and to the general indices of ecosystem quality focused on indicators values of heavy metals class, a smaller version of the Multi-Parametric Quality Index (ICPM) algorithm has been analysed, considering all the heavy metal values. The ICPM values (heavy metals) in the evaluated period (between January and April 2015) ranged from 33% to 38% except for March that was higher, up to 68%, caused by increased sediment transport in a period affected by heavy rainfall.

The addition of these three heavy metal indexes to the global assessment of water quality can lead to a significant improvement of its accuracy, as they become a useful tool for the monitoring of water pollution level and being also able to predict its tendency for the future.

Acknowledgments

This work was financially supported by the National Authority for Scientific Research and Innovation, in the frame of Nucleu Program-Project PN 09 06 02 39, and used raw data from the POST contract Monitoring of Environmental Impact of the Works for Improvement of the Navigation Conditions on the Danube between Calarasi and Braila, km 375 - km 175, available on-line (http://www.afdj.ro/en/content/romomed).

The authors would like to thank the management and employees of National Institute for Research & Development in Environmental Protection for their valuable assistance and suggestions.

REFERENCES

[1] Directive 2000/60/EC of the European Parliament and of the Council establishing a framework for the Community action in the field of water policy.

[2] Solheim A. L., Austnes K., Kristensen P., Peterlin M., Kodes V., Collins R., Semeradova S., Kunitzer A., Filippi R., Prchalova H., Spiteri C., Prins T., *Ecological and chemical status and pressures in European waters*, ATC/ICM Technical Report 1, Prague, 2012.

[3] Anghel A.-M, Ilie M., Ghiță G., Marinescu F., Deák Gy., Assessing the Aquatic Environment Quality Contaminated with Heavy Metals as a Result of Polymetallic Mining in the North-West Region of Romania Using Pollution Indices, *International Journal of Environmental Science and Development*, 8, 111-115, 2017.

[4] Varduca A., *Protecția calității apelor*, *H*G*A*, București, 2000.
[5] Caeiro S., Costa M. H., Ramos T. B., Fernandes F., Silveira N., Coimbra A., Medeiros G., Painho M., Assessing heavy metal contamination in Sado Estuary sediment: An index analysis approach, *Ecological Indicators*, 5, 151-169, 2005.
[6] Qingjie G., Jun D., Yunchuan X., Qingfei W., Liqiang Y., Calculating Pollution Indices by Heavy Metals in Ecological Geochemistry Assessment and a Case Study in Parks of Beijing, *Journal of China University of Geosciences*, 19, 230-241, 2008.
[7] Radu V.-M., Raischi S., Szep R., Tănase G. S., Ionescu P., Evaluation of priority hazardous substances present in the sediments of the Lower Danube section using multivariate statistical analysis, *Water resources, forest, marine and ocean ecosystems, SGEM*, 1, 277-283, 2015.
[8] Resetar-Deac A.-M., Diacu E., Assessment of aquatic environment contamination with heavy metals from abandoned mines of Northwestern Romania, *Rev. Chim. (Bucharest)*, 66, 1535-1539, 2015.
[9] Xu G., Liu J., Pei S., Gao M., Kong X., Transport pathway and depocenter of anthropogenic heavy metals off the Shandong Peninsula, China, *Estuarine, Coastal and Shelf Science*, 180, 168-178, 2016.
[10] Bat L., Yesim Özkan E., Can Öztekin H., The contamination status of trace metals in Sinop coast of the Black Sea, Turkey, *Caspian J. Env. Sci.*, 13, 1-10, 2015.
[11] POS-T Project Monitoring of Environmental Impact of the Works for Improvement of the Navigation Conditions on the Danube between Calarasi and Braila, km 375 - km 175 (http://www.afdj.ro/en/content/romomed).
[12] Ionescu P., Radu V.-M., Deák Gy., Ivanov A.A., Diacu E., Lower Danube water quality assessment using heavy metals indexes, *Rev. Chim. (Bucharest)*, 66, 8, 1088-1092, 2015.
[13] Reza R., Singh G., Assessment of heavy metal contamination and its indexing approach for river water, *Int. J. Environ. Sci. Tech*., 7, 785-792, 2010.
[14] Abdullah E. J., Evaluation of Surface Water Quality Indices for Heavy Metals of Diyala River-Iraq, *Journal of Natural Sciences Research*, 3, 63-69, 2013.
[15] Ministerial Order No. 161, *Approving the Norms on surface water quality classification to determine the ecological status of water bodies*, 2016.
[16] Ameh E. G., Akpah F. A., Heavy metal pollution indexing and multivariate statistical evaluation of hydrogeochemistry of River PovPov in Itakpe Iron-Ore mining area, Kogi State, Nigeria, *Advances in Applied Science Research*, 2, 33-46, 2011.
[17] Radu V.-M., Ivanov A. A., Ionescu P., Deák Gy., Diacu E., Overall assessment of water quality on Lower Danube River using multi-parametric quality index, *Rev. Chim. (Bucharest)*, 67, 391-395, 2016.
[18] Radu V.-M., Ivanov A. A., Ionescu P., Deák Gy., Tudor M., Multiparametric quality index for the ongoing water quality monitoring projects on the Lower Danube, *Environmental Engineering and Management Journal*, 15, 1069-1074, 2016.

ESTIMATION OF HYDROCARBONS BIODEGRADATION RATE FROM SOILS CONTAMINATED WITH OIL

Elena DUMITRESCU*, Andreia VLADIMIRESCU, Ramona VIŞOIU, Ana CRĂCICĂ

OMV PETROM SA, ICPT Campina, 29 Culturii Bvd. Campina, Prahova County, Romania

Abstract

Worldwide, in oilfield areas, there are soils polluted with petroleum hydrocarbons, which need to be remediated by using appropriate treatment technologies. Bioremediation is a cost-effective and environmentally friendly treatment method that uses the ability of microorganisms to degrade organic compounds [1].

The rate of hydrocarbons biodegradability depends on the nature of oil contaminant, soil type and optimal conditions for stimulating of biodegradation activity (presence of appropriate microorganisms in an adequate number, temperature, humidity, nutrients, pH and oxygen availability) [2].

Laboratory bioremediation tests were conducted for two soil types (clay and loam) contaminated with two types of crude oil (light and heavy oil). The efficiency of the bioremediation process was monitored by analysis for total petroleum hydrocarbons (TPH) concentration of all soil samples and by the ratio between C17/pristane and C18/phytane (for soils contaminated with light oil). C17 (N-heptadecane) and C18 (N-octadecane) are more easily biodegradable than pristane (2,6,10,14 tetramethyl pentadecane) and phytane (2,6,10,14 tetramethylhexadecane) that are heavily biodegradable iso-alkanes [3]. These ratios remain constant through evaporation, but decrease very much with oil biodegradation. The lower the C17/pristane and C18/phytane ratios, the more biodegradable the crude oil [4].

The highest rate of biodegradation of crude oil was obtained for loam soil contaminated with light oil, where a decrease in TPH was registered in concentration from 5% to 1% after about 5 months of treatment with inoculum, nutrients, loosening agents, surfactants and microelements. The lower hydrocarbon biodegradation rate was recorded for the variant using clay soil contaminated with heavy oil, where the decrease was from 5% to 3% for the same treatment period.

Based on the results of these tests, a program for the remediation of soils polluted with hydrocarbons has been developed.

Key words: bioremediation, biodegradation, oil, soil, hydrocarbons

* Corresponding author. E-mail address: elena.dumitrescu2@petrom.com

1. Introduction

Petroleum hydrocarbons are very useful to people, but they can also be very dangerous, oil spills and petroleum products posing a major risk to the environment.

Research has been carried out on various decontamination techniques to find cheap methods with minimal environmental impact for the long term. Bioremediation of hydrocarbon-contaminated soil is an efficient, cheap and environmentally friendly treatment method.

Bioremediation is based on the use of soil microorganisms (bacteria or fungi) for the degradation of complex organic contaminants and their transformation into harmless compounds [5]. Microorganisms can adapt their catabolic activity to use toxic organic pollutants from the soil as a source of food, mineralizing complex organic substances to simpler compounds, carbon dioxide and water [6].

Bioremediation can be accomplished:

- in-situ
- ex-situ

In-situ bioremediation is applied for surface contamination with hydrocarbons when the soil is affected to a depth up to 50-60 cm and there is no risk of groundwater contamination. In-situ bioremediation is also appropriate for the treatment of large contaminated surfaces, where the hydrocarbon concentration in the soil does not exceed 5% [7].

In-situ bioremediation takes place at the site of the contamination and no excavation and transport of soil is required. It is a slower process than ex-situ bioremediation, but cheaper.

The advantages of this method are:

- is relatively simple to design and implement;
- allows the soil to be treated without being excavated and transported;
- is a cost effective method;

Limiting factors:

- clay soils are difficult to treat;
- it takes a long time;
- does not apply to soils with a total petroleum hydrocarbons (TPH) content more than 5%.

Ex-situ bioremediation is a method of soil treatment, where soil is excavated and treated in another location. This method is applicable for large soil volume and deep contamination. An impermeable barrier must be provided where contaminated soil is stored, mixed with nutrients and optionally with inoculum. It

is also required an equipment to increase the amount of oxygen in the soil (aeration) and the transport of oxygen and nutrients to bacteria. [8]

The treatment unit could be made on a support (synthetic or clay) to prevent migration of leachate generated during treatment. An irrigation system have to be installed to maintain optimal humidity. The leachate collection system can be coupled with the irrigation system to recirculate the leachate.

Advantages of technology:

- environmental conditions can be easily optimized;
- can be treated soils with a higher hydrocarbon concentration compared to in-situ bioremediation;
- the time required for ex-situ bioremediation is shorter than the in-situ method.

Technology limitations:

- requires soil excavation;
- large space for processed material is required;
- the cost is higher due to excavation;
- composting leads to increased material volume.

The ability of microorganisms to degrade hydrocarbons depends on several factors:

- *type of crude oil*
  - the susceptibility of hydrocarbons for microbial degradation can be generally ranked as follows: linear alkanes> branched alkanes> small aromatics>cyclic alkanes, so lighter crude oil biodegrade faster than heavy oils. [9]
- *the type of soil*
  - soils with coarse particles and unconsolidated materials (sand, gravel) are treated easier. Soils with high percentage of clay are difficult to treat, contaminants are adsorbed on the fine fraction of the soil. For example, soils that tend to clump together (such as clay) are difficult to aerate and result in low oxygen concentrations [7].
- *the presence of bacteria in the soil*
  - normally the soil contains a large number of microorganisms, among which the bacteria represent the most numerous and biochemically active group. In order the hydrocarbons biodegradation take place, it is a necessary to exist bacteria in the soil (minimum number of heterotophic bacteria have to be 10^3 CFU/g soil). A lower number indicates the presence

  - of toxic substances in the soil, which can make the bioremediation process inefficient [7].
- *the presence of oxygen in the soil*
  - oxygen is essential for aerobic bacterial metabolic processes. To ensure the availability of oxygen for bacteria it is necessary to aerate the soil, which was done in the laboratory by mixing the soil in containers and in the field it is made by agricultural works (plowing) or with special equipments (ex-situ bioremediation). Also, to improve the aeration of the soil have to add loosing agents (straw, sawdust).
- *temperature*
  - the highest degradation rates generally occur in the soil temperature range of 10-45^{0}C, the range in which the rate of many biochemical reactions double with temperature increases with each 10^{0}C [7].
- *pH*
  - to support the growth of bacteria, soil pH should be in the range of 6-8, with a value of about 7 (neutral) being optimal. [7].
- *nutrients*
  - biostimulation involves the addition of nutrients (fertilizers) and oxygen to stimulate the development of indigenous microorganisms. These nutrients allow microorganisms to create the enzymes needed to destroy contaminants. All microorganisms require nitrogen, phosphorus, potassium and carbon [7].
- *humidity*
  - microorganisms in soil require water for optimal growth. The ideal range for soil moisture is between 12 percent to 30 percent by weight. Available water is essential for all living organisms and irrigation is required to achieve optimal humidity [7].
- *microelements*
  - microelements play a very important role for microorganisms. Some of the most important trace elements are copper, manganese, cobalt, zinc. [10]
- *salinity*
  - soil salinity results from the accumulation of soluble salts (mainly sodium, calcium, magnesium and potassium salts) in the upper horizon of the soil. Saltwater, which usually accompanies crude oil in the extraction process, can

negatively affect the hydrocarbon biodegradation of hydrocarbons, being a limiting factor of the soil bioremediation process. High concentrations of salts may be lethal to most microorganisms. Biological activity can be properly conducted up to electrical conductivity values of 4000 μS/cm and for sodium adsorbtion ratio (SAR) values <5. [10, 11]

2. Experimental

Two types of crude oil were used to perform bioremediation tests in the laboratory:

- light oil, with density 0.8308 kg/m^3 (API density 38.8), noted A;
- heavy oil, with density 0.9414 kg/m^3 (API density 18.8), noted B.

Oils with API density > 30 are very easily biodegradable and those with an API density < 20 are difficult to biodegrade [12].

Also, two types of soil were used:

- clay soil,
- loam soil.

The higher clay content of the soil, the more difficult it is to treat, because the contaminants adsorb on the fine fraction of the soil (the clay fraction).

For a very good homogenization, soil samples were prepared as a saturated soil paste, according to method 15.2.1 [13].

Soil samples were initially analyzed to see if they were previously contaminated with crude oil or salt water.

The saturated soil paste was filtered through a Baroid filtering device. The obtained extract was analyzed for the determination of pH, electrical conductivity and sodium, calcium and magnesium concentrations.

pH of the aqueous soil extract was determined according to method 4500-H^+ B, the electrical conductivity was determined according to method 2510 B, and the sodium, calcium and magnesium concentrations were analyzed by atomic absorption spectrometry (AAS) according to method 3111 B [14]. Using the concentrations obtained for sodium, calcium and magnesium, SAR was calculated according to method 15.4.4 [13].

From the soil samples the clay content (fraction below 2 μm) according to method 55.2 [13] and the content of microelements soluble in 1N HCl by atomic absorption spectrometry according to method 3111 B [14] were determined.

For determination of total petroleum hydrocarbon (TPH) content, soil samples were dried in air, then milled and extracted with solvent perchlorethylene. Infrared spectra were recorded on the 3100-2800 cm^{-1} range.

Determination was performed on an FT-IR spectrometer, similar to method 5520 C [14].

For determination of the C17/pristane and C18/phytane ratios, a GC-MSD gas chromatograph gas mass spectrometer (GC-MSD) was used.

Caracteristics of the two soils are presented in the Table 1.

Table 1

Results of analyzes performed on soil samples

Parameter	Clay soil	Loam Soil	Recommended values
pH	8,01	6,85	6-8*
SAR, $(me/l)^{1/2}$	0,11	0,05	<5**
TPH, mg/kg	<50	<50	<2000***
Percentage of saturation, %	81	72	-
Electrical conductivity, µS/cm	190	840	<2000**
Clay (<2µm), %	34	23	-
Sand, %	15	29	
Microelements soluble in HCl 1N			
Cu, mg/kg	13,4	13,8	7**
Mn, mg/kg	306	260	250**
Co, mg/kg	2,4	1,3	2,4**
Zn, mg/kg	9	23,2	9**
Heterotophic bacteria, CFU/g sol	$105*10^5$	$115*10^5$	$> 10^3$*

* [7]; ** [10]; *** [15]

Analyzes performed on soil samples highlighted the following:

- the soil has not previously been affected by oil or salt water pollution;
- the presence of bacteria in the soil indicates that the bioremediation process can be effective (there are no toxic concentrations of certain organic or inorganic compounds such as heavy metals or chlorinated compounds).
- the microelements (Cu, Mn, Co, Zn) are present in sufficient quantities in the soil.

Performing of bioremediation tests

To perform the bioremediation tests in the laboratory, the two soils were prepared as saturated paste and each was mixed with crude oil (light or heavy) at a concentration of 5% (relative to dry soil), then divided into containers where it was mixed with various additives: inoculum, fertilizer, straw, biodegradable surfactant in various proportions, as shown in table 2. The amount of saturated paste in each container was calculated so that each one contained 200 grams of dry soil.

Table 2

Distribution in containers

Recipient code loam soil + light oil	**Recipient code clay soil + light oil**	**Recipient code loam soil + heavy oil**	**Recipient code clay soil + heavy oil**	**Inoculum**	**Nutrients**	**Loosing agent (straw)**	**Surfactant**
IIA	2A	IIB	2B	-	X	-	-
IIIA	3A	IIIB	3B	-	-	X	-
IVA	4A	IVB	4B	-	-	-	X
VA	5A	VB	5B	X	X	-	-
VIA	6A	VIB	6B	X	X	X	
VIIA	7A	VIIB	7B	X	X	X	X

Inoculum was obtained as a solution, from an old polluted soil and from biological sludge from wastewater treatment. Microorganisms were grown in inorganic nutrient solution, having hydrocarbons as carbon source. Thus, selection of hydrocarbonoclasts bacteria (able to degradate hydrocarbons) was performed. The amount of inoculum added was 1% based on the total mass of soil saturated paste, corresponding to 10 ml inoculum/kg soil.

Soils with an old oil pollution have a higher percentage of microorganisms that degrade oil and generally have a higher potential for hydrocarbon degradation. Therefore, for the bioremediation of crude oil in environments not previously exposed to crude oil, there may be a delay and adaptation period before occuring a significant biodegradation of crude oil. In the case of very recent pollution, it is necessary to add an inoculum to reduce the delay of biodegradation.

Fertilizators

Biodegradation of crude oil takes place to a large extent at the interface between oil and water. So the efficieny of biostimulation depends on the nutrient concentration in the interstitial pores. The nutrient concentration should be maintained at a enough high level to facilitate bacterial growth.

The source of nitrogen for most microorganisms is ammonium and nitrate, nitrogen is a structural part of proteins and nucleic acids. Phosphorus as phosphate is used for the synthesis of nucleic acids and phospholipids. Potassium is a cofactor for some important enzymes.

Nutrients should be added gradually and in small portions.

The nitrogen dose applied once was 100 mg N/kg soil [16, 17]. For phosphorus, the doses were 30-45 to 90-120 kg P_2O_5/ha and for potassium 50-125 kg K/ha. [10]

In the experiment, soils contaminated with 5% crude oil were treated with nitrogen, phosphorus and potassium fertilizers to stimulate the bioremediation process.

- *Nitrogen*

Considering that the nitrogen fertilizer dose applied once on the soil was 100 mg N/kg soil, then the once-applied ammonium nitrate dose corresponds to 300 mg NH_4NO_3/kg soil.

- *Phosphorus*

Phosphorus can be applied in doses ranging from 30-45 to 90-120 kg P_2O_5/ha. If we consider that 120 kg P_2O_5/ha is applied once, for a depth of application of 20 cm and an average bulk soil density of 1.5 g/cm^3, then the once-applied phosphorus dose corresponds to 17 mg P/kg soil.

- *Potassium*

Potassium is applied at doses of 50-125 kg/ha. If we consider that 70 kg K/ha is applied once, according to the above reasoning, the once-applied potassium dose corresponds to 23 mg K/kg soil.

Nitrogen was applied in the form of ammonium nitrate, and phosphorus and potassium in the form of potassium dihydrogen phosphate.

Corresponding to the above doses, the fertilizer amounts added monthly were: 2.5 ml solution 24 g NH_4NO_3/l and 2.5 ml solution 6 g KH_2PO_4/l.

Loosing agents - Shredded wheat straw was used in the amount of 10 g/container, for aeration improve, corresponding to 50 g straw/kg soil.

Biodegradable surfactant - It is necesary to use surfactants as by their accumulation at the water - polluting petroleum interface, they favour the extraction of hydrocarbon molecules from the soil structure and they became more accessible to bacteria [18].

A 10% biodegradable surfactant solution LCD (having in composition alkyl benzene, sodium sulphonate, laureate sodium sulfate, sodium xylene sulfonate) [19] was added in the laboratory experiments, which was added in 2 mL/container, corresponding to a dose of 10 ml/ kg soil (solution 10%).

Microelements - According to the analyzes performed on the initial soil samples it was found that no additional adding of Cu, Mn, Co and Zn microelements is necessary.

The mixture obtained in each container was homogenized for aeration 2 times a week, adding the amount of water required so that the moisture was between 12-30% (w/w).

3. Results and discussions

In order to determine the effectiveness of treatments applied for biodegradation of hydrocarbons in the soil, the TPH were analyzed in soil

samples after 1.5 months, 3 months and 4.5 months from the beginning of the treatment.

From the initial added TPH (50000 mg/kg) and TPH after 4.5 months of treatment, residual hydrocarbon content (residual TPH) and biodegradable hydrocarbon (TPH biodegradable) content were calculated:

- residual TPH,% = TPH 4.5 months / 10000,
- biodegradate TPH,% = (initial TPH - TPH 4.5 months)/10000,

The results are shown in Tables 3 - 6.

Table 3

Total petroleum hydrocarbons – loam soil + light oil

Container code	TPH, mg/kg after 1,5 months	TPH, mg/kg after 3 months	TPH, mg/kg after 4,5 months	TPH residual , %	TPH biodegradate , %
I A	26300	19900	18200	1,82	3,18
II A	28200	20500	17000	1,7	3,3
III A	24600	19100	15100	1,51	3,49
IV A	25800	20800	20000	2,00	3,00
V A	27300	19300	17100	1,71	3,29
VI A	24100	16800	13700	1,37	3,63
VII A	20300	17400	13200	1,32	3,68

Table 4

Total petroleum hydrocarbons – clay soil + light oil

Container code	TPH, mg/kg after 1,5 months	TPH, mg/kg after 3 months	TPH, mg/kg after 4,5 months	TPH residual, %	TPH biodegradate, %
1A	29800	26700	25800	2,58	2,42
2A	28800	24500	22300	2,23	2,77
3A	26900	23900	21700	2,17	2,83
4A	29400	25200	24900	2,49	2,51
5A	30900	25700	23000	2,30	2,7
6A	26500	24200	20700	2,07	2,93
7A	30600	22700	20700	2,07	2,93

Table 5

Total petroleum hydrocarbons – loam soil + heavy oil

Container code	TPH, mg/kg after 1,5 months	TPH, mg/kg after 3 months	TPH, mg/kg after 4,5 months	TPH residual, %	TPH biodegradate, %
I B	36700	29700	28000	2,80	2,20
II B	35600	29000	29000	2,90	2,10
III B	35500	28500	25300	2,53	2,47
IV B	36200	30100	27500	2,75	2,25

V B	39300	29700	29700	2,97	2,03
VI B	36500	29400	28800	2,88	2,12
VII B	35800	27700	27000	2,70	2,30

Table 6

Total petroleum hydrocarbons – clay soil + heavy oil

Container code	TPH, mg/kg after 1,5 months	TPH, mg/kg after 3 months	TPH, mg/kg after 4,5 months	TPH residual, %	TPH biodegradate, %
1B	39800	36300	35300	3,53	1,47
2B	39200	34200	32800	3,28	1,72
3B	39300	37900	36600	3,66	1,34
4B	40000	33700	32800	3,28	1,72
5B	37000	32300	30000	3,00	2,00
6B	36300	32000	31500	3,15	1,85
7B	36000	33500	32800	3,28	1,72

TPH residual was represented graphical for all cases (Figures 1-4).

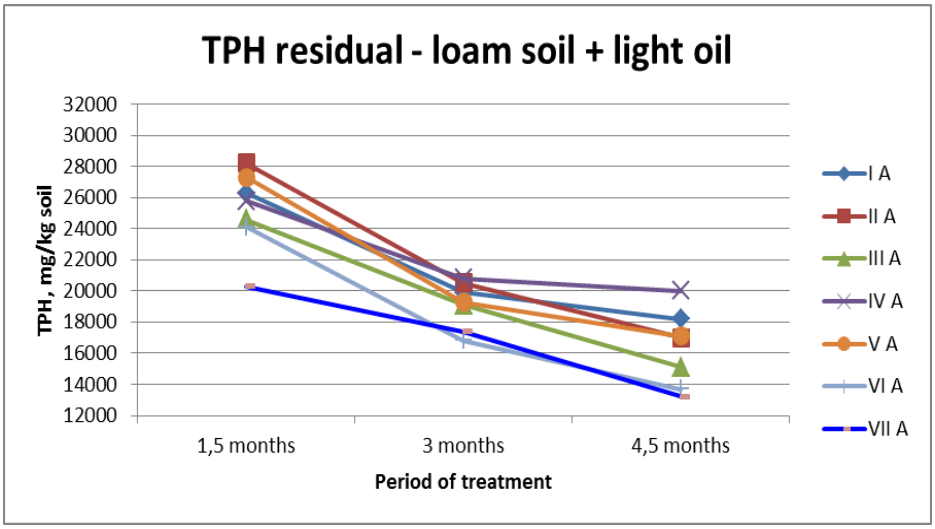

Fig. 1. – TPH residual for loam soil + light oil during 4.5 months of treatment treatment

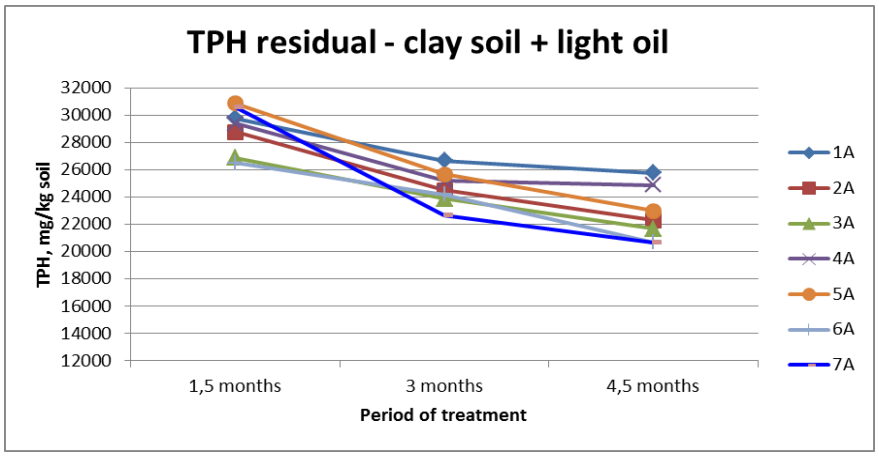

Fig. 2. – TPH residual for clay soil + light oil during 4.5 months of treatment treatment

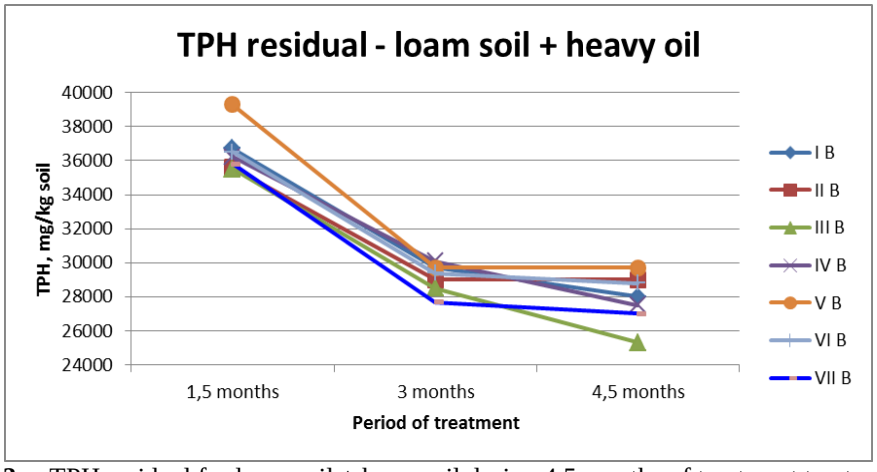

Fig. 3. – TPH residual for loam soil + heavy oil during 4.5 months of treatment treatment

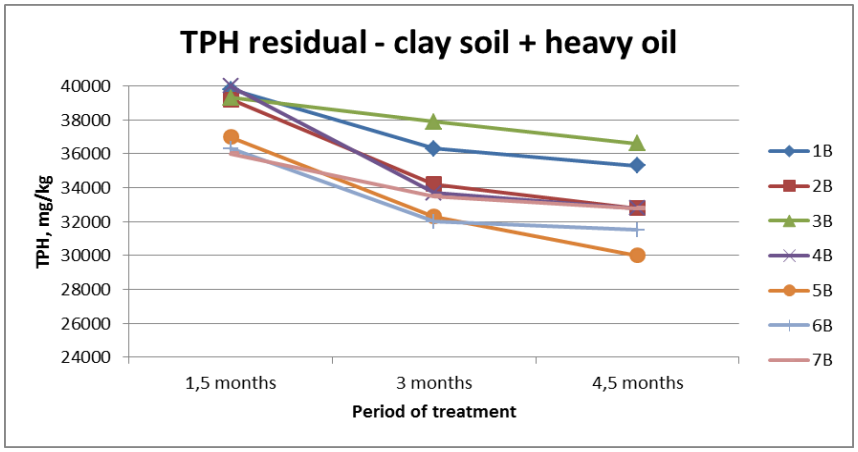

Fig. 4. – TPH residual for clay soil + heavy oil during 4.5 months of treatment treatment

The highest decrease in TPH concentration for soil samples occurred in the case of loam soil contaminated with light oil (from 5% to 1%), after about 5 months treatment with inoculum, NPK nutrients, straw as loosing agents, surfactants. This is due to the fact that:

- light oil is biodegradated faster than an oil that has heavier hydrocarbons in its composition;
- loam soil allows easier penetration of the air into its structure, facilitating access of bacteria to oxygen;
- the straw has also increased soil permeability;
- the surfactant has improved bacterial access to the contaminant in order to degrade it.

The smallest proportion of biodegradable crude oil was recorded in the case of clay soil contaminated with heavy oil (a decrease in TPH concentration from 5% to 3%), both because of the presence of heavier hydrocarbons that are more difficult to biodegrade and due to clay soil in which the oxygen penetrates harder, so that because of these more difficult conditions the bacteria grow more slowly.

For the other cases, intermediate decreases were recorded: for clay soil contaminated with light oil, TPH concentration decreased from 5% to 2% and for loam soil contaminated with heavy oil the decrease was from 5% to 2.5%.

The efficiency of the bioremediation process for soils contaminated with light oil was also evaluated by determining the C17/pristane and C18/phytane ratios. C17 (N-heptadecane) and C18 (N-octadecane) are easily biodegradable than pristane (2,6,10,14 tetramethyl pentadecane) and phythane (2,6,10,14 tetramethyl hexadecane) [3]. These reports remain constant by evaporation, but are greatly reduced by the biodegradation of crude oil. The lower the C17/pristan and C18/fitan ratios, the more biodegradable the oil [4].

The results for C17/pristane and C18/phytane ratios are presentd in Tables 7-10.

Table 7

C17/pristane ratios – loam soil+light oil

	C17/PRISTANE initial analysis	C17/PRISTANE 1,5 months	C17/PRISTANE 3 months	C17/PRISTANE 4,5 months
I A	1,33	1,26	0,35	0,20
II A	1,33	1,26	0,33	0,32
III A	1,33	0,94	0,31	0,20
Container code	1,33	1,21	0,38	0,28
V A	1,33	1,23	0,28	0,15
VI A	1,33	0,93	0,20	0,20
VII A	1,33	0,54	0	0

Table 8

C18/phytane ratios– loam soil+light oil

Container code	C18/PHYTANE initial analysis	C18/PHYTANE 1,5 months	C18/PHYTANE 3 months	C18/PHYTANE 4,5 months
I A	2,25	1,91	0,72	0,43
II A	2,25	2,10	0,73	0,63
III A	2,25	1,69	0,65	0,47
IV A	2,25	1,99	0,76	0,59
V A	2,25	2,05	0,60	0,38
VI A	2,25	1,62	0,33	0,3
VII A	2,25	0,99	0	0

Table 9

C17/pristane ratios – clay soil+light oil

Container code	C17/PRISTANE initial analysis	C17/PRISTANE 1,5 months	C17/PRISTANE 3 months	C17/PRISTANE 4,5 months
1A	1,33	1,31	1,00	1,00
2A	1,33	1,33	0,90	0,78
3A	1,33	1,30	0,91	0,7
4A	1,33	1,30	0,98	0,91
5A	1,33	1,30	0,90	0,90
6A	1,33	1,25	0,89	0,58
7A	1,33	1,27	0,76	0,65

Table 10

C18/phytane ratios– clay soil+light oil

Container code	C18/PHYTANE initial analysis	C18/PHYTANE 1,5 months	C18/PHYTANE 3 months	C18/PHYTANE 4,5 months
1A	2,25	2,15	1,77	1,77
2A	2,25	2,20	1,60	1,41
3A	2,25	2,20	1,48	1,29
4A	2,25	2,25	1,70	1,62
5A	2,25	2,25	1,85	1,51
6A	2,25	2,03	1,52	0,96
7A	2,25	2,11	1,34	1,00

The results obtained for C17/pristane and C18/phytane ratios from soil samples contaminated with light oil confirm that the highest rate of biodegradation occurred for loam soil contaminated with light oil treated with inoculum, NPK nutrients, straw as loosing agents, surfactants, for which C17/pristane decreased from 1.33 to 0 after 3 months of treatment, and

C18/phytanes also decrease from 2.25 to 0 after 3 months of treatment. In the case of clay soil contaminated with light oil, there was a lower decrease for C17/pristane and C18/phytane ratios, due to the fact that the rate of hydrocarbon biodegradability in clay soil was lower than loam soil.

Bioremedition program for soils contaminated with oil

Following the laboratory tests, a bioremediation treatment is proposed for the soils polluted with crude oil, which are added as biodegradation process stimulants: inoculum, fertilizers, loosing agents and biodegradable surfactant:

- adding of :
  - **Inoculum** – 10 ml inoculum/kg soil (for new contamination)
  - **Fertilizers** – added monthly in doses of:
    - 300 mg NH_4NO_3/kg soil
    - 17 mg P/kg soil
    - 23 mg K/kg soil
  - **Loosing agents** (straw, hay, sawdust): 10-50 g straw/kg soil;
  - **Water**: periodically added, depending on weather conditions, so that the humidity is between 12-30% (% by weight);
  - **Biodegradable surfactant** (solution 10%): 10 ml/kg soil;
- aeration, homogenization and incorporation of materials into the soil achieved through agricultural works (plowing) – for in-situ bioremediation or by a special equipment for ex-situ bioremediation.

4. Conclusions

► The rate of biodegradation of crude oil strongly depends on the type of oil and the nature of the soil, the highest rate of biodegradation of crude oil was obtained for loam soil contaminated with light oil and the lowest rate was recorded for clay soil contaminated heavy oil.

► The biodegradation rate was improved by the addition of inoculum, nutrients, loosing agents (straw), biodegradable surfactant.

► Biodegradation of crude oil is an economical method applicable to remediation of contaminated soil under the following conditions: warm season (temperature 10-45^{0}C), adding inoculum, nutrients, loosing agents (straw), biodegradable surfactant and the results were:

- Loam soil + light oil: TPH decreased from 5% to 1% in about 5 months
- Clay soil + light oil: TPH decreased from 5% to 2% in about 5 months

- Loam soil + heavy oil: TPH decreased from 5% to 2,5% in about 5 months
- Clay soil + heavy oil: TPH decreased from 5% to 3% in about 5 months.

REFERENCES

[1] Dumitru M., Toti M., Ceauşu C., Constantin C., Voiculescu A., Căpitanu V., Pârvulescu E., Popa D., Bioremediation of petroleum contaminated soils, *Soil Science*, no.1-2, (1998), 163-165.

[2] Koshlaf E., Ball S. A., Soil bioremediation approaches for petroleum hydrocarbon polluted environments, *AIMS Microbiology*, 3(1), (2017), 25-49.

[3] Connell W. D., *Basic Concepts of Environmental Chemistry*, Second Edition, Taylor & Francis Group, (2005), 116.

[4] Fingas M., *Oil Spill Science and Technology*, Second Edition, Elsevier Inc, (2017), 243.

[5] Macaulay B.M., Rees D., Bioremediation of oil spills: a review of challenges for research advancement, *Annals of Environmental Science*, Vol. 8, (2014), 9-37.

[6] Boopathy R., Factors limiting bioremediation technologies, *Bioresource Technology*, 74(1), (2000), 63-67.

[7] https://www.epa.gov/sites/production/files/2014-03/documents/tum_ch5.pdf

[8] Jergensen K. S., Puustinen J., Suortti A. M., Bioremediation of petroleum hydrocarbon-contaminated soil by composting biopiles, *Environmental Pollution*, 107, (2000), 245-254.

[9] http://dx.doi.org/10.4061/2011/941810

[10] Lixandru G., Caramete C., Marin N., Calancea L., Goian M., Hera C., Borlan Z., Rauta C., *Agrochimie*, Editura Didactica si Pedagogica Bucuresti, (1990), 24-145.

[11] Madjar R., Davidescu V., *Agrochimie*, USAMV Bucuresti, (2009), 99-101.

[12] https://clu-in.org/download/techfocus/bio/Landfarming-OSC.pdf

[13] Canadian Society of Soil Science, *Soil sampling and methods of analysis*, Second Edition, Edited by Carter M. R., Gregorich E. G., (2008), 163-168.

[14] American Water Works Association AWWA, *Standard Methods for the Examination of Water & Wastewater*, 23-nd Edition, Edited by Rodger B. Baird, (2017), 3-20 – 5-45.

[15] Order 756/1997, Minister of Waters, Forests and Environmental Protection, for the approval of the Regulation on environmental pollution assessment, Official Monitor of Romania, part I

[16] Walworth J., Pond A., Snape I., Rayner J, Ferguson S., Harvey P., Nitrogen requirements for maximizing petroleum bioremediation in a sub-Antartic soil, *Cold Regions Science and Technology*, (2007), 48.

[17] Braddock, J.F., Ruth, M.L., Catterall, P.H., Walworth, J.L., McCarthy, K.A., Enhancement and inhibition of microbial activity in hydrocarbon-contaminated Arctic soils: implications for nutrientamended bioremediation, *Environmental Science and Technology*, 31 (7), (1997), 2078–2084.

[18] Dumitran, C., Onutu, I., Environmental Risk analysis for crude oil soil pollution, *Carpathian Journal of Earth and Environmental Sciences*, Vol. 5, No. 1, (2010), 83.

[19] Stoica M. E., Avram L., Cristescu T., Bioremediation Use in Order to Decontaminate Polluted Soils Infested with Liquid Hydrocarbons, *REV. CHEM.* (Bucharest), 65, 12, (2014), 1507.

BREAK-POINT CHLORINATION DRAWBACKS FOR A COMPLEX IMPURIFIED GROUNDWATER SOURCES (NH_4, Fe, Mn) POTABILIZATION TREATMENT

Cristiana COSMA, Ion Viorel PĂTROESCU*, Ioana Alexandra IONESCU, Ionuț CRISTEA, Mirela Alina CONSTANTIN

National Research and Development Institute for Industrial Ecology – ECOIND, 71-73 Drumul Podu Dambovitei Street, 060652, Bucharest, Romania

Abstract

Chlorine is the only chemical oxidant used in drinking water treatment for the ammonium removal. Break point chlorination takes place at a pH range of 7-8 with significant efficiencies, the chlorine demand for oxidation of $N\text{-}NH_4^+$ being influenced by pH, $N\text{-}NH_4^+$ concentration, Cl_2: $N\text{-}NH_4^+$ ratio and temperature. Taking into consideration chlorine reactivity against most of the inorganically oxidable compounds (NH_4^+, NO_2^-, SO_3^{2-}, S^{2-}, Fe^{2+}, Mn^{2+}, Br^-) and organic compounds (humic acids, organic compounds with nitrogen within the molecule) the chlorine dose for $N\text{-}NH_4^+$ oxidation varies across a large domain Cl_2: $N\text{-}NH_4^+$ = (7.6 ÷ 20) : 1, being experimentally determined for each source that requires treatment. For a special case of an impurification matrix resulting from the association between $N\text{-}NH_4^+$ concentrations above 1 mg /L, alkalinity < 200 mg HCO_3^-/L and organic nitrogen compounds (organic N > 1 mg/L), the impossibility of a practical treatment was demonstrated do to: (1) the chlorine action on the organic nitrogen structures that leads to their degradation with ammonium release, there for the chlorine demand for initial NH_4^+ + the formed NH_4^+ oxidation being very high, above 60 mg/L and (2) the water pH becomes acid (pH = 3-5) during the chlorination process due to the low buffering capacity of the water. In this paper chlorine treatment at different Cl_2: NH_4^+ ratios under specific work conditions is presented comparatively for a few groundwater containing a variable amount of $N\text{-}NH_4$ (0.96 ÷ 2.35 mg/L) and organic N (0.04 – 1 mg/L). The article presents the reagent selection (Cl_2, $KMnO_4$, ClO_2) and the oxidation parameters (pH, dose, reaction time) of Mn^{2+} found in the groundwater source in concentrations of 83-92 µg/L. Furthermore, the adapted water treatment flow for groundwater with this type of impurification matrix is also presented.

Key words: groundwater, manganese, ammonium, organic nitrogen, break-point chlorination, water treatment flow

1. Introduction

It is estimated that in the European Union, raw and groundwater sources provide approx. 90% of consumed drinking water, approx. 50% of which comes from underground sources [1]. Although Romania did not submit data to be included in the previous assessment, the use of groundwater in water treatment flows is

* Corresponding author; E-mail address: viorel.patroescu@incdecoind.ro

widespread in our country. Among the main polluters often found in Romania groundwater sources are iron, manganese and ammonia [2], [3].
Even without a proved direct relevance to human health, drinking water ammonium concentration is limited to 0.5 mg/L, due to the main disinfectant used in Romania which is chlorine. Ammonium reacts with chlorine and therefore compromises the water disinfection prior to consumers delivery. Another operational problem induced by the ammonium presence is the formation of secondary chlorine reaction products (chloramines), which can organoleptically affect the drinking water quality.
Although they generally do not cause health problems in the usual groundwater concentrations, they can affect the drinking water organoleptic characteristics and may create operational problems, the concentrations of iron and manganese in drinking water are restricted to 200 μg/L and, respectively, 50 μg/L [4].
Common methods applied for ammonium removal from groundwater sources are represented by break-point chlorination, described in reaction (1) and biological nitrification [5], [6].

$$NH_4^+ + 1.5HOCl \rightarrow 0.5N_2 + 1.5H_2O + 2.5H^+ + 1.5Cl^- \quad (1)$$

The main removal methods for dissolved iron and manganese from groundwater are the oxidative ones [7], [8], [9] using various reagents (O_2, O_3, HOCl, $KMnO_4$, ClO_2). The processes of interest for the present paper are described by the following reactions:

$$2Fe^{2+} + 1/2O_2\,(aq) + 5H_2O \rightarrow 2Fe(OH)_3\,(s) + 4H^+ \quad (2)$$
$$Mn^{2+} + HOCl + H_2O \rightarrow MnO_2\,(s) + Cl^- + 3H^+ \quad (3)$$
$$3Mn^{2+} + 2MnO_4^- + 2H_2O \rightarrow 5MnO_2\,(s) + 4H^+ \quad (4)$$
$$Mn^{2+} + 2ClO_2 + 2H_2O \rightarrow MnO_2\,(s) + 2ClO_2^- + 4H \quad (5)$$

The paper presents a case study of a southwest Romanian location (Rovinari, Gorj), where it is intended to supply the existing drinking water system with additional groundwater sources (4 wells and their mixing) that have a complex impurification (ammonium, manganese, iron). The study main objectives were to evaluate the possibility of ammonium oxidation by break-point chlorination and manganese oxidation with various oxidizing agents by choosing the most suitable reagent and setting the reaction conditions, at experimental laboratory level, as well as establishing the recommended water treatment flow according to the groundwater sources contamination.

2. Materials and methods

Parameters determination was done according to standard methods: iron – SR 13315:1996/C91:2008, manganese – SR 8662-2:1996, ammonium – SR EN ISO

14911:2006, total Kjeldahl nitrogen (TKN) – SR EN 25663:2000, total organic carbon (TOC) – SR EN 1484:2006, trihalomethanes (THM) – SR EN ISO 10301:2003, chlorine – SR EN ISO 7393-1:2002, pH – SR EN ISO 10523:2012, alkalinity – SR EN ISO 9963-1:2002.

3. Results and discussions

3.1. Groundwater noncompliant parameters identification

Analytical investigations have shown that the major pollution, common to all sources intended for potabilisation - four wells and their mixing, is due to the presence of ammonium, iron and manganese:

- ammonium - NH_4^+ (MAC = 0,5 mg/L): 0.21-3.86 mg/L;
- total iron - Fe_t (MAC = 200 µg/L): 105-1282 µg/l (of which Fe^{2+} = 1 - 5% of Fe_t);
- total manganese - Mn_t (MAC = 50 µg/L): 4-130 µg/l (of which Mn^{2+} = 75 - 91% of Mn_t).

3.2 Treatability tests

3.2.1 Ammonium oxidation by break - point chlorination

Prior to the break-point chlorination experiments, preliminary experiments were conducted in order to determine the trihalomethanes formation potential. The results are shown graphically in Fig. 1, with the following conclusions:

- ammonium oxidation by break-point chlorination leads to THMs concentrations much lower than the maximum admissible concentration (MAC = 100 µg/L). This fact can be explained by the low reactivity of the organic load present in the raw water (globally evaluated by TOC <1 mg/L) towards chlorine;
- therefore, break-point chlorination can be applied in this case without the danger of exceeding the maximum admissible concentration for trihalomethanes.

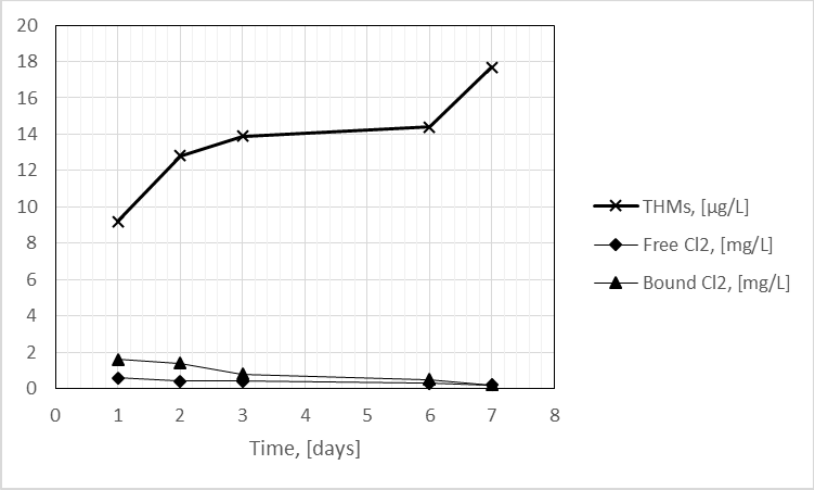

Fig. 1. Evolution of THMs, free Cl_2 and bound Cl_2 concentrations vs. time, within initial conditions TOC = 0.9 mg/L, NH_4^+ = 1.4 mg/L, Cl_2:NH_4-N = 10:1, pH = 7.2

NH_4^+ oxidation tests by break-point chlorination led to the results graphically presented in Fig.2 and Fig.3.

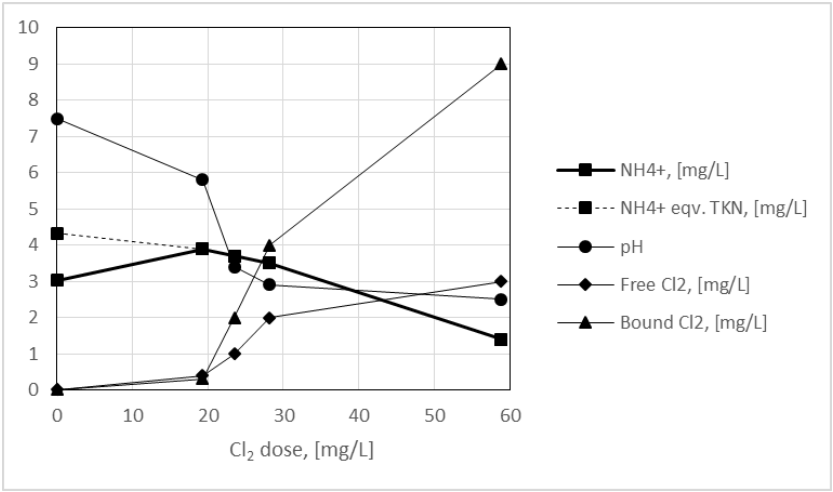

Fig. 2. Chlorine dose influence on NH_4^+, free Cl_2, bound Cl_2 concentrations and pH at ammonium oxidation by break-point chlorination for 40 minutes, within initial conditions NH_4-N = 2.35 mg/L, TKN = 3.36 mg/L

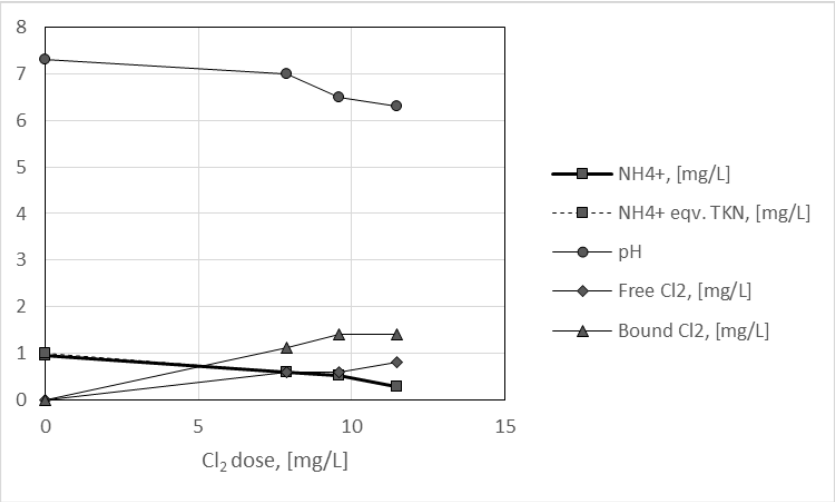

Fig. 3. Chlorine dose influence on NH_4^+, free Cl_2, bound Cl_2 concentrations and pH at ammonium oxidation by break-point chlorination for 40 minutes, within initial conditions NH_4-N = 0.96 mg/L, TKN = 1 mg/L

The graphical data analysis led to the following conclusions:

- at ammonium oxidation by break-point chlorination oxidation, the presence of organic nitrogen in the water results in an increased effect of the initial ammonium concentration up to TKN equivalent by organic nitrogen compounds oxidation. This leads to a significant increase of the needed chlorine dose. In the example presented in Fig.2, at a significant initial concentration of organic nitrogen (1 mg/L), the applied dose (Cl_2: TKN = 17.5) is much higher than the stoichiometric dose (Cl_2: NH_4-N = 7.6) and much higher than the dose used in the example presented in Fig. 3 (Cl_2:TKN = 11.5) for an initial low concentration of organic nitrogen (0.04 mg/L);
- in the case of large initial TKN concentrations (Fig. 2), chlorine break-point oxidation, even at high doses, does not achieve the maximum admissible ammonium value (MAC = 0.5 mg/ L);
- in the case of large initial TKN concentrations (Fig.2), chlorine break-point oxidation leads to high free and bound residual chlorine values situated above the maximum admissible value (MAC = 0.5 mg/L);
- in the case of large initial TKN concentrations (Fig. 2), chlorine break-point oxidation leads to a severe pH drop due to the high chlorine dose used and poor water buffering capacity (alkalinity < 200 mg HCO_3^-/L);
- therefore, ammonium chlorine oxidation is not recommended for NH_4-N concentrations > 1 mg/L.

3.2.2 Manganese oxidation and precipitation

Oxidation tests for Mn (reduced state/Mn^{2+}) present in the raw groundwater were carried out using three chemical agents: Cl_2, $KMnO_4$, ClO_2, under specific pH, contact time and doses conditions. The results are graphically presented in Fig. 4, Fig.5 and Fig.6.

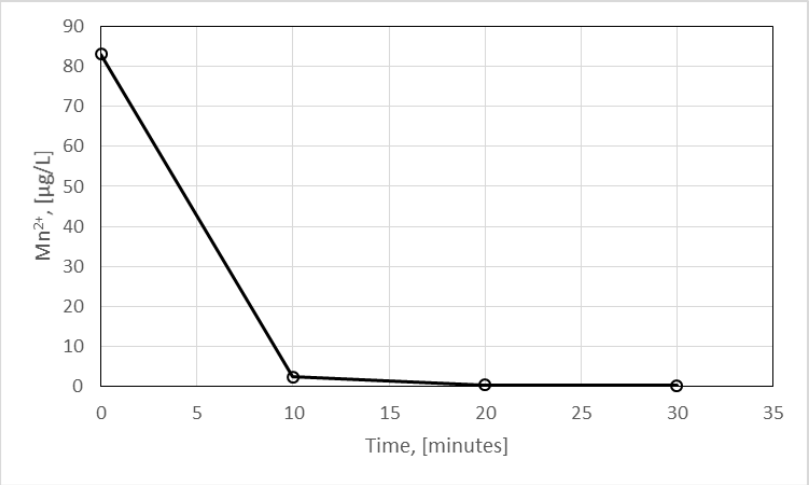

Fig. 4. Evolution of Mn^{2+} concentration vs. time for manganese oxidation with Cl_2, for an applied Cl_2 dose of 1 mg/L and a pH initially adjusted from 7.1 to 8.5 with 28 mg NaOH/L

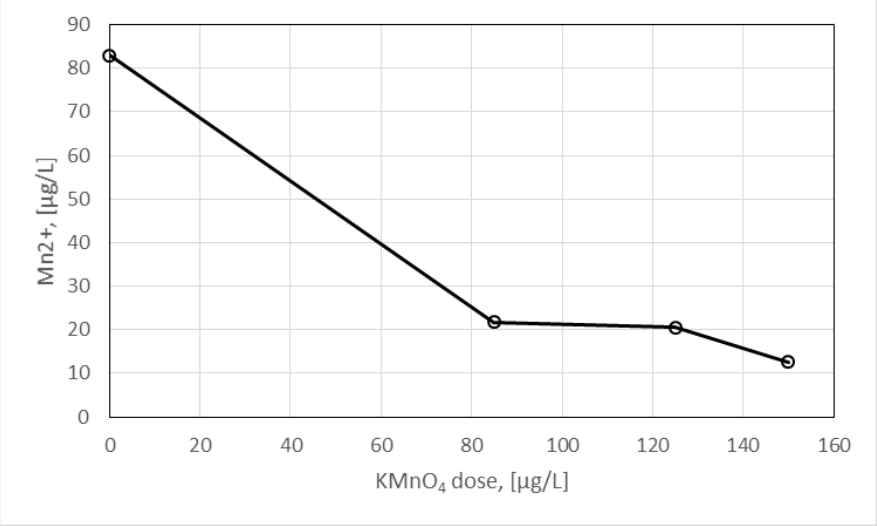

Fig. 5. $KMnO_4$ dose influence over Mn^{2+} concentration for 30 minutes manganese oxidation (initial pH = 7.1, final pH = 7.4-7.7)

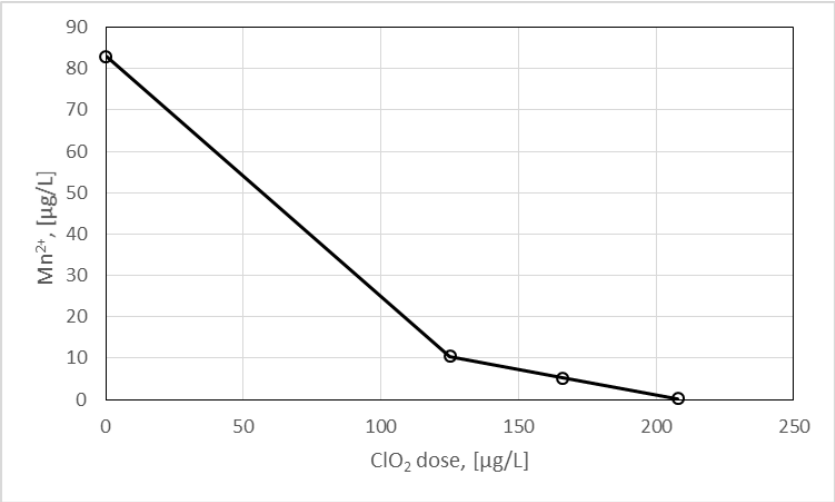

Fig. 6. ClO_2 dose influence over Mn^{2+} concentration for 30 minutes manganese oxidation (initial pH = 7.1, final pH = 76.5 – 6.9)

The analysis of graphical data presented in Fig.4, 5 and 6 led to the following conclusions:

- Mn^{2+} oxidation with Cl_2, leads to a residual concentrations of soluble manganese lower than MAC = 50 µg/L, takes place at a weak alkaline pH obtained by correcting the raw water, within less than 30 minutes reaction time at a Cl_2 dose = 1 mg/L, approx. nine times higher than the stoichiometric dose (1.3 mg Cl_2/mg Mn^{2+} + 0.63 mg Cl_2/mg Fe^{2+});
- Mn^{2+} oxidation with $KMnO_4$, leads to a residual concentrations of soluble manganese lower than MAC = 50 µg/L, takes place at doses lower than the stoichiometric one (1.92 mg $KMnO_4$/mg Mn^{2+}) within less than 30 minutes reaction time and a recommended pH of at least 7.2;
- Mn^{2+} oxidation with ClO_2, results in residual concentrations of soluble manganese lower than MAC = 50 µg/L, takes place at doses close to the stoichiometric one (2.45 mg ClO_2/ mg Mn^{2+}) and a 30 minutes reaction time.
- taking into consideration the obtained results and subsequent implications of chlorinated compounds use (Cl_2 - pH correction, bound chlorine formation; ClO_2 - secondary products formation such as chlorites, chlorates), the recommended oxidant is $KMnO_4$ (dose below stoichiometric requirements, reaction times less than 30 minutes).

3.3 Setting up treatment options

In order to correct the nonconformities pointed out in paragraph 3.1. and taking into consideration the conclusions of the treatability tests presented in paragraph 3.2. the following water treatment flow for the compliance of drinking water quality with the imposed legislation was proposed. The following steps are included:

- aeration for Fe^{2+} oxidation and iron oxyhydroxide precipitation;
- Mn^{2+} oxidation and MnO_2 precipitation in the presence of $KMnO_4$ at doses below the stoichiometric requirement ($KMnO_4 \leq 0{,}15$ g/m^3);
- sand filtration in order to retain the precipitates formed in previous oxidation steps;
- aerobic biological nitrification in a biofilter system for NH_4^+ to NO_3^- oxidation;
- sand filtration for suspended solids retention;
- chlorine disinfection.

***Acknowledgement**: Experimental results were obtain within the PN 18 - 05 03 01, carried out with the Ministry of Research and Innovation support.*

REFERENCES

[1]. van der Hoek, J. P., Bertelkamp, C., Verliefde A. R., Singhal, N., Practical Paper. Drinking water treatment technologies in Europe: state of the art-challengies-research needs, *Journal of Water Supply: Research and Technology-AQUA*, 63(2), (2014), 124-130.

[2]. Racoviteanu, G., Vulpasu, E., Iron and manganese removal from difficult ground water sources, *Acta Technica Napocensis: Civil Engineering & Architecture*, 56(4), (2013), 22-32.

[3]. Adumitroaei, M. V., Gavriloaiei, T., Sandu, A. V., Iancu, G. O., Distribution of Mineral Compounds in Groundwater in Vaslui County (Romania), *Rev. Chim.(Bucharest)*, 67(12), (2016), 2530-2536.

[4]. Parlamentul Romaniei, Legea nr. 458(r1)/2002 privind calitatea apei potabile, actualizata, *Buletinul Oficial al Romaniei*, Partea I, nr. 875, (2011).

[5]. US Environmental Protection Agency, Office of Research and Development, Office of Water, Manual: Nitrogen Control, *EPA/625R-93/010*, (1993), 44-97.
[6]. Johnson, M., Ratnayaka, D. D., Brandt, M. J., Twort's Water Supply, 6th Edition, *Elsevier Ltd.*, (2009), 390-435.
[7]. AWWA Research Foundation, Compagne General des Eaux, Ozone in Water Treatment: Application and Engineering, Cooperative Research Report, *Lewis Publishers Inc*., (1991), 138-143.
[8]. Tobiason, J. E., Bazilio, A., Goodwill J., Mai, X., Nguyen, C., Manganese Removal from Drinking Water Sources, *Current Pollution Reports*, 2, (2016), 124-130.
[9]. Elsheikh M., Guirguis, H., Fathy A., Removal of iron and manganese from groundwater: a study of using potassium permanganate and sedimentation, BCEE3-2017, *MATEC Web of Conferences*, vol.162, art. no. 05018, (2018).

EMPHASIZING THE CELLULOSE CONTAINING WASTES PRETREATMENT, IN ORDER TO MAKE THEM MORE AVAILABLE TO FURTHER BIOSYNTHESIS

Ana-Despina IONESCU*, Angela CĂŞĂRICĂ, Irina LUPESCU, Roxana-Mădălina STOICA

National Institute for Chemical-Pharmaceutical Research and Development – ICCF,
112 Vitan Avenue, District 3, 031299, Bucharest, Romania

Abstract

This paper presents the obtained results concerning the optimization of the cellulose containing wastes pretreatment, in order to make them more available for the fungal enzymatic attack. The cellulase is an enzyme complex which breaks down cellulose to beta-glucose. It is produced mainly by symbiotic bacteria in the ruminating chambers of herbivores. Aside from ruminants, most animals (including humans) do not produce cellulase, and are therefore unable to use most of the energy contained in plant material. Cellulase refers to a family of enzymes which act in concert to hydrolyze cellulose. Cellulases are widely distributed throughout the biosphere and are most manifest in fungal and microbial organisms [1]. Our studies were carried out by using fungal strains, selected from the natural sources by a specific screening and without any genetic engineering applications, in order to realize a technology friendly with the environment. The studied parameters were represented by a thermal pretreatment and then the use of different doses of some chemical reagents. The substrates consisted in few mixed wild plants or a mix containing straw and stalks [2].

When the hydrolysis tests were conducted only with a complex based on cellulases, the obtained glucose was further used as a substrate for obtaining yeasts biomass or ethyl alcohol, while an additional step of hydrolysis made by using the laccase may conduct us to obtain biogas from lignocellulosic grain wastes like straw and stalks.

Key words: cellulose, wastes, pretreatment

* Corresponding author: Email address: ionescudespina@yahoo.com

1. Introduction

This paper presents the obtained results concerning the optimization of the cellulose containing wastes pretreatment, in order to make them more available for the fungal enzymatic attack.

The cellulase is an enzyme complex which breaks down cellulose to beta glucose. It is produced mainly by symbiotic bacteria in the ruminating chambers of herbivores. Aside from ruminants, most animals (including humans) do not produce cellulase, and are therefore unable to use most of the energy contained in plant material.

Cellulase refers to a family of enzymes which act in concert to hydrolyze cellulose. Cellulases are widely distributed throughout the biosphere and are most manifest in fungal and microbial organisms [1].

Our studies were carried out by using fungal strains, selected from the natural sources by a specific screening and without any genetic engineering applications, in order to realize a technology friendly with the environment.

Our studies were carried out by using fungal strains, selected from the natural sources by a specific screening and without any genetic engineering applications, in order to realize a technology friendly with the environment.

The studied parameters were represented by a thermal pretreatment and then the use of different doses of some chemical reagents. The substrates consisted in few mixed wild plants or a mix containing straw and stalks [2].

When the hydrolysis tests were conducted only with a complex based on cellulases, the obtained glucose was further used as a substrate for obtaining yeasts biomass or ethyl alcohol, while an additional step of hydrolysis made by using the laccase may conduct us to obtain biogas from lignocellulosic grain wastes like straw and stalks. While the final expected result is to obtain the biogas, our study describes a new procedure for a controlled hydrolysis of the lignocellulosic grain wastes, in order to obtain a higher level of biogas by using available raw materials and a better protection of the environment.

Biogas typically refers to a gas produced by the biological breakdown of organic matter in the absence of oxygen. Modern technologies for biogas obtaining aimed not only to use the organic wastes traditionally used for this purpose, but also the pre-and post-food wastes, green wastes (grass cuttings, wood chips from logging), waste paper, waste lipids sewage with plant and animal origin and the wastewaters. In many European countries there are used for biogas production, some

mixtures of animal manure and vegetable substrates, energy plants grown specifically for this purpose and which are used entirely, i.e. maize and sunflower [1].

The gases methane, hydrogen and carbon monoxide can be combusted or oxidized with oxygen. This energy release allows biogas to be used as a fuel. Biogas can be used as a low-cost fuel in any country for any heating purpose, such as cooking. It can also be utilized in modern waste management facilities where it can be used to run any type of heat engine, to generate either mechanical or electrical power. Biogas is a renewable fuel and electricity produced from it can be used to attract renewable energy subsidies in some parts of the world.

Biogas can be produced utilizing anaerobic digesters. The composition of biogas varies depending upon the origin of the anaerobic digestion process. Landfill gas typically has methane concentrations around 50 %. Advanced waste treatment technologies can produce biogas with 55-75 % CH_4.

Methane within biogas can be concentrated to the same standards as natural gas, when it is, it is called biomethane. If the local gas network permits it, the producer of the biogas may be able to utilize the local gas distribution networks. Gas must be very clean and must be of the correct composition for the local distribution network to accept. Carbon dioxide, water, hydrogen sulfide and particulates must be removed if present. If concentrated and compressed it can be also used in vehicle transportation [3, 4]. The European Union presently has some of the strictest legislation regarding waste management and landfill sites, called the Landfill Directive. The average composition of the biogas is presented in Table 1.

Table 1

Literature data concerning typical composition of biogas

Matter	**%**
Methane, CH_4	50-75
Carbon dioxide , CO_2	25-50
Nitrogen , N_2	0-10
Hydrogen, H_2	0-1
Hydrogen sulfide , H_2S	0-3
Oxygen , O_2	0-2

2. Materials and methods

For the case of obtaining the glucose as final product, two types of substrates are presented here. That one named “A” consists in a mixture of *Dactylis glomerulata* and *Medicago sativa* (alfalfa). The variant named “B” was brought from a grassland with unfertilized soil.

Both substrates were first milled and dried for 30 min at 80°C and then they were sterilized 30 min at 120°C, each bottle containing 2 g of substrate and 100 mL water. The next step was represented by the 1- 4 ml H_2SO4 or NaOH addition, followed by a new sterilization during 45 min at 120°C.

After this pretreatment, the substrates were supplemented with some cellulases complexes, previously obtained in our laboratory by using different selected *Aspergillus sp*. strains and named as AnM3 (24.14 Cx activity U/mL/h/50 °C), AN6 (22,65 Cx activity U/mL/h/50°C and AN48 (22,72 Cx activity U/mL/h/50°C). The witness sample did not received any chemical supplement. The hydrolysis results were expressed as sugar concentration (wt. %) after 48 hours of enzymes attack at 50°C. For the second research pattern, when the biogas represents the final task, the used materials and methods are more complicated.

2.1. The substrates

Using agricultural grain wastes as single carbon and energy source for biogas production is not yet described in the literature. There is presented only the lignocellulosic grain wastes recovery especially for bioethanol [2], while for biogas production are mentioned recently only wastes resulted from vegetables and fruits [3].

Unfortunately, a large part of lignocellulosic wastes are lost by burning them on the field, a process extended to the entire planet, although huge quantities of biomass (made up of plant wastes) represent a potential source of useful byproducts.

This new technology can be applied also by using as substrates some wastes resulted from wood and paper industry, or large amounts of wastes generated by the agricultural and forestry processing, which raises serious environmental pollution problems.

Numerous residues [5] are available as lignocellulosic biomass resources, as shown in Table 2.

Regardless of their origin, the lignocellulosic materials are composed of the same major components: cellulose, hemicellulose and lignin, to varying degrees, as shown in Table 3 [6, 7].

Table 2

Types of lignocellulosic materials and their current use [5]

The source of lignocellulosic materials	The agricultural waste	The waste's current use
Grain harvest (wheat, rice, barley, oats and maize)	Straw, corn cobs, stalks, husks)	Feed, fuel (burning), soil care
Grain processing (maize, wheat, barley, soy)	Wastewater, bran	Feed
Harvesting of fruits and vegetables	Seeds, shells, kernel, fallen whole fruits, juice	Animal and fish feed, oil extraction from certain grains
Fruits and vegetables processing	Seeds, shells, kernel, degraded whole fruits. Wastewater	
Cane and other sugary products	Pulp	Fuel (burning)
Oil plants and seeds, nuts, cottonseed, olives, soy	Shells, fibers, pressed sludge. Wastewater	Feed, fertilizers, fuel
Animal manure	Manure	Soil care
Forestry, wood and paper industry		
Logs harvesting	Wood residues, bark, leaves	Soil care, fuel
Waste timber and plywood	Shavings, wood powder, sawdust	Pulp and paper industry, cardboard from shavings and fibers
Pulp and paper plants	Waste fibers, sulfite lye	Reused as fuel in paper and cardboard industry
Lignocellulosic waste of the Community	Old newspapers, papers, cartons, furniture	Recycling (a small percentage), the rest as fuel
Grass	Unused grass	Burning

Of these 3 components, lignin is the most resistant to degradation, while the cellulose (due to its crystalline structure) is more resistant to hydrolysis than the hemicellulose. In these conditions, the efficiency of plant biomass recovery is possible only in case of existing efficient methods for lignocellulosic complex hydrolysis.

The bioprocess proposed in this paper comprises some steps of physical and enzymatic pre-treatment of the natural vegetable wastes, in order of dismissal carbohydrate polymers, which can then be used, as a hydrolyzed preparation, for a biogas producing anaerobic fermentation.

By the process proposed by us, there are obtained the delignification, decristallyzation and a partial hydrolysis of wastes resulted from the harvesting and the processing of grain, for example straw and stalks, as shown in Table 4.

Table 3

The lignocellulosic content of some lignocellulosic wastes [6, 7]

The lignocellulosic material	Cellulose (%)	Hemicellulose (%)	Lignin (%)
Strain of hardwood	40 -55	24 - 40	18 - 25
Strain of softwood	45 - 50	25 - 35	25 - 35
Nutshell	25 - 30	25 - 30	30 - 40
Corncobs	45	35	15
Paper	85 -99	0	0 - 15
Wheat straw	30	50	15
Rice straw	32	24	18
Scrap wood sorted	60	20	20
Leaves	15 -20	80 - 85	0
Fibers of cottonseeds	80 - 95	5 - 20	0
Newspapers	40 - 55	25 - 40	18 - 30
Paper residue from chemical processing	60 - 70	10 - 20	
Solid materials from primary aqueous wastes	8 - 15	NA	24 - 29
Fresh mash or pulp	33,4	30	18,9
Pig manure	6	28	NA
Solid manure of cattle	1,6 – 4,7	1,4 – 3,3	2,7 – 5,7
Herbs (average)	25 - 40	25 - 50	10 - 30

Table 4

The lignocellulosic wastes used and their characteristics

Current No.	The lignocellulosic material	Dry substance (%)	Cellulose content (%)	Lignin content (%)
1	Wheat straw	85	39,4	15
2	Barley straw	87	37 - 42	18
3	Corncobs	85	50,2	20,4

2.2. The enzimes

The new enzyme mixture used in order to get our task contains laccase (which is a phenol- oxidase) and another enzyme complex containing cellulases, beta-glucanase and xylanase. Some of these enzymes can be obtained also into our laboratory. Thus, we had carried out some experiments in order to obtain the cellulases, using different strains of *Aspergillus niger* and *Trichoderma viride* grown on different natural substrates, in batch systems or surface cultures (for example a medium with soybeans wastes and ground corn cobs, during 120 hours at a temperature of 28-30°C, in shaken flasks).

2.3. Methods used for the hydrolysis

In the first step of the hydrolysis, the substrate chopped by grinding is suspended in a minimum amount of water required to obtain a suspension fluid and then is subjected to thermal degradation, under steam pressure, by autoclaving. This done soaking up with water of the plant tissues until the supra-expansion state, lowering their strength and resistance to the action of enzymic hydrolysis.

In the second stage, the heat-pretreated material is treated successively with laccase and then with an enzyme complex containing cellulases, beta-glucanase and xylanase. Treatment with laccase allows partial delignification of the plant material. Laccase is added in a proportion of 0.5-15% compared with the weight of dry waste, within its aqueous suspension, at pH 5.5. The mixture must be incubated at 55°C with stirring for 10-20 hours. Subsequently laccase action is stopped, by heating the reaction mixture for 15 min at 95°C. Inactivation of laccase action is required because of its dangerous action over the enzymes to be used in further. The partial hydrolysis is carried further by treating plant material, already delignified, with the aforementioned enzyme complex. The enzymic preparation is added in a proportion of 1-20% compared with the weight of the dry plant material and the reaction mixture is incubated at 55-60°C, under stirring, for 4-10 hours. It results as a dense suspension containing the soluble reducing sugars at a level of 25-30 mg/ml, corresponding to a degree of hydrolysis of lignocellulosic substrate between 25-55%.

2.4. The quantitative determination of reducing sugars

In order to determine the concentration of reducing sugars resulted from each step of the experimental process, it was used the spectrophotometer method based on color reaction of reducing carbohydrates with 3,5-dinitrosalicylic acid reagent.

3. Results and discussion

The results obtained for the case of glucose as final expected product (substrate formed by *Dactylis glomerulata* and *Medicago sativa*, or by a grassland with unfertilized soil) are presented in the Table 5.

Table 5

The chemical influence on the plants mixtures hydrolysis

Sample no.	Substrate	Chemical pretreatment	Enzyme' source	Sugar concentration (wt. %) 0 hour	Sugar concentration (wt. %) 24 hours	Sugar concentration (wt. %) 48 hours
1	A	0	AnM3	0,08	0,248	0,450
2	A	0	AnM3	0	0,186	0,310
3	A	1mL H_2SO4	AnM3	0	0,093	0,240
4	A	1mL NaOH	AnM3	0	0,124	0,300
5	A	2mL NaOH	AnM3	0.09	0,186	0,500
6	A	2mL H_2SO4	AnM3	0,10	O,403	0,980
7	5	0	AnM3	0	0,155	0,348
8	5	0	AnM3	0,09	0,186	0,350
9	5	1mL H_2SO4	AnM3	0.10	0,248	0,540
10	5	1mL NaOH	AnM3	0	0,155	0,350
11	5	2mL NaOH	AnM3	0,10	0,300	0,600
12	5	2mL H_2SO4	AnM3	0,10	0,442	1,100
13	5	0	AN6	0	0,250	0,520
14	5	4mL H_2SO4	AN6	0	0,310	0,620
15	5	4mL H_2SO4	AN48	0	0,240	0,600
16	A	0	AN6	0	0,260	0,450
17	A	4mL H_2SO4	AN6	0	0,510	0,980
18	A	4mL H_2SO4	AN48	0	0,430	0,860

For the hydrolysis of the wheat straw barley straw and corncobs, the results obtained under different alkaline pretreatment parameters are presented in the following 3 Tables.

Table 6

The influence of the alkaline pretreatment on the wheat straw hydrolysis

Var	Iniţial mg/mL	2 h		4 h		20 h	
		mg/mL	□	mg/mL	□	mg/mL	□
1.	0,468	1,827	1,359	3,469	3,001	9,410	8,942
2.	0,510	2,120	1,610	8,379	7,869	16,915	16,405
3.	0,828	2,566	1,738	8,875	8,046	21,037	20,208
4.	0,708	2,674	1,966	9,007	8,299	24,597	23,888
5.	0,651	2,727	2,076	9,071	8,421	26,350	25,699

Table 7

The influence of the alkaline pretreatment on the barley straw hydrolysis

Var.	Iniţial mg/mL	2 h		4 h		20 h	
		mg/mL	□	mg/mL	□	mg/mL	□
1.	0,615	1,855	1,240	4,714	4,100	9,563	8,948
2.	0,665	2,246	1,582	8,641	7,976	18,202	17,538
3.	0,721	2,616	1,895	8,954	8,234	21,302	20,581
4.	0,651	2,647	1,997	9,093	8,443	24,990	24,339
5.	0,627	2,764	2,137	9,174	8,547	27,561	26,933

Table 8

The influence of the alkaline pretreatment on the corncobs hydrolysis

Var.	Iniţial mg/mL	2 h		4 h		20 h	
		mg/mL	□	mg/mL	□	mg/mL	□
1.	0,740	1,140	0,400	1,950	1,210	3,300	2,560
2.	0,770	1,260	0,490	3,290	2,520	6,295	5,525
3.	0,816	1,406	0,590	3,446	2,630	7,476	6,660

4. Conclusions

1. This paper presents the obtained results concerning the optimization of the cellulose containing wastes pretreatment, in order to make them more available for the fungal enzymatic attack.
2. Our studies were carried out by using fungal strains, selected from the natural sources by a specific screening and without any genetic engineering applications, in order to realize a technology friendly with the environment.
3. When the hydrolysis tests were conducted only with a complex based on cellulases, the obtained glucose was further used as a substrate for obtaining yeasts biomass or ethyl alcohol, while an additional step of hydrolysis made by using the laccase may conduct us to obtain biogas from lignocellulosic grain wastes like straw and stalks.
4. In both cases, the chemical and thermal pretreatment play a very important role for getting a more efficient vegetable wastes hydrolysis.
5. All around the world, there are obviously many restrictions on available material resources, which has made from their recycling a real necessity, and our technology can respond effectively to this problem.

REFERENCES

[1] IndoGulfGroup.com, 2011
[2] Ionescu A. D., Lupescu I., Moscovici M., Pattern 125 230, Procedeu biotehnologic de obtinere a biogazului pornind de la deseuri cerealiere lignocelulozice, The International Fair for Innovation, Timisoara, Romania, 2015.
[3] Varga E., Reczey K., Zacchi G., Optimization of steam pretreatment of corn stover to enhance enzymatic digestibility *Appl. Biochem. Biotechnol*., 114(1-3), (2004), 509-523.
[4] Costa-Fereira M., Matos de Sousa J., *Procedeengs of Bioenergy-I: From concept to Commercial Processes*, Tomar, Portugalia, 5-10.03.2006.
[5] Sun Y., Cheng J., Hydrolysis of lignocellulosic materials for ethanol production: a review, *Biores. Technol*., 83, (2002), 1-11.
[6] Kamm B., Kamm M., Schmidt M., Sarke I., Kelinpeter E., Chemical and biochemical generation of carbohydrates from lignocellulose-feedstock (*Lupinus nootkatensis*)—quantification of glucose, *Chemosphere*, 62(1), 97-105, 2006
[7] Kanuf M., Monirussaman M., *International Sugar Journal*, 106: 147-150, 2004

NOBLE METAL NANOPARTICLES FROM KOHLRABI PEEL: GREEN SYNTHESIS AND ANTIOXIDANT ACTIVITY

Ana-Alexandra SORESCU[1,2•], Alexandrina NUTA[1,3], Rodica-Mariana ION[1,2], Lorena IANCU[1], Cristina Lavinia NISTOR[1]

[1] The National Research and Development Institute for Chemistry and Petrochemistry – ICECHIM, 202 Splaiul Independentei Street, district 6, 060021, Bucharest,Romania
[2]Valahia University, Materials Dept., 13th Sinaia Alley,130004, Targoviste, Romania
[3]The Romanian Academy "Stefan S. Nicolau" Institute of Virology, 285 Mihai Bravu Avenue, Bucharest, Sector 3, Zip Code 030304

Abstract

In recent years there has been a constant progress regarding the methods used for the synthesis of different shaped metallic nanoparticles, focusing especially on noble metal nanoparticles such as silver nanoparticles (AgNPs) and gold nanoparticles (AuNPs) due to their numerous applications in different scientific fields. Different methods are used for the preparation of both AgNPs and AuNPs, involving both chemical and green routes. The present paper describes the green synthesis of silver nanoparticles (AgNPs) and gold nanoparticles (AuNPs) using aqueous extracts of pale-green and purple Kohlrabi peel (Brassica Oleracea Gongylodes Group), a vegetable with numerous health benefits. The potential capacity of the two species of Kohlrabi to bioreduce Ag^{+} to Ag^{0} was investigated by means of different spectral techniques (e.g.: FTIR, UV-Vis, absorption). UV-Vis spectra were recorded for both AgNPs and AuNPs at different times (0, 30, 60, 120 minutes and 24 h after synthesis) and the results are specific for both metallic nanoparticles. The size of the biosynthesized metallic nanoparticles was determined by means of diffraction light scattering measurements (DLS) and the results are in the nanometer range.

Key words: silver nanoparticles, gold nanoparticles, kohlrabi, green chemistry, phytochemicals

• Corresponding author: E-mail address: anaalexandrasorescu@yahoo.com

1. Introduction

Noble metal nanoparticles are of huge importance in the continuously growing field of nanotechnology due to their versatile properties and numerous applications in various scientific field [1-3]. Among noble metal nanoparticles, silver (Ag) and gold (Au) are of particular interest mostly because of their proven antibacterial properties that are known to mankind from prehistoric times but could only recent be understood at the nanoscale level [4]. Silver nanoparticles (AgNPs) do not modify the structure of living cells and, therefore, are unable to cause microbial resistance while gold nanoparticles (AuNPs) are gaining more and more importance as drug delivery platforms due to their surface that allows an easy, low toxicity and efficient functionalization with both chemical and biological molecules [5, 6].

Numerous conventional methods are used to obtain metallic nanoparticles (AgNPs and AuNPs) such as: solution, chemical/photochemical reactions in reverse micelles, thermal decomposition of different silver or gold compounds, electrochemical and microwave-assisted routes but these methods usually involve the use of hazardous chemicals are require high energy and wasteful purifications [7 - 9].

An affordable and cost-effective method is constantly gaining importance in recent years which involves the use of plants as both bio-reducing and stabilizing agents [10].

Kohlrabi (*Brassica oleracea* Gongylodes group) is a bulbous vegetable rich in vitamin C from which both root and leaves are recommended for human consumption as they contain important quantities of nutrients (Fig. 1.) [11].

Fig. 1. Health benefits of Kohlrabi

The present paper describes the green synthesis of AgNPs and AuNPs using aqueous extracts of pale-green and purple Kohlrabi peel. The potential capacity of the two species of Kohlrabi to bio-reduce metal ions was investigated by UV-Vis and FTIR. The size of the biosynthesized metallic nanoparticles was confirmed by diffraction light scattering measurements (DLS).

2. Experimental

Materials

Silver nitrate ($AgNO_3$), tetrachloauric acid ($HAuCl_4$), sodium citrate, DPPH, (2,2 – diphenyl – 1 – picryl – hydrazyl – hydrate stable free radical), hydrochloric acid (HCl), sulphuric acid (H_2SO_4), Benedict reagent and glacial acetic acid (CH_3COOH) were purchased from Sigma – Aldricht (Germany) and ethanol (C_2H_5OH) was purchased from Scharlau (Spain). The distilled water used in our experiments was freshly prepared in the laboratory using a Liston distiller. Both species of Kohlrabi were purchased fresh from the local market and dried at room temperature for further use.

Preparation of aqueous Kohlrabi extracts

Both types of Kohlrabi used in our experiments were purchased fresh from the supermarket, thoroughly washed twice with tap water and thrice with distilled water, followed by a clear separation between core and peel and leaves that were then left to dry at room temperature for 4-6 days. After drying, the peel of both types of Kohlrabi was finely grinded and further used for the preparation of two aqueous extracts following the same protocol:

- 25 g dried peel was transferred into a "French press" type extractor (distinctive for each Kohlrabi peel) and 250 mL distilled water were added;
- the resulted mixture was left for 24 hours, at 4^0 C (in a refrigerator) to infuse so that all the intracellular materials could be released;
- the resulted aqueous extract was filtered until a clear liquid is obtained;
- the aqueous extract is stable at 4^0 C for more than 12 weeks.

Synthesis of AgNPs and AuNPs

A 10^{-3} M aqueous solution of silver nitrate ($AgNO_3$) was prepared and used for the biosynthesis of AgNPs from pale-gren and purple Kohlrabi peel by the following method: 5 mL aqueous extract was mixed with 50 mL 10^{-3} M $AgNO_3$ solution and left 24 hours in the dark, at room temperature. After the 24 hours, the AgNPs – aqueous extract solution was agitated for 30 minutes in an ultrasound bath, at 50 rpm.

AuNPs were biosynthesized from Kohlrabi peel by the following method: 5 mL aqueous peel extract were mixed with 5 mL 10^{-3} M $HAuCl_4$, heated at 50^0 C with continuous stirring (450 rpm) for 30 minutes. The heat was turned off and the resulted solution was agitated at room temperature for 1 hour and then left for 24 hours in the dark. After the 24 hours, the AuNPs – aqueous extract solution was agitated in an ultrasound bath, at 50 rpm, for 30 minutes.

Characterization methods

The absorption spectra were recorded using a M 400 Carl Zeiss Jena UV – Vis spectrometer in the wavelength range of 250 – 800 nm. Fourier transform infrared spectroscopy (FTIR) spectra were recorded using a Vertex 80 FT-IR spectrometer equipped with high-resolution Hyperion 3000 microscope, in the range of 8000 – 400 cm^{-1}. Dynamic light scattering (DLS) spectra were recorded using a Zetasizer Nano SZ – Malvern instrument that has a computer connected with preinstalled Zetasizer software that allows an accurate control of the measurements.

Antioxidant activity was determined using a standard method: a DPPH solution was prepared in ethanol and 0.5 mL aqueous extract was mixed with 1 mL 0.02 mg/mL DPPH solution. The resulted mixtures were tested by recording the absorbance at 517 nm. A blank was prepared in parallel by mixing 0.5 mL distilled water with 1 mL 0.02 mg/mL DPPH solution and the spectrum was recorded at the same wavelength [12, 13]. The antioxidant activity (AA %) was calculated with the following formula:

$$AA\ \% = [A_{Control} - A_{Sample} / A_{Control}] \times 100,$$

where: $A_{Control}$ is the absorbance of the blank DPPH solution and A_{Sample} is the absorbance of the aqueous extracts mixed with 0,02 mg/mL DPPH solution.

The quantitative determination of phytochemicals (Table 1) was carried out to determine the total content of tannins (TCF), total content of flavonoids (TCF), total content of polyphenols (TCP) and total content of terpenoids (TCTp) [14-16].

3. Results and discussions

Quantitative determination of phytochemicals

The amount of total tannins is described as mg catechin/L and the two aqueous extracts were analyzed in triplicate. To determine the total content of flavonoids, catechin was used as standard. The total content of polyphenols uses gallic acid as standard calibration curve. Linalool was used as standard calibration curve for the determination of total content of terpenoids. The results of the

quantitative screening of phytochemicals in aqueous extracts o pale-green Kohlrabi and purple Kohlrabi are detailed in Table 2.

Table 1:

Quantitative methods for the determination of phytochemicals

Crt. No.	Assay	Reagents	Reaction parameters	Recordings
1	Total Tannins Content	0.5 mL extract+3 mL 4% vanillin-MeOH and 1.5 mL HCl	15 min. incubation at room temperature	Absorbance at 500 nm (catechin curve calibration standard)
2	Total Flavonoids Content	1 mL extract+4 mL distilled water and 0.3 mL 5% $NaNO_2$; after 5 minutes: 0.3 mL 10% $AlCl_3$; after other 5 minutes: 2 mL 1M NaOH and 2.4 mL distilled water	30 min. incubation at room temperature	Absorbance at 510 nm (catechin curve calibration standard)
3	Total Polyphenols Content	1 mL diluted extract and 5 mL Folin-Ciocalteu reagent; after 8 minutes: 4 mL Na_2CO_3	60 min. incubation at room temperature	Absorbance at 765 nm (gallic acid curve calibration standard)
4	Total Terpenoids Content	2 mL extract and 1 mL 2% vanillin-H_2SO_4	Heated at 60^0C for 20 min., cooled at 25^0C for 5 min.	Absorbance at 608 nm (linalool curve calibration standard)

Table 2

Quantitative results of the quantitative screening of phytochemicals

Aqueous extract	TCT (mg/L)	TCF (mg/L)	TCP (mg/L)	TCTp (mg/L)
Pale-green Kohlrabi	34,400	73,93	423,728	14,115
Purple Kohlrabi	34,692	75,06	435,986	14,869

Antioxidant activity of AgNPs and AuNPs

The easiest way to observe the formation of AgNPs and AuNPs is the visual change in color of the aqueous extracts from peel of pale-green and purple Kohlrabi once $AgNO_3$ 10^{-3} M or $HAuCl_4$ 10^{-3} M solutions were added. The results for the antioxidant activity (AA) (%) are presented in comparison between the two metallic nanoparticles and their extracts, clearly proving that both pale-green Kohlrabi and purple Kohlrabi exhibit good antioxidant properties, as it is observed from Table 3.

Table 3

Antioxidant activity for the aqueous extracts and metallic nanoparticles

Aqueous extract	AA (%) aq. extract	AA (%) AgNPs	AA (%) AuNPs
Pale-green Kohlrabi	79,28	86,76	83,45
Purple Kohlrabi	80,21	87,39	84,98

Characterization of AgNPs and AuNPs by UV-Vis spectroscopy

The aqueous extracts from peel of pale-green and purple Kohlrabi were analyzed using UV-Vis spectroscopy at well-established time intervals: 0s, 5 min, 30 min, 60 min, 120 min and at 24 hours after the biosynthesis. The bioreduction of both AgNps and AuNPs was analyzed using UV-Vis spectrometry between wavelengths of 220 and 800 nm.

The visual change of color for the aqueous extracts prepared from peel of pale-green and purple Kohlrabi are clearly observed immediately after the $AgNO_3$ 10^{-3} M or $HAuCl_4$ 10^{-3} M solutions were added as follows:

- the solutions turned yellow-brown in case of AgNPs for both solutions prepared from peel of pale-green and purple Kohlrabi and, respectively,
- the solutions turned dark-red in case of AuNPs for both solutions prepared from peel of pale-green and purple Kohlrabi.

The absorption recorded at a wavelength of 272 nm and 375 nm respectively is characteristic for phenolic acids and their derivates such as: flavones, flavonols and quinones [17]. To be more specific, phenolic compounds were found at 282 nm in the case of aqueous extract prepared from peel of pale-green Kohlrabi and at 285 nm in the case of aqueous extract prepared from peel of purple Kohlrabi.

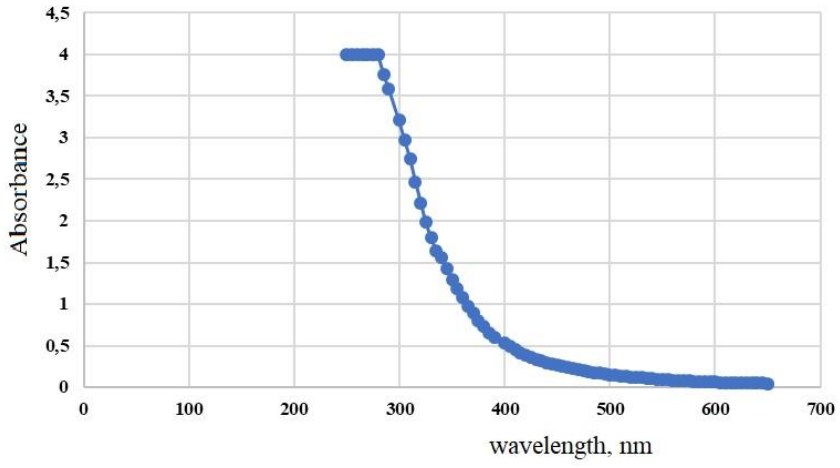

Fig. 2. UV-Vis spectra of aqueous extract from peel of pale-green Kohlrabi

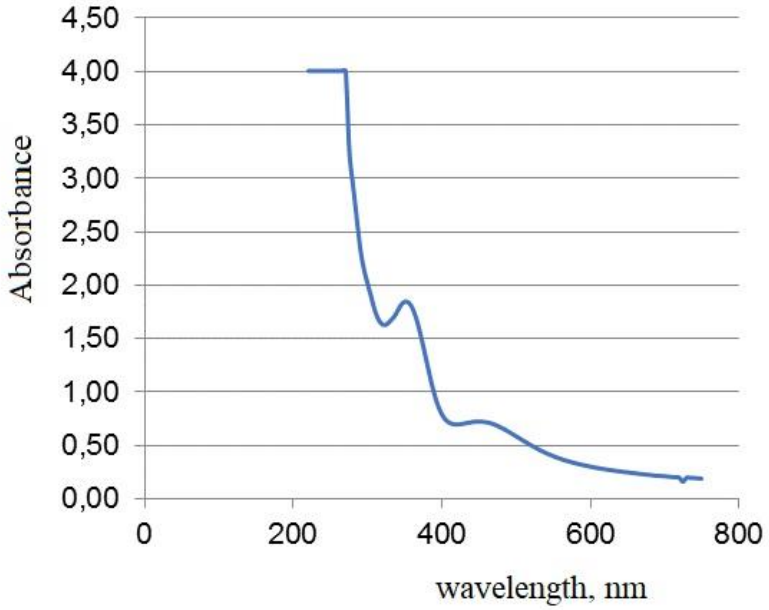

Fig. 3. UV-Vis spectra of AgNPs - peel of pale-green Kohlrabi

The bioreduction of Ag^+ was observed at 450 nm in the case of the aqueous extract from peel of pale-green Kohlrabi and at 455 nm in the case of aqueous extract from peel of purple Kohlrabi. By comparison, the bioreduction of Au^+ was observed at 548 nm in the case of the aqueous extract from peel of pale-green Kohlrabi and at 552 nm in the case of aqueous extract from peel of purple Kohlrabi.

Characterization of AgNPs and AuNPs by FTIR spectroscopy

All the studied samples were first dried and then analyzed using Fourier Transform Infrared spectroscopy (FTIR), a technique used to precisely indicate various functional groups found at different wavelengths in the recorded spectra.

FTIR spectra (Fig.4) exhibit specific peaks for pale-green Kohlrabi and purple Kohlrabi that are at at 3337 cm^{-1} (pale-green Kohlrabi) and 3325 cm^{-1} (purple Kohlrabi) assigned to hydroxyl (- OH) groups. The band that appears at 2948 cm^{-1} (pale-green Kohlrabi) and 2945 cm^{-1} (purple Kohlrabi) is specific to methine (-CH) groups while the bands C = C and C = O were easily identified at 1590 cm^{-1} and 1453 cm^{-1} (pale-green Kohlrabi) respectively 1586 cm^{-1} and 1458 cm^{-1} (purple Kohlrabi).

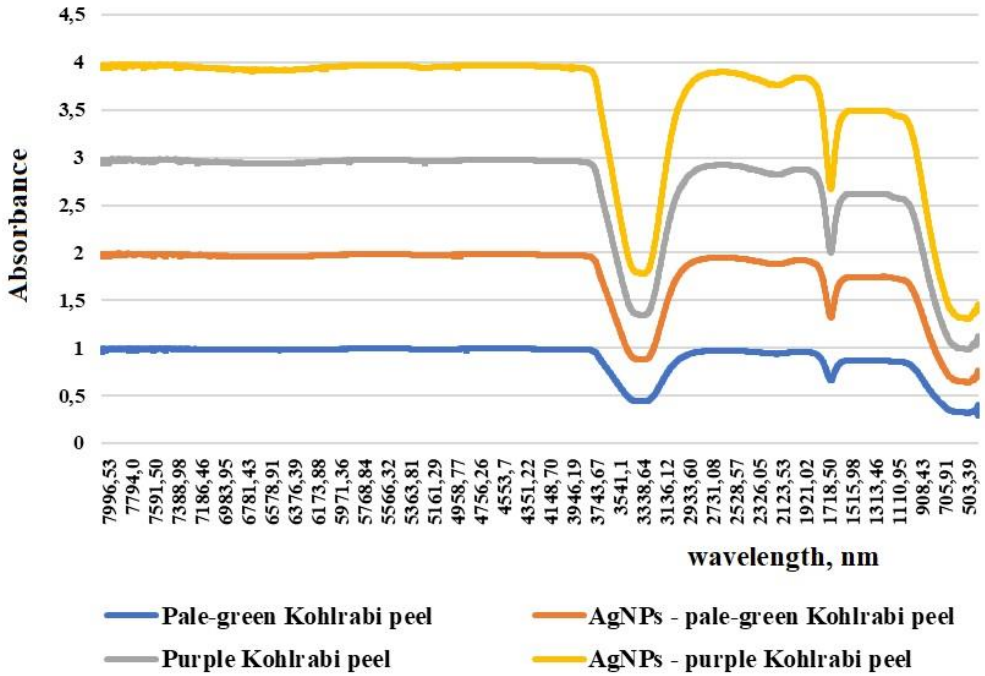

Fig. 4. Comparative FTIR spectra of the aqueous extracts and AgNPs

The aromatic amide I and amide II group were found in the range of 1386 cm^{-1} and 1321 cm^{-1} (pale-green Kohlrabi) respectively 1385 $cm^{-1}$and 1320 cm^{-1} (purple Kohlrabi). The C – O groups specific for esters, catechins and type III amides were situated between 1262 – 1120 cm^{-1} (pale-green Kohlrabi) respectively 1265 – 1126 cm^{-1} (purple Kohlrabi). Specific bands found between 1500 – 1300 cm^{-1} were attributed to amides, proteins and enzymes that contribute to the reduction of Ag ions. All the bio – synthesized AgNPs exhibited specific FTIR bands attributed to polyphenols in the range of 1655 cm^{-1} and 1659 cm^{-1}.

Characterization of AgNPs and AuNPs by DLS

In order to determine the size of the biosynthesized metallic nanoparticles, dynamic light scattering (DLS) measurements were carried out for both pale-green Kohlrabi and purple Kohlrabi. Also, zeta potential was also determined for all the studied samples.

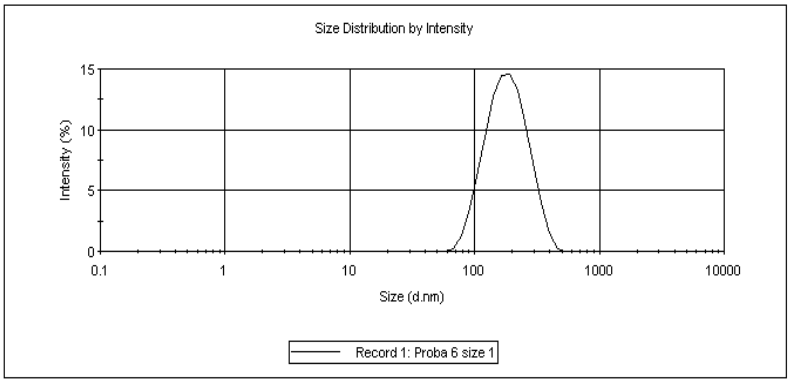

Fig.5. DLS spectrum for AgNPs – pale-green Kohlrabi peel

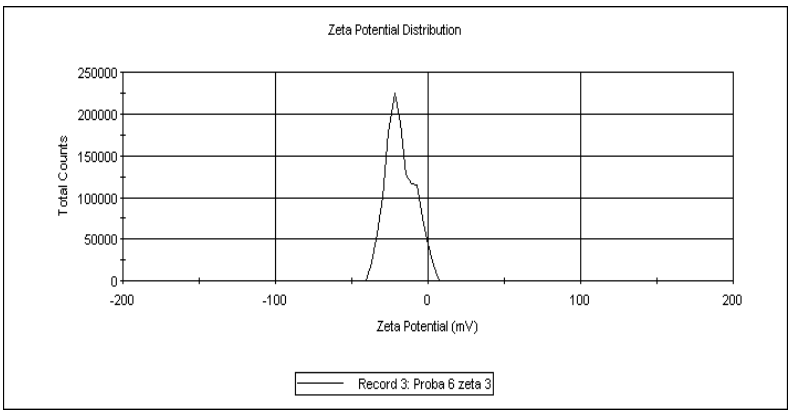

Fig.6. Zeta potential measurements for AgNPs – purple Kohlrabi peel

Table 4

Particle size and zeta potential for AgNPs – Kohlrabi peel

Sample	Dm (d.nm)	P_1...i (d.nm)	PdI	PZ (mV)
AgNPs – pale-green Kohlrabi peel	153	P_1 = 191	0.199	- 18
AgNPs – purple Kohlrabi peel	158	P_1 = 180	0.186	-16

4. Conclusions

The present research paper fully describes the biosynthesis of two metallic nanoparticles, namely silver nanoparticles (AgNPs) and gold nanoparticles (AuNPs) from aqueous extracts prepared from the peel of pale-green Kohlrabi and purple Kohlrabi, a versatile vegetable with numerous health benefits. Both aqueous extracts were analyzed by means of quantitative phytochemicals 'content using standard analytical techniques showing excellent results for total content of polyphenols (TCP) for the two aqueous extracts.

The AgNPs showed a significant increase of the antioxidant activity compared to the aqueous extracts alone thus proving that AgNPs can be used to treat many diseases. From the FTIR – ATR spectra it was clear that the phytocomponents (especially proteins and flavonoids) act as reducing agents.

The visual change of color was observed for both AgNPs and AuNPs and was confirmed by recording the UV-Vis spectra at different time intervals. Also, the antioxidant activity (AA, %) showed a considerable increase of the metallic nanoparticles compared to the aqueous extracts alone.

Acknowledgment: This research paper was prepared with the financial support of the project PN 18.22.04.01.02.

REFERENCES

[1] Sreeprasad T. S., Predeep T., *Noble Metal Nanoparticles*, Springer Handbook of Nanomaterials, Berlin, Heidelberg 2013.
[2] Arvizo R. R., Bhattacharyya S., Kudgus R., Giri K., Bhattacharyya R., Mukherjee P, Intrinsic therapeutic applications of noble metal nanoparticles: past, present and future, *Chem Soc Rev*, 41(7), (2012), 2943-2970.
[3] Conde J., Doria G., Baptista P., Noble metal nanoparticles applications in cancer, *Journal of Drug Delivery*, Article ID 751075, (2012), 56-68, doi:10.1155/2012/751075.
[4] Krystek P., Brandsma S., Leonards P., DeBoer J., Exploring moethods for compositional and particle size analysis of noble metal nanoparticles in Daphnia magna, *Talanta*, 147, (2016), 289-295.
[5] Dykman L. A., Khlebtsov N. G., Gold nanoparticles in biology and medicine: recent advances and prospects, *Acta Naturae*, 3(2), (2011), 34-55.
[6] Papasani M. R., Wang G., Hill R. A., Gold nanoparticles: the importance of physiological principles to devise strategies for targeted drug delivery, *Nanomedicine*, 8(6), (2012), 804-814.
[7] Mourato A., Gadanho M., Lino A.R., Tenreiro R., Biosynthesis of crystalline silver and gold nanoparticles by extremophilic yeasts, *Bioinorganic Chemistry and Applications*, (2011), 2010-2018.
[8] Galdiero S., Falanga A., Vitiello M., Marra V., Galdiero M., Silver nanoparticles as potential antiviral agents, *Molecules*, 16, (2011), 8894-8918.
[9] Bayazit M. K., Yue J., Cao E., Gavrilidis A., Tang J., Controllable synthesis of gold nanoparticles in aqueous solutions by microwave assisted flow chemistry, *ACS Sustainable Chem. Eng.*, 4(12), (2016), 6435-6442.
[10] Mittal A. K., Chisti Y., Banerjee U. C., Synthesis of metallic nanoparticles using plant extracts, *Biotechnology Advances*, 31(2), (2013), 346-356.
[11] Escalona VH, Aguayo E, Artes F. Metabolic activity and quality changes of whole and fresh-cut kohlrabi (*Brassica oleracea* L. *gongylodes* group) stored under controlled atmosphere, *Postharvest Biology and Technology*, 41, (2006), 181-190.
[12] Mosquera O. M., Correra Y. M., Nino, J., Antioxidant activity of plant extracts from Colombian flora, *Braz. J. of Pharmacog.*, 19(2A), (2009), 382-387.

[13] Bunghez I. R., Raduly M., Doncea S. M., Aksahin I., Ion R. M., Lycopene determination in tomatoes by different spectral techniques (UV-Vis, FTIR and HPLC), *Dig. J. Nanomater. Bios*, 4, (2011), 1349-1356.
[14] Biju J., Sulaiman C. T., Satheesh G., Reddy V. R. K., Total phenolics and flavonoids in selected medicinal plants from Kerala, *Intl. J. of Pharm. and Pharm. Sci.*, 6(1), (2014), 406-408.
[15] Alam N., Hossain M., Khalil M. I., Moniruzzaman M., Sulaiman S. A., Gan S. H., High catechin concentrations detected in Withania somnifera (Ashwagandha) by high performance liquis chromatography analysis, *BMC Compl. And Altern. Med.*, 11(65), (2011), 208-211.
[16] Zhishe, J., Menhcheng T., Jianming W., The determination of flavonoid contents in mulberry and their scavenging effects on superoxide radicals, *Food Chemistry*, 64, (1999), 555-559.
[17] Bunghez F., Socaciu C., Zagrean F.,Pop M., Ranga F., Romanciuc F., Characterisation of an aromatic plant-based formula using UV-Vis Spectroscopy, LC–ESI(+)QTOF-MS and HPLC-DAD analysis, *Bull. USAMV Food Sci Technol*, 70, (2013), 16-24.

A NEW PHYTOTHERAPEUTIC PRODUCT WITH HEALTH-PROMOTING EFFECTS IN RHEUMATIC AILMENTS

Viorica CARABELA, Viorica TAMAȘ, Gabriel C. IVOPOL, Andreea M. NEAGU*

S.C. Hofigal Export Import SA, 2 Intrarea Serelor Street, District 4, Bucharest, Romania

Abstract

This paper presents the studies carried out by the authors for identifying a combination of native plant sources that are rich in certain natural compounds having anti-inflammatory and analgesic effects, and on this basis developing new products with an increased efficiency in rheumatic ailments.

The following plants were selected for this purpose: willow bark (Salix alba cortex), well-known as containing precursors of aspirin that have inhibitory effects upon the activity of enzymes that generate inflammation and pain; rosemary, aerial parts (Rosmarinus officinalis herba) and oregano, aerial parts (Origanum vulgare herba), that bring other important anti-rheumatic compounds. We mention tri-terpenic acids (ursolic acid and its isomers) that have an anti-inflammatory effect, significant anti-inflammatory and analgesic flavonoids and tannins, choline, vitamins B3 and C, amino acids and peptides, essential oils, and minerals that have analgesic and soothing effects, and support local blood circulation and repair of the affected area.

The complex of plant compounds obtained as a concentrated extract, by the association of three plant products in certain processing conditions, was used in preparing a new anti-rheumatic product – Salicilol gel. This is presented in the form of a gel for topical use, and was tested with very good results in the "Alexandra" Natural Therapy Centre in Breaza, Prahova County, Romania.

Key words: Salicin, white willow, rosemary, oregano

1. Introduction

All of the structures of the inferior limbs (e.g. bone, cartilage, synovium, joint capsules, muscles, and ligaments) can contribute to rheumatic ailments.

* Corresponding author: E-mail address: cercetare@hofigal.eu (Andreea M. Neagu)

Rheumatic complaints generally cause different degrees of inflammation and discomfort to the human body, from mild pain and difficulties in moving easily, to intense prolonged pain that's hard to bear and advanced degrees of immobilisation. Due to the fact that rheumatic inflammation and pain can increase over time as the limb's structures deteriorate and transform, it is best to intervene in the earliest possible stages of mild rheumatic complaints, with mild natural products. Natural products are efficient in these early stages, and unlike many chemical preparations, in most people don't produce undesirable secondary effects (that are often initially silent and may adversely affect other systems such as the liver or delicate metabolic enzymes).
Therefore the authors have proposed to develop an easy to administer phytotherapeutic product, for external use, which intervenes locally in reducing the inflammatory process, pain, and associated muscular contraction.

2. Materials and methods

In order to develop this new product, a natural intermediate product was used. The intermediate product is a liquid extract of white willow bark, together with rosemary *herba* and oregano *herba*, which are rich in compounds (presented in Table 1), that are useful for the products proposed purpose.
From the studies carried out with this extract (called "phytocomplex A"), it was found that it is necessary to increase the quantity of salicylic derivatives, that have an important contribution for the product's intended purpose, from approximately 0.5% to a minimum of 1.3%.

In this sense research was carried out on white willow bark from different parts of the country and during different seasons.

White willow bark represents the main source of salicin and other salicylic derivatives (e.g., salicortin, 2'-O-acetylsalicortin, and tremulin), compounds that share a similar structure to aspirin (acetyl salicylic acid), white willow is thus also known as "nature's aspirin".
Salicin can be cleaved (by enzymatic hydrolysis induced by emulsin and diastase) into glucose and saligenin (o-oxybenzylic alcohol or saligenol) [1]. Saligenin, in turn, produces salicylic acid via oxidation, with notable analgesic, anti-pyretic and anti-rheumatic properties, thus generating, stepwise, a prolonged effect. [2, 9]. Likewise, tannins present in white willow bark have a tonic, astringent, coagulant and mildly haemostatic effect [3].

Table 1

Description of the natural ingredients used and their beneficial effects

Common name	Scientific name	Active chemical compounds of interest	Compound's effects
White willow	*Salix alba (cortex)*	• salicylic compounds: • salicin, fragilin, populin. • phenolic compounds: • triandrin, cafeic acid, ferulic acid, salicylic acid, p-cumaric acid • flavonoids, quercitin, luteolin, naringenin • tannins	• anti-inflammatory • analgesic • antipyretic • sedative • coagulant • astringent
Rosemary	*Rosmarinus officinalis (herba)*	• essential oil • polyphenolcarboxylic acids • rosmarinic, cafeic, chlorogenic acid • diterpenoids • carnosol, rosmanol, rosmadial • triterpenic acids • ursolic, oleanolic acid • phytosterols • flavonic derivatives • apigenol, luteolin, diosmetin, diosmin	• antirheumatic • antiseptic • stomachic • powerful stimulant of blood circulation, especially good for cerebral blood circulation and oxygenation • general tonic
Oregano	*Origanum vulgare (herba)*	• essential oil (thymol, carvacrol), • ursolic acid, • tannins, • anthocyanides, • flavonoids, • minerals.	• anti-inflammatory, • sedative, • sedative-bronchodilator, • antiseptic, • antispastic, • stomachic.

As analgesics that act on peripheral vasculature and tissues, salicylic acid and aspirin belong to a group of anionic medicines that inhibit the generation of pain signals in the body's nociceptors, while concurrently acting as anti-inflammatories due to their concentration in tissue that has become acidic due to the inflammatory process.

Pain signals are triggered in the body's nociceptors via a series of chemical mediators that are released concurrently with tissular changes, while the body's sensitivity to pain is exacerbated in the affected area due to PGE1, and PGE2

(prostaglandin E1 and E2 respectively). Salicylic acid generated by the metabolisis of salicin and its related glucosides intervenes in the arachidonic acid metabolic pathway by inhibiting cyclooxygenase (COX, i.e., prostaglandin-endoperoxide synthase), and therefore the synthesis of PG (prostaglandin), PGI_2 (prostacyclin) and its antagonist, TXA_2 (thromboxane). As the concentration of PG decreases at the site of inflammation, pain intensity subsides even to the point of disparition [4].

For the selection of sources of white willow bark that is rich in salicylic derivatives, multiple samples were taken, from different geographical regions, young (2-3 years) and mature, harvested in spring and summer (Fig.1).

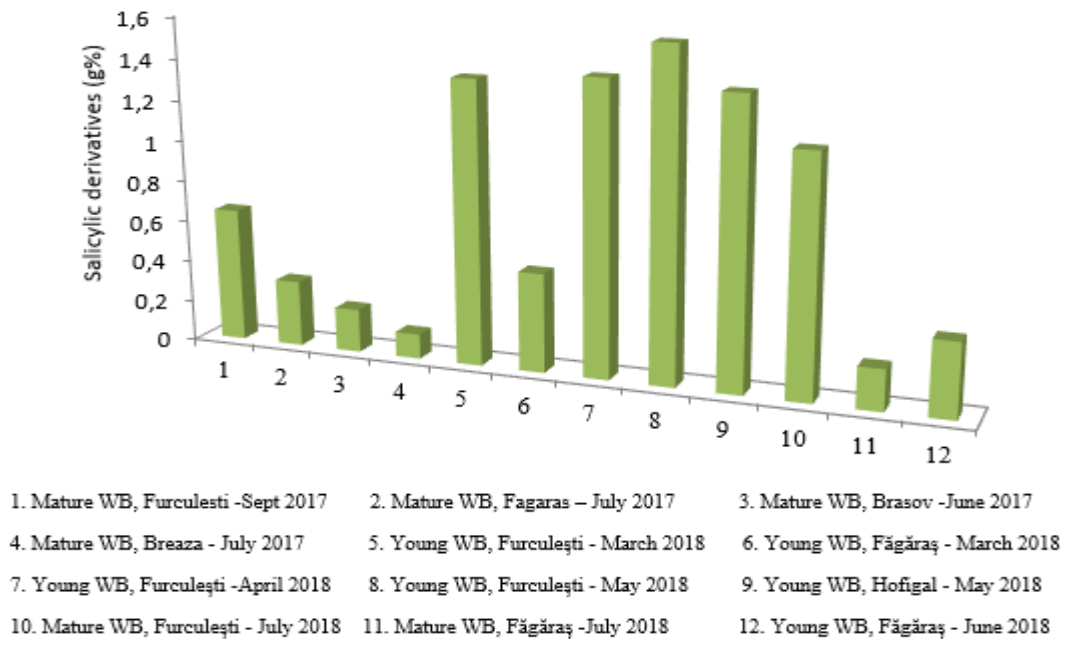

Fig. 1 Variation in the content of salicylic derivatives, in different samples of white willow bark.

The studies were carried out directly on phytocomplex A with different samples of white willow bark.

From the results depicted in Fig. 1, it can be seen that the most suitable white willow bark for phytocomplex A is from young trees (2-3 years old), from the south of the country (Furculesti, Teleorman), harvested in the spring, with a

content of at least 1.58% salicylic derivatives. This agrees with the hypothesis that these salicylic derivatives may be part of the white willow's defence mechanism against insect damage in spring, transported more easily in young tissues, in lowland southerly climes where there are higher populations of insects that feed on the white willow.

Rosemary complements phytocomplex A due to its content of polyphenylcarboxylic acids, expressed as rosmarinic acid. Unlike NSAIDs (non-steroidal anti-inflammatory drugs) that act by inhibiting COX and/or 5-lipoxygenase, rosmarinic acid inhibits the cleavage of C3 (complement component 3) into C3a and C3b fragments. C3a would also act as a pro-inflammatory agent, exacerbating inflammation by increasing vascular permeability, and attracting mastocytes and neutrophils to the site of inflammation [6].

Concurrently, the effect of the salicylic acid derivatives in phytocomplex A is potentiated by the polyphenolic compounds present in oregano, that inhibit COX-2 [7].

As a result, the use of high quality white willow bark in the preparation of the new phytocomplex has led to the development of phytocomplex B, in liquid extract form, having at least 1.35% salicylic derivatives, that was analysed and characterised physico-chemically (q.v. Table 2).

Phytocomplex B was used in the creation of the new product "Salicylol Gel", that has anti-inflammatory and analgesic effects, easing joint, muscle and skin discomfort, and stimulating peripheral blood circulation.

3. Results and discussions

In order to maximise the content of salicylic derivatives from white willow bark, it was necessary to carry out a comparative study regarding the extractive conditions (e.g., aqueous or hydroalcoholic media, decoctions, tinctures) (Fig.2).

Thus, it was found that extraction in an aqueous medium is the most efficient, resulting in an extract with the highest concentration of salicylic derivatives.

In phytocomplex B, with an elevated content of salicylic derivatives, other compounds are found that have a synergistic effect such as: polyphenols, tannins, flavonoids, minerals, and essential oils that have an anti-inflammatory and analgesic effect.

Phytocomplex B was characterised according to salicylic derivatives content (wt.,%), tannins expressed as pyrogalol content (wt.,%), and polyphenol content

expressed as chlorogenic acid (wt.,%). The main physico-chemical characteristics of phytocomplex B are shown in Tab. 2.

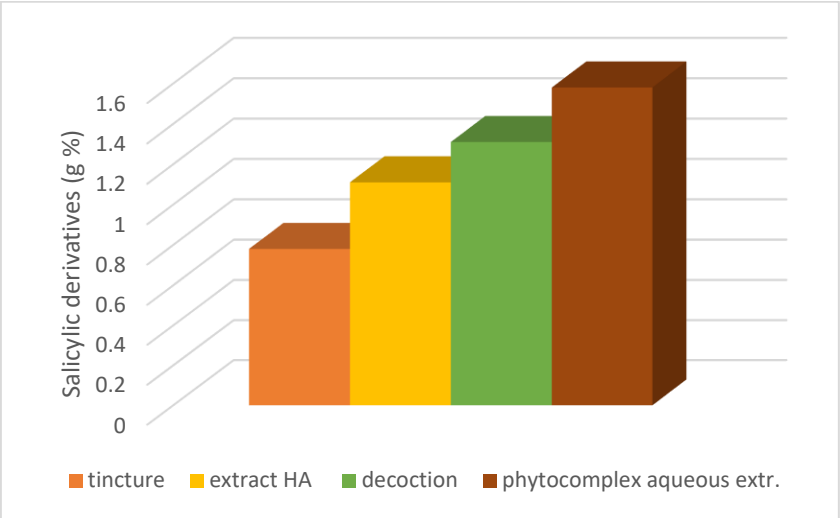

Fig. 2 Percentage content of salicylic derivatives, for different extraction conditions.

Table 2

The main physico-chemical characteristics of phytocomplex B.

Characteristic	**Quality parameters**
Description: aspect/colour; smell/taste	opalescent liquid / red-brown; characteristic / intensely bitter
Relative density,d_{20}^{20}	0.990-1.200
Evaporation residue, %, min.	15.0
Content in salicylic derivates, expressed as salicin, %, min.	1.35
Total polyphenol content expressed in: - Chlorogenic acid,%,min. - Gallic acid,% , min.	 13.00 8.00
Tannins content expressed in pyrogalol , %, min.	1.15

"Salicilol Gel" for massage with extracts of white willow, rosemary, oregano, chili pepper and essential oils of rosemary, mint, and pine is a product especially created to care for and ease discomfort of the joints and muscles. Besides phytocomplex B, Salicilol Gel contains chili pepper extract, that has a role in improving peripheral blood circulation, and certain essential oils such as mint,

rosemary, and pine with a revulsive (i.e. dispersing and diverting a complaint away from an affected area) and calming effect.
The high content of active natural compounds and their synergism favours the relaxation of the muscles and joints, gives an anti-inflammatory effect, and stimulates blood flow, being therefore beneficial in rheumatic or muscular pain. It is also beneficial as an adjuvant in other pains, such as those caused by neuralgias, contusions, sprains, or in the healing phase following fractures of other minor traumas. (Fig.3).

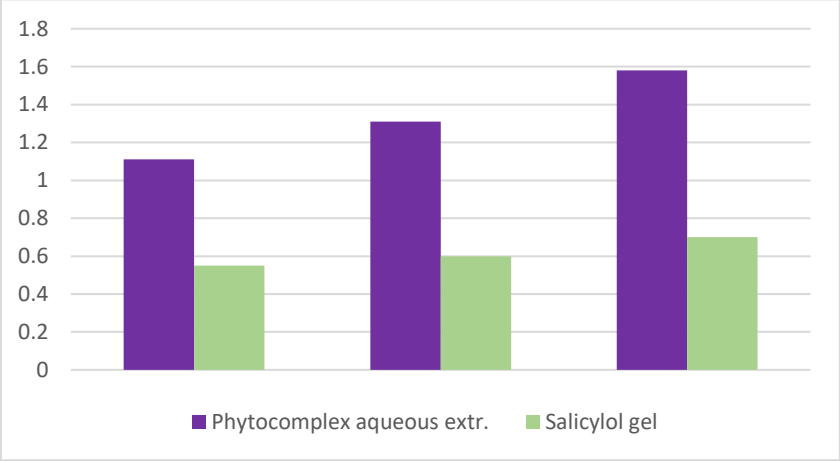

Fig. 3 Salicylic derivatives content (wt. %) for phytocomplex B and salicilol gel

Salicilol Gel was studied and analysed, *inter alia*, physico-chemically, by HPLC (high performance liquid chromatography), and spectrophotometrically. Salicilol gel as a final product was thus characterised by establishing a minimum concentration of 0.25% salicylic derivatives. The tannins content (expressed as 0.100% pyrogalol) and identification of capsaicin (via TLC - thin layer chromatography) were likewise established. (Tab.3).
Salicilol Gel forms a thin film on the skin's surface, favouring the transport of its synergistic plant-compounds down to the cutaneous tissue's deeper layers. The mechanism of action comprises a modulation of the inflammatory process and acts via neuropeptides and cytokines attaining an equilibrium between pro-inflammatory cytokines (TNFα, IL1, IL6, IL8) that are inhibited/decreased and

anti-inflammatory cytokines (TGFβ, IL10) that are stimulated/activated, facilitating a better repair of damaged tissue [8].

Table 3

The main physico-chemical characteristics of Salicilol Gel.

Characteristic	**Quality parameters**
Description: aspect/colour; smell/taste	Homogenous gel / red-brown; characteristic / intensely bitter
pH	5.0 – 7.0
Relative density, d_{20}^{20}	0.950 – 0.990
Content in salicylic derivates, expressed as salicin, %, min.	0.25
Tannins content expressed in pyrogalol , %, min.	0.100
Identification of capsaicin (TLC)	Positive

During the period of August 2016, a test was carried out for verifying the compatibility of Salicilol Gel with the skin. This was done by a single dermal application in an occlusive environment (a patch test), under exaggerated experimental conditions. The results of the study showed no adverse reactions of the irritative or inflammatory type.

The product's efficacy was tested at the "Alexandra" Natural Therapy Centre in Breaza. The parameters considered were: pain diminishment, improved mobility, reduced oedema, recovery of normal functions, an evaluation of overall activity.

The results are good, contributing to an amelioration in the discomfort of the joints, muscles, and skin, having anti-inflammatory effects, and peripheral blood circulation stimulating effects [9].

4. Summary of activities

- A concentrated plant-complex extract (rich in natural salicylic compounds) was developed; including, amongst other plants, white willow, rosemary and oregano.
- A quantitative and qualitative formula for Salicilol Gel was created.
- Technical documentation was compiled for Salicilol Gel, in accordance with current requirements for production (product file, technical specifications, stability studies)
- An evaluative report was generated with regards to the risks to human health. The results of the evaluative tests show that the product is suitable, in accordance with Dermotest Pauna SRL Bucharest.

- Methods of analysis were developed for determining the content in tannins and salicylic derivatives in Salicilol Gel.

5. Conclusions

The synergistic combination of active natural plant products that include white willow, rosemary, oregano, chili pepper and essential oils of rosemary, mint, and pine in "Salicilol Gel", by processes and effects described in this paper, including salicylic derivatives, makes it an efficacious massage preparation that favours the relaxation of the muscles and joints, gives an anti-inflammatory effect, and stimulates peripheral blood flow, being therefore beneficial in rheumatic and/or muscular pain.

REFERENCES

[1] European Medicines Agency. Assessment Report on Salicis Cortex (Willow Bark) and Herbal Preparation(S) thereof with Well-Established Use and Traditional Use. Doc. Ref.: EMEA/HMPC/295337/2007, 26 September 2009.
[2] http://en.wikipedia.org/wiki/Salicin
[3] Farmacopeea Botanica Americana (1999).
[4] Dannhardt G, Kiefer W. Cyclooxygenase inhibitors--current status and future prospects, *Eur J Med Chem*., 36(2), (2001), 109-26.
[5] World Health Organization (WHO). WHO monographs on selected medicinal plants. Geneva, Switzerland: WHO Press, 2009.
[6] Englberger W, Hadding U, Etschenberg E, Garf E, Leyck S, Winkelmann J, Parnham MJ, Nattermann Research Laboratories, Cologne F.R.G. Rosmarinic acid: a new inhibitor of complement C-convertzse with anti-inflammatory activity, *Int. J. Immunopharmacol*, 10(6), (1988), 729-37.
[7] Stănescu U., Hăncianu M., Cioancă O., Plante medicinale de la A la Z, Ed. Polirom, Iasi, 2014. pag.1102
[8] Julkunen-Tiitto R, Meier B. The enzymatic decomposition of salicin and its derivatives obtained from *Salicaceae* species. *Journal of Natural Products*, 55, (1992), 1204-12.
[9] Greyn J et al. COX-1 and COX-2 inhibition: current status and future perspective. *Acta Anaesthesiol Belg.*, 49(3), (1998), 175-83.